Model based process analysis and scale-up in membrane chromatography

Inaugural dissertation

for the attainment of the title of doctor
in the Faculties of Mathematics and Natural Sciences
at the Heinrich Heine University Düsseldorf

presented by

Pranay Kumar Ghosh
from Bhagalpur

Jülich, Dec 2013

from the Institute of Bio- and Geosciences, IBG1: Biotechnology
at the Forschungszentrum Juelich GmbH

Published by permission of the
Faculty of Mathematics and Natural Sciences at
Heinrich Hein University Düsseldorf

Supervisor: Prof. Dr. Wolfgang Wiechert
Co-supervisor: Prof. Dr. Martin Lercher
Ph.D. Advisor: Dr.-Ing. Eric von Lieres

Date of the oral examination: 27/05/2014

Declaration of Authorship

I, Pranay Kumar Ghosh, hereby declare that, to the best of my knowledge, I have worked on this thesis titled, *Model based process analysis and scale-up in membrane chromatography* without external help and without the use of sources other than mentioned. I have not submitted this work or similar kind of work at any other institution for evaluation. Any statements or data etc. which are quoted from other sources are acknowledged or cited accordingly.

(Ich, Pranay Kumar Ghosh, versichere, dass ich die vorliegende Arbeit *Method development for model based process analysis in membrane chromatography* ohne fremde Hilfe und ohne Benutzung anderer als der angegebenen Quellen angefertigt habe und dass die Arbeit in gleicher oder ähnlicher Form noch keiner anderen Prüfungsbehörde vorgelegen hat und von dieser als Teil einer Prüfungsleistung angenommen wurde. Alle Ausführungen, die wörtlich oder sinngemäß übernommen wurden, sind als solche gekennzeichnet.)

Signed: _____

Date: _____

"You have control over your respective duty only, but no control or claim over the results. The fruits of work should not be your motive. You should never be inactive."

Bhagwad Gita (2.47)

Abstract

Membrane chromatography (MC) is gaining wider acceptance in downstream processing of biopharmaceuticals. MC offers the advantage of higher operational flow-rates and thus, provides an attractive alternative to traditionally employed packed bed chromatography. With increased commercial usage, in-depth understanding of different mechanisms within MC capsules is desirable in order to achieve optimum performance.

MC capsules are characterized by the sharpness of their breakthrough curves (BTCs). However, BTCs frequently suffer from tailing near the saturation. Furthermore, the degree of tailing differs not only between MC capsules from different vendors but also varies between MC capsules at lab and large scales from the same vendor. A lab scale MC capsule, built as a physical scale-down model of a large scale MC capsule, therefore, cannot be accurately used for optimization of large scale purification processes. Hence, mathematical model-based approaches are required for holistic process analysis and scale-up in MC.

Several works have been performed in modeling BTC behaviour of MC capsules in the past. However, although, the traditionally used modeling approach works in performing stand-alone process analysis in MC on one scale of operation, it completely fails in providing a holistic model based scale-up. Hence, in this work, two advanced modeling approaches, the zonal rate model (ZRM) and the computational fluid dynamics (CFD), are developed for providing model based scale-up in MC capsules. Both modeling approaches have been shown to accurately predict the breakthrough performances of large scale MC capsules as compared to the traditionally used modeling approach.

MC capsules exhibit several non-idealities at different scales: Non-ideal hydrodynamics, non-ideal protein adsorption and non-linear scaling, all influencing the shape of measured BTCs. The developed modeling approaches holistically capture these non-idealities and decouple their influence on the observed BTCs. Thus, the developed models are universal in nature and can be applied for rational model-based process design employing MC capsules with different flow configurations, membrane types and scales.

Kurzfassung

Membranchromatographie (MC) Membrane findet in der Aufarbeitung biopharmazeutischer Wirkstoffe zunehmend Akzeptanz. MC bietet den Vorteil höherer Flussraten und ist deshalb eine attraktive Alternative zur traditionell eingesetzten Festbettchromatographie. Mit zunehmender kommerzieller Nutzung wird ein vertieftes Verständnis verschiedener Mechanismen in MC-Kapseln erforderlich, um optimale Prozessperformanz zu erreichen.

MC-Kapseln sind durch die Form ihrer Durchbruchskurven (DBK) charakterisiert. Die DBK flachen jedoch oft in der Nähe des Sättigungsbereiches ab. Darüber hinaus unterscheidet sich dieses Abflachen nicht nur zwischen MC-Kapseln verschiedener Hersteller, sondern auch zwischen MC-Kapseln des gleichen Herstellers auf Labor- und Produktions-Skalen. Eine MC-Kapsel auf der Labor-Skala, hergestellt als physikalisches, herunterskaliertes Modell einer MC-Kapsel auf der Produktionsskala, kann daher nicht für eine präzise Optimierung von Aufreinigungsprozessen auf der Produktionsskala verwendet werden. Deshalb werden mathematische, modell-basierte Ansätze für eine holistische Prozessanalyse und Hochskalierung in der Membranchromatographie benötigt.

In der Vergangenheit wurden verschiedene Arbeiten zur Modellierung des DBK-Verhaltens von MC-Kapseln durchgeführt. Obwohl der traditionell angewendete Modellierungsansatz funktioniert, um einzelne Prozessanalysen von MC-Kapseln auf ein und derselben Skala durchzuführen, versagt er bei der holistischen, modell-basierten Hochskalierung dennoch vollständig. Deshalb werden in dieser Arbeit zwei weiterentwickelte Modellierungsansätze, das Zonale Ratenmodell (ZRM) und Computational Fluid Dynamics (CFD), für die modellbasierte Hochskalierung von MC-Kapseln eingesetzt. Es wird gezeigt, dass beide Modellierungsansätze die DBK von MC-Kapseln auf der Produktionsskala präzise vorhersagen können, im Gegensatz zum traditionell angewandten Modellierungsansatz.

MC-Kapseln auf verschiedenen Skalen weisen unterschiedliche Nichtidealitäten auf, die die Form der gemessenen DBK beeinflussen: Nichtideale Hydrodynamik, nichtideale Proteinadsorption und nichtlineare Skalierung. Die weiterentwickelten Modellierungsansätze erfassen diese Nichtidealitäten und entkoppeln ihren Einfluss auf die beobachteten DKB. Deshalb sind die entwickelten Modelle von universeller Natur und können für eine rationale, modell-basierte Prozessauslegung verwendet werden, unter Verwendung von MC-Kapseln mit verschiedenen Flussschemata, Membrantypen und auf unterschiedlichen Skalen.

List of Publications

Journals

- Ghosh, P., Vahedipour, K., Lin, M., Vogel, J. H., Haynes, C. A. and von Lieres, E., Zonal rate model for axial and radial flow membrane chromatography. Part I: Knowledge transfer across operating conditions and scales. Biotechnology and Bioengineering 110 (2013) 1129-1141. [*Journal Impact Factor: 3.648*]

- Ghosh, P., Vahedipour, K., Lin, M., Vogel, J. H., Haynes, C. A. and von Lieres, E, Computational fluid dynamic simulation of axial and radial flow membrane chromatography: mechanisms of non-ideality and validation of the zonal rate model. Journal of Chromatography A 1305 (2013) 114-122. [*Journal Impact Factor: 4.612*]

- Kiefer, J., Rasul, N.H., Ghosh, P.K. and von Lieres, E., Surface and Bulk Porosity Mapping of Polymer Membranes using Infrared Spectroscopy. Journal of Membrane science 452 (2014) 152-156. [*Journal Impact Factor: 4.093*]

- Ghosh, P., Lin, M., Vogel, J. H., Choy, D.,Haynes, C. A. and von Lieres, E., Zonal rate model for axial and radial flow membrane chromatography. Part II: Model-based scale-up. Biotechnology and Bioengineering 111 (2014) 1587-1594. [*Journal Impact Factor: 3.648*]

- Ghosh, P., Vahedipour, K., Leuthold, M., and von Lieres, E., Model-based analysis and quantitative prediction of membrane chromatography: Extreme scale-up from 0.08 ml to 1200 ml. Journal of Chromatography A 1332 (2014) 8-13. [*Journal Impact Factor: 4.612*]

Conference proceedings

- Ghosh, P.; von Lieres, E.: Mechanistic and semi-empirical approaches for modelling inhomogeneous flow in membrane chromatography. Proceedings of 14$^{\text{th}}$ Aachener Membran Kolloqium, 14 (2012) 512-524.

Conference talks

- Ghosh, P.; von Lieres, E.: Mechanistic and semi-empirical approaches for modeling inhomogeneous flow in membrane chromatography, 9^{th} International PhD Seminar on Chromatographic Separation Science, Weggis, Switzerland, 24 - 26 February 2013.
- Ghosh, P.; von Lieres, E.: Mechanistic and semi-empirical approaches for modeling inhomogeneous flow in membrane chromatography, ESBES+ISPPP conference, Istanbul, 23 - 26 September 2012.
- Ghosh, P.; von Lieres, E.: Mechanistic and semi-empirical approaches for modeling inhomogeneous flow in membrane chromatography, Processnet conference, Karlsruhe, 10 - 13 September 2012.
- Ghosh, P.; Lin, M.; Vogel, J; von Lieres, E.: Model based scale-up with zonal rate model for membrane chromatography, ACS conference, San Diego, 25 - 29 March 2012.
- Ghosh, P.; Pohl, M.; Wiechert, W.; von Lieres, E.: Spatial homogeneity analysis of stacked membrane chromatography, 3^{rd} CLIB international conference, Cologne, 22 - 24 February 2012.
- Ghosh, P.; Francis, P.; Haynes, C.; Pohl, M.; Wiechert, W.; von Lieres, E.: Spatial homogeneity analysis of stacked membrane chromatography, ECCE/ECAB conference, Berlin, 25 - 29 September 2011.
- Ghosh, P.; Francis, P.; Haynes, C.; Pohl, M.; Wiechert, W.; von Lieres, E.: Modeling of stacked and spiral wound membrane chromatography- Zonal rate model approach, ECCE/ECAB conference, Berlin, 25 - 29 September 2011.
- Ghosh, P.; Lin, M.; Vogel, J.; Pohl, M.; Wiechert, W.; von Lieres, E.: Modeling of stacked and spiral wound membrane chromatography- Zonal rate model approach, PREP conference, Boston,10 - 13 July 2011.
- Ghosh, P.; Pohl, M.; Wiechert, W.; von Lieres, E.: Spatial homogeneity analysis of stacked membrane chromatography, 2^{nd} CLIB international conference, Düsseldorf, 5 - 6 April 2011.

Posters

- Ghosh, P.; von Lieres, E.: Mechanistic and semi-empirical approaches for modeling inhomogeneous flow in membrane chromatography, 14th Aachener Membran Kolloqium, Aachen, 7- 8 November 2012.
- Ghosh, P.; Pohl, M.; Wiechert, W.; von Lieres, E.: Spatial homogeneity analysis of stacked membrane chromatography, 3rd CLIB international conference, Cologne, 22 - 24 February 2012.
- Ghosh, P.; Pohl, M.; Wiechert, W.; von Lieres, E.: Spatial homogeneity analysis of stacked membrane chromatography, 2nd CLIB international conference, Duesseldorf, 5 - 6 April 2011.
- Ghosh, P.; Francis, P.; Haynes,C.; Wiechert, W.; von Lieres, E.: Spatial homogeneity analysis of stacked membrane chromatography, ACS conference, Anaheim, 27 - 31 March 2011.

Acknowledgements

I take this opportunity to express my heartfelt thanks to all the people involved with me in this project. First and foremost, I would like to express my deepest gratitude towards Dr.-Ing. Eric von Lieres, my advisor at IBG1: Biotechnology for his guidance, suggestions and support all throughout this project.
I would like to thank Prof. Dr. Wolfgang Wiechert for giving me the opportunity to work in his Institute and being the official supervisor. I would also like to thank Prof. Dr. Martin Lercher for agreeing to take up the role of co-supervisor.
I am grateful to Cluster Industrialle Biotechnologie (CLIB) for providing me financial assistance during the entire duration of the project.
I am extremely thankful to Dr. Min Lin and Dr. Jens Vogel at Bayer Healthcare, Berkeley for providing the required infrastructure to perform expensive large scale experiments. I also would like to thank Dr. Kaveh Vahedipour, INM4, FZ Juelich , for mentoring the MRI investigations. I would like to thank Dr. Martin Leuthold, Sartorius Stedim Biotech, Göttingen for collaborating with us and providing data sets that help in further validation of the developed models.
I am grateful to Prof. Dr. Martina Pohl for allowing me to perform experiments in her lab. I wish to take this opportunity to especially thank Ursula Mackfeld, Heike Offerman, and Lilia Arnold for helping me in the lab.
Special Thanks goes to my colleagues, Sebastian Schnittert, Andreas Püttmann and Birgit Stute for discussing and explaining various computational topics in a very "understandable" manner to a process engineer.
Last but not the least; I would like to thank my family for their patience and mental support throughout this project.

Contents

Abbreviations

BTC	**B**reak**T**hrough **C**urves
CFD	**C**omputational **F**luid **D**ynamics
MC	**M**embrane **C**hromatography
CSTR	**C**ontinuous **S**tirred **T**ank **R**egion
HIC	**H**ydrophobic **I**nteraction **C**hromatography
IEX	**I**on **EX**change Chromatography
IEX-MC	**I**on **EX**change-**M**embrane **C**hromatography
MRI	**M**agnetic **R**esonance **I**maging
MV	**M**embrane **V**olume
ODE	**O**rdinary **D**ifferential **E**quations
PDE	**P**artial **D**ifferential **E**quations
PFR	**P**lug **F**low **R**egion
SEC	**S**ize **E**xclusion **C**hromatography
ZRM	**Z**onal **R**ate **M**odel

For ma, papaji, da, and mou

Chapter 1

Introduction

1.1 General introduction

Modern biotechnology industry has grown much beyond from alcoholic fermentation and breweries to large scale production of bio-pharmaceuticals. With impressive advances in genetic engineering, scientists have achieved incredible success in modifying and harnessing cellular processes of living cells to produce bio-pharmaceuticals. These bio-pharmaceuticals, today, are helping in preventing and treating previously incurable diseases such as cancer, HIV and inherited genetic disorders such as sickle-cell anemia and Down syndrome. With such developments, immense demand of such bio-pharmaceuticals is insuppressible. Hence, the main challenge, before the industry, lies in the design and engineering of efficient production facilities in order to meet the rising demand for these drugs at affordable costs.

A bio-pharmaceutical is commercially manufactured in large tanks, referred to as fermenters or bioreactors. The entire production chain can be divided into two main categories namely *upstream processing* and *downstream processing*. All the operations from cell culture to process development at lab scale and so on, until the production of the bio-pharmaceutical in the fermenter are categorized as upstream processing. At the end of upstream processing, the fermentation broth is usually centrifuged to obtain a clear broth. This broth consists of the bio-pharmaceutical but is highly contaminated with several side-products of the manufacturing process such as metabolites added for cell growth, host cell proteins, viruses, DNA, endotoxins and so on. These contaminants must be removed so that the bio-pharmaceutical is delivered in its purest form. All the unit operations employed to tackle this specific separation and formulation task are categorized as downstream processing. Since, the bio-pharmaceuticals are for human usage, strict regulations are imposed by drug agencies to ensure their stability and

Product	*Downstream processing cost* (%)
Crude cellular extract	20-25
Gums and polymers	40-50
Antibiotics	20-60
Industrial enzymes	40-65
Non recombinant product	50-70
rDNA product	60-80
Monoclonal antibodies	50-70
Plasma protein	70-80

TABLE 1.1: Contribution of the downstream processing to the overall manufacturing cost of various products.

safety. These regulations make downstream processing a challenging task and one single unit operation is seldom capable of delivering a bio-pharmaceutical of desired standard. Hence, many expensive unit operations are required before the final delivery. These expensive unit operations make downstream processing a major contributor to the overall manufacturing cost. Table 1.1 shows the contribution of downstream processing to the overall manufacturing costs for various products arranged according to their value in market [1].

For a low value product such as crude cellular extracts, the downstream processing contributes only 20-25% of the overall manufacturing cost. On the other hand, for high value biopharmaceutical products such as monoclonal antibodies and plasma proteins, the contribution can be as high as 85% of the total manufacturing cost. Thus, the market price of a bio-pharmaceutical is directly correlated to the costs incurred in downstream processing. If the expenses in downstream processing can be reduced, bio-pharmaceuticals can be produced at reduced costs and thus, also sold at lower prices.

The downstream processing can be further divided into four distinct steps - Removal, Isolation, Purification and Polishing [1]. Each step comprises of one or more unit operations. A downstream process begins with application of removal and isolation steps. These steps constitute of unit operations that aim at reducing the large process volume of the broth. Filtration, crystallization, precipitation, and centrifugation are commonly applied unit operations in these steps. These are high-throughput processes and are often faster. However, the product after the removal and isolation steps remains only partially purified. In order to obtain a pure product, the purification step is applied.

It constitutes of unit operations that aims to selectively capture the target product. Purification is also commonly referred to as capture. Finally, before the end product is delivered, another set of unit operations is applied in order to ensure that the product standard adheres to regulatory guidelines. This step is called polishing step. In a polishing step, the goal is to selectively capture trace impurities such as DNA, viruses, and endotoxins that remain in the process volume. Chromatography, affinity separation, and electrophoresis are commonly applied unit operations in the purification as well as in the polishing step. Although the purification and polishing steps have high resolution, they are low-throughput processes due to low operational flow rates and therefore often hinder overall productivity. They also have a high capital and operational costs and are the main reasons for higher downstream processing costs. Therefore, there is an increasing need for the development of alternative purification and polishing techniques that could reduce the overall costs while maintaining high purity and productivity.
Membrane chromatography (MC) has emerged as an attractive alternative bioseparation technique that offers virtues of having higher throughput as well as better resolution. With advances in membrane chemistries, many MC capsules are available for commercial usage and are routinely applied in capture as well as polishing step. As MC is becoming increasingly accepted in the biopharmaceutical industry, accurate modeling approaches have become important for rational process analysis and design. In this dissertation, two different modeling approaches have been developed that semi-empirically and mechanistically capture the fundamental mechanisms affecting the performance of MC capsules. These advanced modeling approaches address the shortcomings of traditional modeling approaches that are commonly applied in the scientific community and provide a better strategy for model based process analysis and scale-up in MC. The proposed models provide a universal mathematical approach that can be applied to analyze and predict performance of MC capsules -
- With different membrane properties,
- Using different protein molecules,
- Exhibiting different capsule geometries,
- At different operating conditions,
- And at different scales of operation.

The dissertation is divided into four chapters. This chapter, *chapter 1*, discusses the fundamentals of chromatography, various modes of operation, and different chromatography column types. Membrane chromatography and its advantages are then discussed. The motivation and project goals are finally discussed in detail at the end of this chapter. *Chapter 2* and *chapter 3* discuss the developed semi-empirical zonal rate model

(ZRM) approach and mechanistic computational fluid dynamics (CFD) approach respectively. Each of these chapters consists of two articles published and submitted during the project duration. *Chapter 4* finally discusses the entire model building process from a broader perspective and highlights the main results of the project. In the end, practical applications of the developed models are discussed.

1.2 Background

The term *Chromatography* was first coined by Mikhail Tswett in 1906, when he applied the separation principles to purify plant pigments. In 1952, Martin and Synge received the Nobel Prize in chemistry for their work in partition chromatography that established chromatography as a prime analytical tool which is since then widely applied in different fields of chemistry, biology and medicine [2]. Today, usage of chromatography is not only limited to analytical purposes but has become the *central dogma* in large scale bioseparation and is applied in the capture as well as polishing step.

1.2.1 Different adsorption mechanisms in chromatography

A typical chromatography process involves two distinct physical phases, a mobile phase and a stationary phase. Depending on the application, these phases vary from gas, liquid or solid. In biotechnology, liquid-solid chromatography, or more commonly referred to as liquid chromatography, is used. Here, the mobile phase is liquid and the stationary phase is solid. In principle, the mobile phase flows or percolates through the stationary phase and carries the target components which are to be separated. The stationary phase carries functionalized groups or ligands that selectively interact with the target component. Depending on the objective of separation (capture or polishing), the "target component" may be the protein of interest (capture) or the impurities (polishing). Nonetheless, irrespective of the nature of the target component, the first step in a chromatographic process is selective adsorption of the target component onto the stationary phase. There are five main mechanisms by which the selective adsorption is typically implemented in chromatography columns.

- **Ion exchange chromatography:** Ion exchange chromatography (IEX) is a relatively inexpensive and widely used technique. Electrostatic interaction between charges of the target component and the adsorber surface is the main principle

of separation [3, 4]. The stationary phase is an insoluble solid support containing fixed charge-carrying groups. Counter-ions of opposite charge are loosely attached to these groups. IEX are further classified into anion and cation exchange chromatography. In cation exchange chromatography positively charged groups are attached to a negatively charged solid support. Conversely, in anion exchange chromatography, negatively charged groups are attached to a positively charged solid support.

To achieve separation, the target component in the liquid mobile phase is also ionized with the same charge as the counter-ions. When the mobile phase is passed through the system, the target components displace the loosely attached counter-ions and gets attached to the fixed charge-carrying groups. Thus, the target components get selectively adsorbed.

- **Affinity chromatography:** Affinity chromatography is a highly selective technique as it separates the target components based on their unique biological or chemical interaction with ligands present at the stationary phase surface [5, 6]. For example, Protein A, a protein anchored in the cell wall of *Staphylococcus aureus* has the ability to selectively interact with immunoglobulin G, which makes it a highly specific ligand for capturing monoclonal antibodies [7, 8]. Protein A affinity chromatography is widely applied as initial unit operation in the capture step of large scale purification of monoclonal antibodies, IgG.

- **Hydrophobic interaction chromatography:** Hydrophobic interaction chromatography (HIC) separates the target components based on their polarity [9, 10]. The more polar a component is, the more strongly it is adsorbed to a polar stationary phase, whereas a non-polar protein will adsorb to a non-polar stationary phase.

- **Size exclusion chromatography:** Size exclusion chromatography (SEC) is also known as gel filtration. In the SEC, the target components are separated based on their molecular size [11, 12]. Highly cross linked porous gels such as dextrans and polyacrylamide gels, are used as stationary phases. To achieve separation, the mixture containing target components is passed through a bed of the porous stationary phase. The components with larger molecular sizes are not able to enter the pores and come out earlier while the components with smaller molecular sizes diffuse into the pores and are more strongly retained, thus, leading to late retrieval. The SEC is commonly used for fractionation and buffer exchange.

- **Mixed-mode chromatography:** Mixed-mode chromatography (also known as multimodal chromatography) utilizes ligands that provide multiple modes of interactions, most commonly ion exchange and hydrophobic interaction. This combination can enhance the selectivity of a protein purification process. [13].

1.2.2 Chromatography systems

Several automated chromatography systems are offered on the market that provide integrated workflows for efficient protein purification. A typical system constitutes of pumps, a chromatography column, UV-VIS spectroscopy, pH and conductivity meters, and several buffer lines. The buffer lines provide different buffers and feed mixture to the chromatography system. The pumps control the flow rate and the flow of different buffers through the chromatography column. UV-Visible spectroscopy is used as a detector to measure protein concentration at the outlet while the pH and conductivity meter measures the pH and conductivity of the effluent buffer respectively. Figure 1.1 shows a typical scheme of such chromatography system.

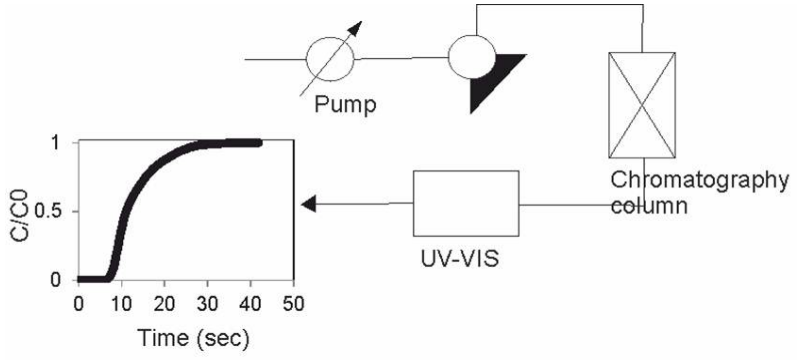

FIGURE 1.1: Flowscheme of a typical chromatography system.

1.2.3 Modes of Operation

There are two main modes of operation in a chromatographic process, namely, *bind-and-elute mode* and *flow-through mode*. In the bind-and-elute mode, operating conditions (pH, ionic strength, temperature, flow rate) are chosen so that the component of interest binds to the stationary phase, while in the flow-through mode, the operating conditions are chosen so that the component of interest does not bind to the stationary phase. Adsorption mechanisms described earlier can be employed in both these modes. The SEC is an exception as it is, essentially, a sieving mechanism and does not involve any binding process.

A chromatography operation constitutes of five main steps:

- Loading step: In the loading step, the feed, containing the protein of interest and impurities, is mixed with a loading buffer and passed through the column. In the bind-and-elute mode, the operating conditions of the loading buffer are selected to facilitate complete binding of the protein of interest to the column. The impurities generally flow through the column. However, there are certain impurities that also bind to the column along with the protein of interest. In the flow-through mode, the operating conditions of the loading buffer are selected so that the protein of interest completely flows through the column. Generally most of the impurities are retained in the column. However, there are certain impurities that also flow through the column.

- Washing step: A wash step involves passing the loading buffer, without the feed, through the column. In the bind-and-elute mode, the objective of the wash step is to remove unbound impurities from the column after the loading step. In the flow-through mode, the objective is to capture the protein of interest remaining in the load line and in the column after the load step. The washing step is continued until the detector signal reaches a predefined baseline.

- Elution step: An elution step involves the removal of the protein of interest from the column and collection in a highly pure and concentrated form. Elution step is not important in the flow-through mode as the protein of interest is not retained in the column and is collected during the loading step, however design of the elution step is crucial in the bind-and-elute mode. The elution buffer is carefully selected so that the protein of interest maintains its biological activity. The operating condition is also carefully chosen in order to maximize product recovery and purity. In practice, ionic strength of the elution buffer is usually changed to recover the protein of interest from the column. This is done by changing the salt concentration in the elution buffer. However, there has been recent trends to change the pH of the elution buffer as well. There are two main ways by which changes in ionic strength or pH is implemented in the elution step. They are *gradient elution* and *step elution*. Gradient elution involves gradually changing the ionic strength or pH of the elution buffer. The gradient elution is useful to fractionate proteins that have different strength of interactions with the stationary phase. Thus, when the salt concentration is gradually increased from low to high, weakly bound proteins elute first at low salt concentration while the strongly bound proteins elute late at high salt concentration.

  A step elution involves changing the operating conditions in steps. A salt step or a pH step can be used. The step elution strategy works best when the salt concentration at which the protein of interest elutes, is already known. Step elution is generally faster to run and the protein is eluted in a smaller volume as compared

to the gradient elution. A combination of the gradient and the step elution is also used to optimize the elution process.

- Regeneration/cleaning step: In this step, any strongly adsorbing impurities are removed from the column so that the column is ready for another cycle of loading. Regeneration buffer with extreme pH value or high salt concentration is normally used. Selecting an appropriate cleaning buffer is important as it also affects the stability of the stationary phase.

- Equilibration step: An equilibration step is also performed before the next loading cycle in order to restore the column to its original condition. The loading buffer is normally used in this step. The equilibration step is performed until the inlet and effluent of the column are equal in terms of critical operational parameters.

1.2.4 A typical chromatogram

The output of the chromatography operation, measured as UV-visible signal at the column outlet, is referred to as a chromatogram. Figure 1.2 shows a representative chromatogram for the bind-and-elute mode of operation. For simplicity, it is assumed that three different species are present in the mixture to be processed, namely non-adsorbing impurities, target component and strongly adsorbing impurities. The goal of the chromatographic separation is to isolate the target component from this mixture. In the first step of loading, operating conditions of the loading buffer are chosen so that the target component is retained in the column while the non-adsorbing impurities flow through (shown in the red line). The strongly adsorbing impurities are also retained in the column at this loading operating condition. In order to avoid product loss, the loading process is stopped when 1% of the target component appears in the chromatogram. The wash step is followed to bring the detector signal for the impurities and the target component to a predefined baseline. This is followed by elution, where a pure fraction of the target component is collected in the elution buffer. The target component appears as a peak as shown in blue the Figure 1.2. In the regeneration step, the regeneration buffer of extreme pH or salt is used to remove strongly adsorbing impurities. The strongly adsorbing impurities eluting in the regeneration step are shown in the green line in the figure.

Ideally, the shape of a chromatogram should appear as a sharp step for each species. As shown by the dotted line in Figure 1.2, the impurities should come out in a step form while loading and the target component should form a sharp rectangular pulse while

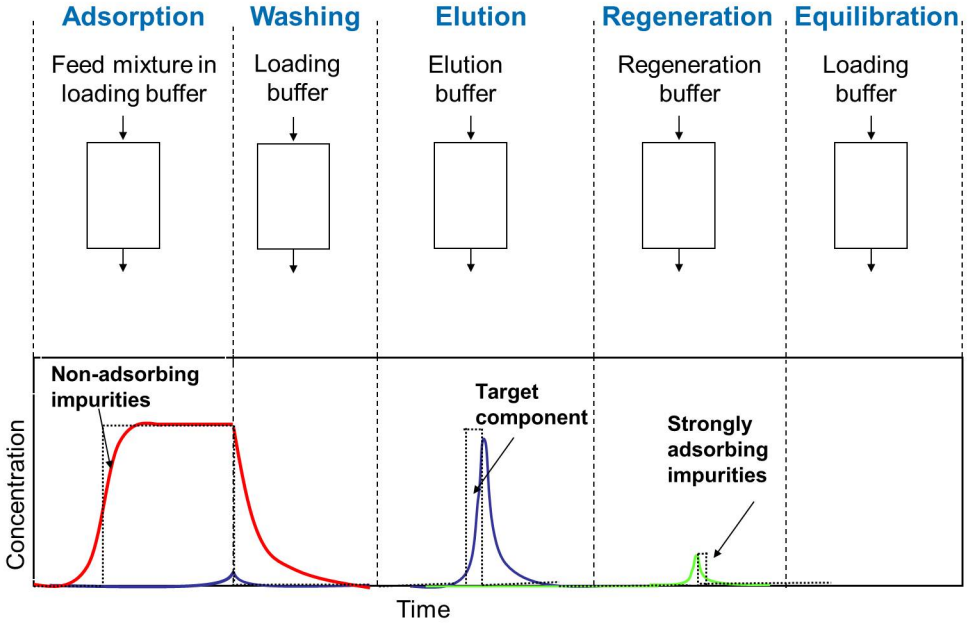

FIGURE 1.2: A chromatogram showing different steps in the chromatography operation.

elution. However, in reality such is not the case. The breakthrough of non-binding impurities in the loading step and the elution profile in the elution step are greatly dispersed and exhibit long tailing. A majority of research activities in the field of liquid chromatography is devoted to fundamentally understand the causes of such non-idealities in the chromatogram. Several factors influence the shape of a chromatogram. These constitute inherent chemical attribute such as non-idealities in adsorption and operational factors such as column design, flow hydrodynamics, pH, temperature, ionic strength. The primary objective of the chromatography column manufacturers and bioseparation scientist is to optimally design the column and the separation process so that the shape of a chromatogram is as close as possible to the ideal case.

1.2.5 Chromatography column types

A chromatography column is the device where actual separation occurs. It is the central element in a chromatography system. Therefore, the selection of an appropriate type of column is a pre-requisite for optimizing a separation task. Packed bed columns are the traditional and most widely used chromatography column type in downstream processing of biomolecules. They exhibit high resolution power and today, with several decades of research devoted to the optimization of packed bed processes, they can be employed to separate any kind of complex mixture. However, due to large bed height and mass

transfer limitations, packed bed columns are often limited in operational flow rates. This poses a bottleneck in current requirements of faster downstream unit operations and has led to the development of several alternatives. Membrane chromatography and monolith chromatography have emerged as the most prominent alternative techniques. Figure 1.3 represents the packed bed, the monolith and the membrane chromatography column.

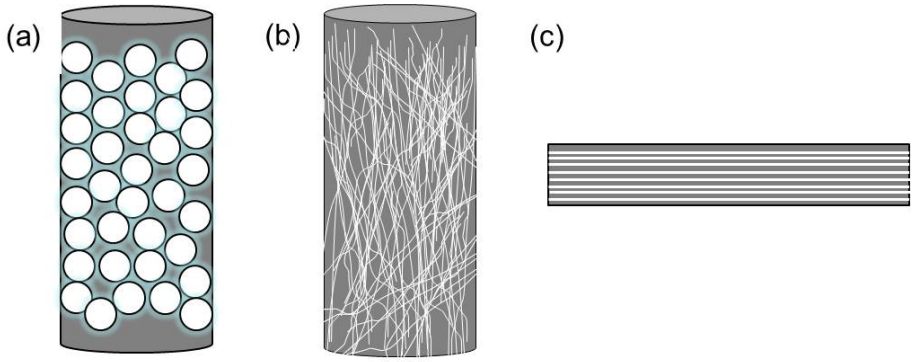

FIGURE 1.3: Different types of chromatography columns: (a) Packed bed, (b) monolith, (c) membrane chromatography column.

A packed bed column is packed with functionalized beads, a monolith column has functionalized porous channels and a membrane chromatography capsule contains stacked sheets of functionalized porous membranes. Due to their highly porous structure, the monolith and the membrane chromatography can be operated at a much higher flow-rates in comparison with the packed bed column. With respect to design, MC capsules havea much smaller bed height and larger cross section in comparison to a packed bed and monolith columns.

Packed bed and monolith columns usually maintain the same design at different scales of operations. A large scale packed bed or monolith column has the same bed height as a corresponding lab scale column but the column diameter is increased in order to process more volume. Thus the flow through the column in a lab or a large scale packed bed or monolith operation is axial. On the other hand, MC capsules can have fundamentally different capsule designs at different scales of operations. A typical lab scale MC capsule has a flat sheet arrangement and flow occurs axially through the capsule while large scale MC capsules are available in spiral wound or pleated structure and flow occurs radially across the capsules. The different MC capsule designs are shown in Figure 1.4. With a spirally wound or pleated membrane around a solid core, large scale MC capsules offer the advantage of processing same volumes as packed bed or monolith columns but have a much smaller footprint. MC capsules are often designed to be disposable and therefore expensive cleaning steps are not required [14, 15]. Today being a faster process and offering lower operational costs, MC, arguably, holds more promise than monoliths in developing as a viable alternative to packed bed columns.

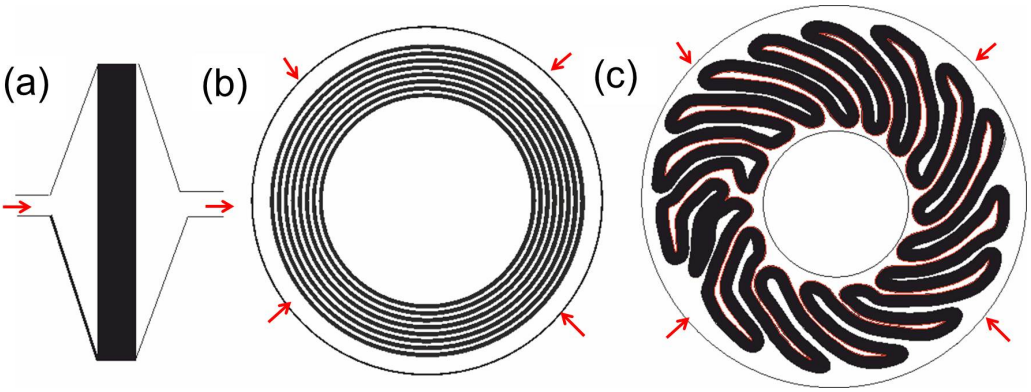

FIGURE 1.4: Different geometries of membrane chromatography capsules. (Figures not drawn to scale; Black stacks shows membrane): (a) Lateral cross section of a flat sheet arrangement (b) axial cross section of a spiral wound arrangement, (c) axial cross section of a pleated arrangement.

1.2.6 Comparison of packed bed chromatography and membrane chromatography

The performance differences between packed bed and membrane chromatography are mainly caused by different flow dynamic properties. As discussed earlier, the chromatography process starts with the loading step. The target protein to be separated gets selectively adsorbed on the functionalized surface, while other impurities flow through the column. The speed of the loading process is governed by different physical and chemical phenomena. Figure 1.5 shows different factors governing mass transfer for packed bed and membrane chromatography. In a packed bed column, the target protein is first transported to the bead surface through convection. This is a fast process. The bead surface is surrounded by a thin film of stagnant liquid. The target protein has to diffuse through this layer in order to reach the pores in the bead. This diffusion process is referred as film diffusion and the speed of transfer is dependent on the thickness of the film. The target protein then diffuses through the pores in the beads to finally reach the functionalized surface where the protein gets adsorbed. The adsorption is usually fast; however the diffusive flow through the pores is often slow as it depends on the pore diameter. The beads, typically, have pore diameters ranging from 0.01 to 0.1 μm making pore diffusion a rate limiting step.

In membrane chromatography, the protein solution is forced convectively through the stacks of membrane sheet. Membranes have greater pore diameters of order 0.8 to 2 μm and thereby binding sites are better accessible, because the mass transfer from the bulk fluid to the binding sites is predominantly through convection. The protein molecules are transferred across a thin film layer and immediately bound to the adsorption sites. There is no mass transfer limitation due to pore diffusion, and film diffusion can be

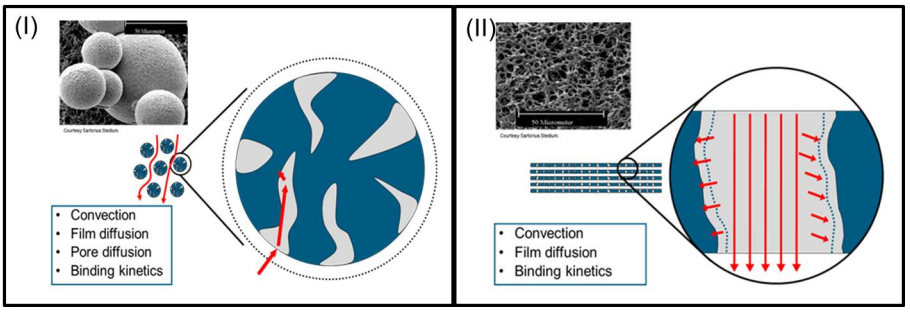

FIGURE 1.5: Different factors governing mass transfer in (a) packed bed chromatography, and (b) membrane chromatography.

neglected in many cases [16, 17]. Therefore, the overall mass transfer process is comparably fast in membrane chromatography. Greater pore sizes offer lower pressure drop and therefore, the system can be operated at a much higher flow-rate in comparison to a packed bed chromatography [18, 19]. Larger pore sizes also allow bigger molecules to reach the binding sites and thus to be separated more easily.

MC can be used in all the different modes of adsorption as described earlier. However, ion exchange membrane chromatography (IEX-MC) has found prominent use in large scale purification platforms. Particularly IEX-MC is routinely used in polishing steps in the downstream processing of monoclonal antibodies. The polishing step is applied at the end of flow scheme in order to remove trace contaminants such as viruses, DNA, host cell protein, and endotoxins before the product is finally formulated. Many of these contaminants are negatively charged at neutral pH while the antibodies are typically positively charged. Thus, anion exchange membrane chromatography is aptly applied for selective removal of these large contaminants. With the recent advances in membrane surface chemistry that allows binding capacities comparable to conventional packed bed chromatography, ion exchange membrane chromatography is now also being reported to be used in the capture step [20]. Here, MC is applied in order to selectively capture high molecular weight species such as DNA vectors, Factor VIII, and viral vectors from large volumes of impure fermentation broth [21–24].

Other adsorption modes based on interaction types such as biospecificity [25–27], hydrophobicity [28], molecular size and shape [29] and metals-complex formations [30] are also possible in membrane chromatography but are not as widely used as ion exchange.

1.3 Scope

1.3.1 Mathematical modeling in Biotechnology

Models are objects or concepts that are used to partly represent reality. A model can be a simple physical object such as a small device crafted in order to calculate actual drag forces on a real plane through wind-tunnel experiments or a complex mathematical formulation that explains disease progression in a population and thus aid in deciding a beneficial large scale health intervention scheme.
In biotechnology, mathematical modeling is an indispensable tool for process optimization. Process engineers are generally interested in optimizing large scale purification process in order to obtain the maximum yield of the product. Since purification processes are influenced by several operational parameters, large numbers of experiments must be performed in order to select the best operating conditions. However, considering the high value of the processed bio-pharmaceutical, performing such large scale experiments is commercially unfeasible. Therefore, scale-down physical experimental models, that can mimic the large scale purification process, are used. Scale-down approaches aim at conserving the essential characteristics of large scale equipment in the smaller model. Performing experiments on smaller models is much cheaper and scientists seek to optimize the process at the laboratory scale and transfer the operating parameters to large scale. Unfortunately accurate conservation of all essential characteristics in a scale-down model is not possible in most cases. Quite often, different behaviors are observed in physical large and lab scale devices. This poses quite a challenge in designing optimal processes but, mathematical modeling can help to understand various physical and chemical processes involved at different scales.

1.3.2 Project goals

This proposed dissertation primarily aims at developing different modeling approaches for understanding the causes of non-ideal outputs of MC capsules. Once the causes of non-idealities are understood and characterized for the lab scale MC capsules, identified model parameters can be transferred across scales to predict the output of large scale MC capsules. Thus, the project has two distinct aspects, model-based process analysis and model-based scale-up.

Model-based process analysis

The performance of MC capsules is measured by the sharpness of their breakthrough curves (BTCs). A BTC is the measured effluent concentration of an MC capsule obtained on loading. The shape of a measured BTC at a given scale is an outcome of the

physical nature of fluid flow and the chemical nature of protein adsorption in the MC capsule. *Therefore, the first objective is to devise appropriate models for independently capturing fluid flow in MC capsules.* Several models of protein adsorption will be then combined with the developed flow models to enable a holistic process analysis of lab scale MC capsules. Such decoupling of fluid flow will allow to rationally select the most appropriate model that accurately describes protein adsorption on a given membrane surface. This allows a holistic model-based process analysis at a given scale of operation.

Model-based scale-up

As discussed earlier, MC capsules have different capsule geometries at different scales. The flow patterns at different scales are also different; axial flow in the studied lab scale MC capsules and radial flow in the studied large scale capsules. Figure 1.6 shows the BTC data obtained from lab scale and large scale MC capsules from Pall Inc. The measurements are performed using 1mg/ml BSA loaded at a flow-rate of 12 MV/min. Since the lab scale capsule is developed as a physical scale down model of the corresponding large scale MC capsule, the BTC obtained should exhibit the same shape. However, such is not the case. Although both capsules exhibit the same breakthrough points, they differ significantly after approx. 60% breakthrough is reached. BTC from the large scale MC capsule exhibits longer tailing and take longer time to reach complete saturation. However, since the protein is loaded to the MC capsules at the same operating conditions, the chemical nature of protein adsorption on a given membrane surface is conserved, irrespective of the scale of operation. Therefore, the hydrodynamics within these capsules must have a defining role in the shape of the measured BTCs. Hence, once the hydrodynamics is coherently captured in the lab and large scale MC capsules using the developed flow models, the parameters of the most appropriate binding model obtained from lab scale analysis can be directly transferred across scales in order to predict BTC data of the large scale MC capsule.

Similar non-identical BTC behavior is also observed at different scales for MC capsules from Sartorius Stedim GmbH (see Figure 1.7). Although, both BTCs are obtained for same operating conditions (2mg/ml at a flow rate of 4MV/min), in this case, they exhibit different breakthrough points. In contrast to MC capsules from Pall Inc., the lab scale MC capsules from Sartorius exhibit greater tailing than the large scale MC capsule from Sartorius. Thus the scale-down physical lab MC models are of limited use in both these cases. *Therefore, the final objective of this dissertation is to provide a universal modeling approach for holistic scale-up that can be applied to MC capsules with different properties, scales and geometries.*

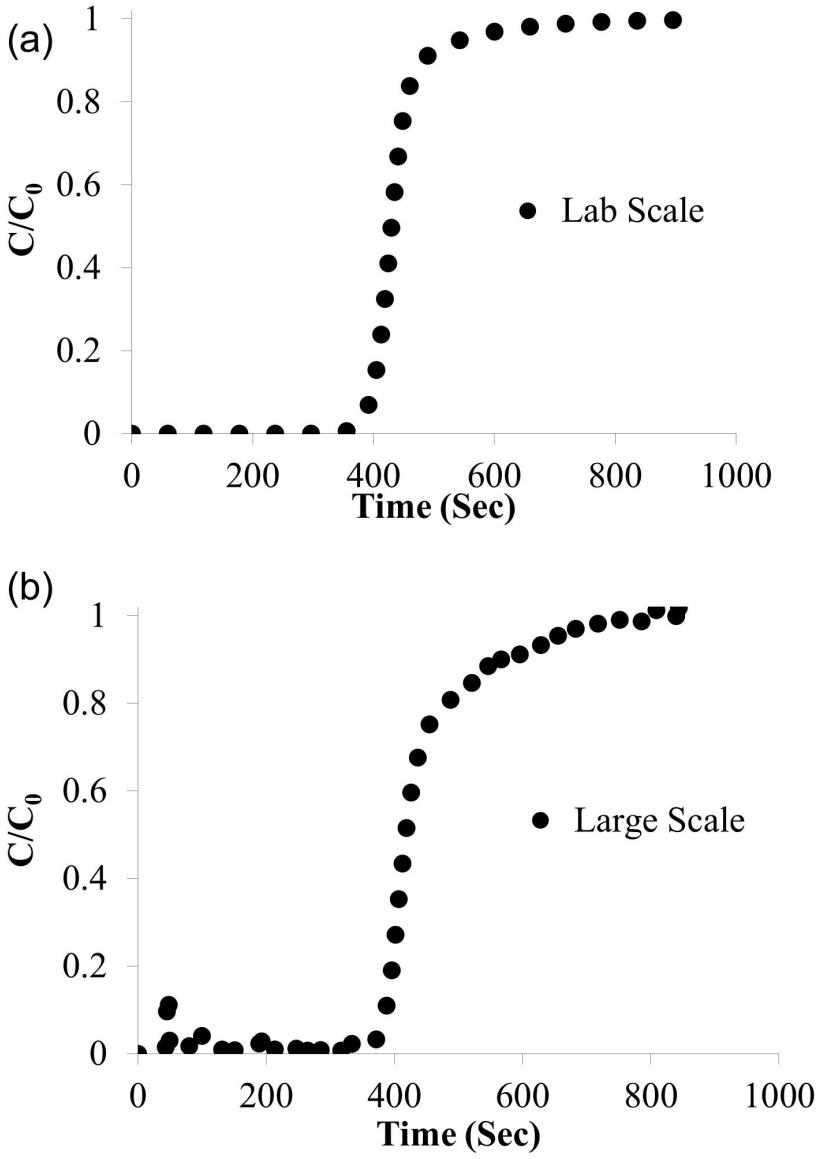

FIGURE 1.6: BTC obtained under binding conditions for 1mg/ml BSA at 12MV/min: (a) lab scale MC capsule from Pall, (b) (a) large scale MC capsule from Pall.

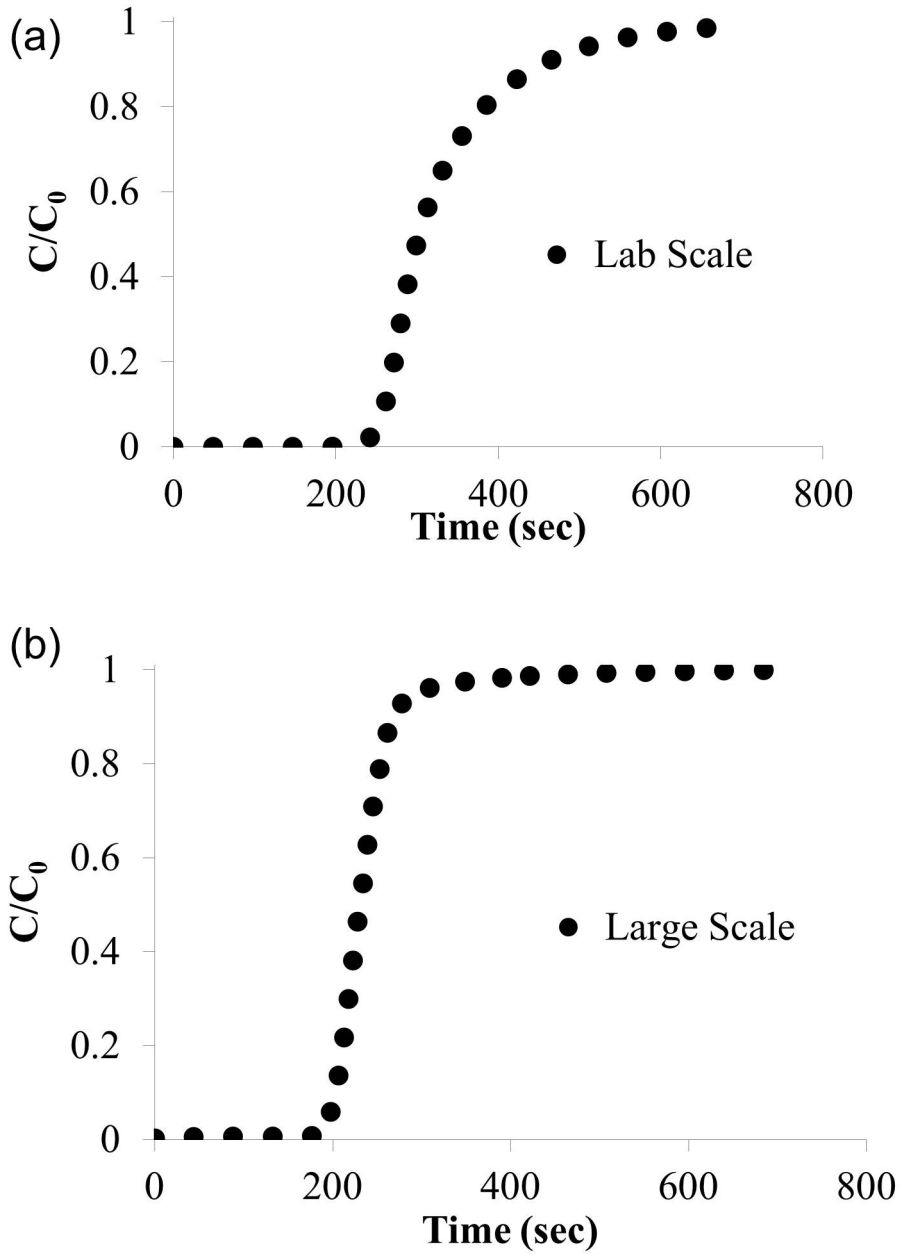

FIGURE 1.7: BTC obtained under binding conditions for 2mg/ml BSA at 4MV/min: (a) lab scale MC capsule from Sartorius Stedim Biotech, (b) large scale MC capsule from Sartorius Stedim Biotech.

REFERENCES

[1] R. Ghosh, *Principles of Bioseparation Engineering*. McMaster University, Canada: World Scientific Publishing Co. Pte.Ltd., 2006.

[2] A. J. P. Martin and R. L. M. Synge, "A new form of chromatogram employing two liquid phases I. A theory of chromatography 2. Application to the micro-determination of the higher monoamino-acids in proteins," *Biochemical Journal*, vol. 35, pp. 1358–1368, 1941.

[3] B. Noller and N. Currey, "The evaluation of ammonium ion determination in waters by cation exchange ion chromatography over wide concentration ranges," *Water Research*, vol. 24, pp. 471–476, Apr. 1990.

[4] G. Corthier, E. Boschetti, and J. Charley-Poulain, "Improved method for IgG purification from various animal species by ion exchange chromatography," *Journal of Immunological Methods*, vol. 66, pp. 75–79, Jan. 1984.

[5] W. H. Scouten, "Affinity chromatography for protein isolation," *Current Opinion in Biotechnology*, vol. 2, pp. 37–43, Feb. 1991.

[6] A. Liapis, "Theoretical aspects of affinity chromatography," *Journal of Biotechnology*, vol. 11, pp. 143–160, Aug. 1989.

[7] H. Aono, D. Wen, L. Zang, D. Houde, R. B. Pepinsky, and D. R. H. Evans, "Efficient on-column conversion of IgG1 trisulfide linkages to native disulfides in tandem with Protein A affinity chromatography.," *Journal of chromatography. A*, vol. 1217, pp. 5225–32, Aug. 2010.

[8] P. Füglistaller, "Comparison of immunoglobulin binding capacities and ligand leakage using eight different protein A affinity chromatography matrices," *Journal of Immunological Methods*, vol. 124, pp. 171–177, Nov. 1989.

[9] B. H. Hofstee and N. F. Otillio, "Non-ionic adsorption chromatography of proteins.," *Journal of chromatography*, vol. 159, pp. 57–69, Feb. 1978.

[10] H. P. Jennissen and L. M. Heilmeyer, "General aspects of hydrophobic chromatography. Adsorption and elution characteristics of some skeletal muscle enzymes.," *Biochemistry*, vol. 14, pp. 754–60, Feb. 1975.

[11] K. Unger, B. Anspach, and H. Giesche, "Optimum support properties for protein separations by high-performance size exclusion chromatography," *Journal of Pharmaceutical and Biomedical Analysis*, vol. 2, pp. 139–151, Jan. 1984.

[12] S. Lesieur, C. Grabielle-Madelmont, M. Paternostre, and M. Ollivon, "Study of size distribution and stability of liposomes by high performance gel exclusion chromatography," *Chemistry and Physics of Lipids*, vol. 64, pp. 57–82, Sept. 1993.

[13] S. Burton and D. Harding, "Hydrophobic charge induction chromatography: salt independent protein adsorption and facile elution with aqueous buffers," *Journal of Chromatography A*, vol. 814, pp. 71–81, July 1998.

[14] J. X. Zhou and T. Tressel, "Basic concepts in Q membrane chromatography for large-scale antibody production.," *Biotechnology progress*, vol. 22, no. 2, pp. 341–9, 2006.

[15] J. X. Zhou, T. Tressel, U. Gottschalk, F. Solamo, A. Pastor, S. Dermawan, T. Hong, O. Reif, J. Mora, F. Hutchison, and M. Murphy, "New Q membrane scale-down model for process-scale antibody purification.," *Journal of chromatography. A*, vol. 1134, pp. 66–73, Nov. 2006.

[16] P. Francis, E. von Lieres, and C. Haynes, "Zonal rate model for stacked membrane chromatography part II: Characterizing ion-exchange membrane chromatography under protein retention conditions," *Biotechnology Bioengineering*, vol. 109, no. 31, pp. 615–629, 2012.

[17] P. Francis, E. von Lieres, and C. A. Haynes, "Zonal rate model for stacked membrane chromatography. I: characterizing solute dispersion under flow-through conditions," *J Chromatography A*, vol. 1218, no. 31, pp. 5071–5078, 2011.

[18] R. Ghosh, "Protein separation using membrane chromatography: opportunities and challenges," *Journal of Chromatography A*, vol. 952, no. 1-2, pp. 13–27, 2002.

[19] C. Charcosset, "Membrane processes in biotechnology: an overview," *Biotechnoogyl Advances*, vol. 24, no. 5, pp. 482–492, 2006.

[20] J. H. Vogel, H. Nguyen, R. Giovannini, J. Ignowski, S. Garger, A. Salgotra, and J. Tom, "A new large-scale manufacturing platform for complex biopharmaceuticals.," *Biotechnology and bioengineering*, vol. 109, pp. 3049–58, Dec. 2012.

[21] Y. M. Li, J. L. Liao, K. Nakazato, J. Mohammad, L. Terenius, and S. Hjerten, "Continuous Beds for Microchromatography - Cation-Exchange Chromatography," *Analytical Biochemistry*, vol. 223, no. 1, pp. 153–158, 1994.

[22] J. Luksa, V. Menart, S. Milicic, B. Kus, V. Gabercporekar, and D. Josic, "Purification of Human Tumor-Necrosis-Factor by Membrane Chromatography," *Journal of Chromatography A*, vol. 661, no. 1-2, pp. 161–168, 1994.

[23] O. W. Reif and R. Freitag, "Characterization and Application of Strong Ion-Exchange Membrane Adsorbers as Stationary Phases in High-Performance Liquid-Chromatography of Proteins," *Journal of Chromatography A*, vol. 654, no. 1, pp. 29–41, 1993.

[24] D. A. Wells, G. L. Lensmeyer, and D. A. Wiebe, "Particle-Loaded Membranes as an Alternative to Traditional Packed-Column Sorbents for Drug Extraction - in-Depth Comparative-Study," *Journal of Chromatographic Science*, vol. 33, no. 7, pp. 386–392, 1995.

[25] S. M. A. Bueno, K. Haupt, and M. A. Vijayalakshmi, "In-Vitro Removal of Human-Igg by Pseudobiospecific Affinity Membrane Filtration on a Large-Scale - a Preliminary-Report," *International Journal of Artificial Organs*, vol. 18, no. 7, pp. 392–398, 1995.

[26] D. M. Zhou, H. F. Zou, J. Y. Ni, L. Yang, L. Y. Jia, Q. Zhang, and Y. K. Zhang, "Membrane supports as the stationary phase in high performance immunoaffinity chromatography," *Analytical Chemistry*, vol. 71, no. 1, pp. 115–118, 1999.

[27] D. M. Zhou, H. F. Zou, J. Y. Ni, H. L. Wang, L. Yang, and Y. K. Zhang, "Membrane affinity chromatography for analysis and purification of biopolymers," *Chromatographia*, vol. 50, no. 1-2, pp. 27–34, 1999.

[28] R. Ghosh, "Fractionation of human plasma proteins by hydrophobic interaction membrane chromatography," *Journal of membrane Science*, vol. 260, no. 1-2, pp. 112–118, 2005.

[29] R. T. Kurnik, A. W. Yu, G. S. Blank, A. R. Burton, D. Smith, A. M. Athalye, and R. Vanreis, "Buffer Exchange-Using Size-Exclusion Chromatography, Countercurrent Dialysis, and Tangential Flow Filtration - Models, Development, and Industrial Application," *Biotechnology and Bioengineering*, vol. 45, no. 2, pp. 149–157, 1995.

[30] D. Josic, J. Reusch, K. Loster, O. Baum, and W. Reutter, "High-Performance Membrane Chromatography of Serum and Plasma-Membrane Proteins," *Journal of Chromatography*, vol. 590, no. 1, pp. 59–76, 1992.

Chapter 2

Zonal rate model (ZRM)

2.1 Publication I

"Zonal Rate Model for Axial and Radial Membrane Chromatography. Part I: Knowledge Transfer Across Operating Conditions and Scales."

(Biotechnology and Bioengineering, 110 (2013) 1129-1141)

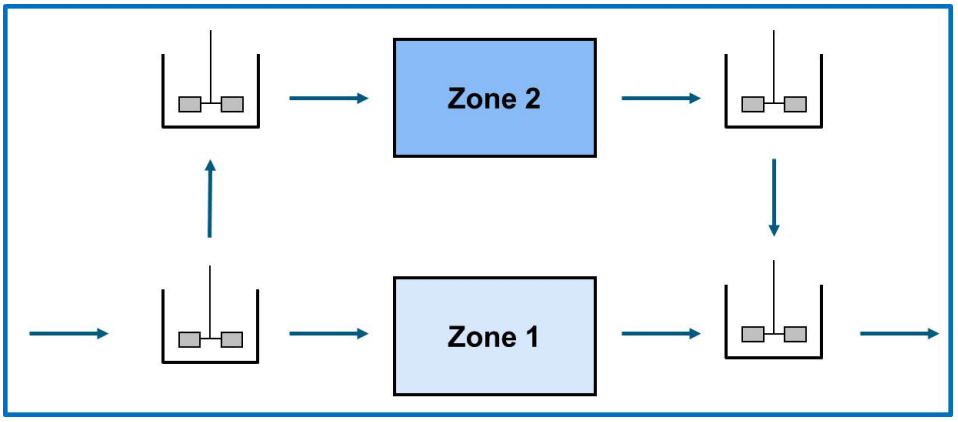

Pranay Ghosh, Kaveh Vahedipour, Min Lin, Jens H. Vogel, Charles Haynes, Eric von Lieres

ARTICLE

BIOTECHNOLOGY and BIOENGINEERING

Zonal Rate Model for Axial and Radial Flow Membrane Chromatography. Part I: Knowledge Transfer Across Operating Conditions and Scales

Pranay Ghosh,[1] Kaveh Vahedipour,[2] Min Lin,[3] Jens H. Vogel,[3] Charles A. Haynes,[4] Eric von Lieres[1]

[1]IBG1: Biotechnology, Forschungszentrum Jülich, Wilhelm-Johnen-Strasse 1, 52425 Jülich, Germany; telephone: +49-2461-61-2168; fax: 49-2461-61-3870; e-mail: e.von.lieres@fz-juelich.de

[2]INM-4: Medical Imaging Physics, Forschungszentrum, Jülich, Germany

[3]Isolation and Purification Department, Global Biologics Development, Bayer Healthcare, Berkeley, California

[4]Michael Smith Laboratories, University of British Columbia, Vancouver, British Columbia, Canada

ABSTRACT: The zonal rate model (ZRM) has previously been applied for analyzing the performance of axial flow membrane chromatography capsules by independently determining the impacts of flow and binding related non-idealities on measured breakthrough curves. In the present study, the ZRM is extended to radial flow configurations, which are commonly used at larger scales. The axial flow XT5 capsule and the radial flow XT140 capsule from Pall are rigorously analyzed under binding and non-binding conditions with bovine serum albumin (BSA) as test molecule. The binding data of this molecule is much better reproduced by the spreading model, which hypothesizes different binding orientations, than by the well-known Langmuir model. Moreover, a revised cleaning protocol with NaCl instead of NaOH and minimizing the storage time has been identified as most critical for quantitatively reproducing the measured breakthrough curves. The internal geometry of both capsules is visualized by magnetic resonance imaging (MRI). The flow in the external hold-up volumes of the XT140 capsule was found to be more homogeneous as in the previously studied XT5 capsule. An attempt for model-based scale-up was apparently impeded by irregular pleat structures in the used XT140 capsule, which might lead to local variations in the linear velocity through the membrane stack. However, the presented approach is universal and can be applied to different capsules. The ZRM is shown to potentially help saving valuable material and time, as the experiments required for model calibration are much cheaper than the predicted large-scale experiment at binding conditions.

Biotechnol. Bioeng. 2013;110: 1129–1141.

KEYWORDS: membrane chromatography; modeling; process analysis

Introduction

Packed bed chromatography is one of the most widely employed purification steps in biopharmaceutical industry. High resolution makes it an indispensable unit operation in the recovery of therapeutic proteins and recombinant drugs where purity is of utmost importance. In the recent past, an ever-growing market demand of drugs has led to the production of large batch volumes, which has put an enormous pressure on downstream processing for including higher throughput operations than conventional packed bed chromatography for rapid product isolation (Levine, 2002; Przybycien and Pujar, 2004). Membrane chromatography is a very attractive alternative due to many beneficial features (Endres et al., 2003; Ghosh, 2001; Klein, 2000; Przybycien and Pujar, 2004; Saxena et al., 2009; Teeters et al., 2003; Vogel et al., 2012), such as the potential of working at higher flow rates while maintaining binding capacities at comparable levels to packed bed chromatography. Membrane chromatography occupies smaller footprints because of the smaller size of membrane chromatography capsules as compared to packed bed chromatography columns with similar volume processing capacities (Zhou and Tressel, 2006). Membrane chromatography capsules are often disposable, which can offer additional advantages over packed bed chromatography, as cleaning steps are not required.

Jens H. Vogel's present address is Boehringer Ingelheim, Fremont, CA.
Correspondence to: E. von Lieres
Contract grant sponsor: Cluster Industrial Biotechnology (CLIB)
Received 7 September 2012; Revision received 8 October 2012;
Accepted 15 October 2012
Accepted manuscript online 23 October 2012;
Article first published online 23 November 2012 in Wiley Online Library (http://onlinelibrary.wiley.com/doi/10.1002/bit.24771/abstract)
DOI 10.1002/bit.24771

The performance differences between resin based and membrane chromatography are mainly caused by different mass transfer regimes (Klein, 2000; Sarfert and Etzel, 1997; Suen and Etzel, 1994). In packed bed chromatography a column is filled with porous beads whose inner surfaces are functionalized with specific adsorption sites. During the loading step, a feed stream that contains target molecules, for example proteins, and various impurities is passed through this column. The target molecules (and the strongly binding impurities) are bound to the adsorption sites. The solute molecules are transferred from the bulk fluid to the binding sites by the successive mechanisms of convection, external mass transfer through a stagnant boundary layer around the beads, pore diffusion within the bead pores, and finally by adsorption. In packed bed chromatography, the pore diffusion step is often rate limiting and can prevent rapid mass transfer to the binding sites.

Membranes have much larger pores and the binding sites are better accessible, because the mass transfer from the bulk fluid to the binding sites is predominantly through convection. The protein molecules are transferred across a thin film layer and immediately bound to the adsorption sites. There is no mass transfer limitation due to pore diffusion, and film diffusion can be neglected in many cases (Dimartino et al., 2011; Francis et al., 2011; Frey et al., 1992; Gerstner et al., 1992; Shiosaki et al., 1994). Due to smaller bed height, membrane chromatography has lower pressure drops and can consequently be operated at higher flow rates. These advantages have been successfully utilized for the industrial removal of trace impurities such as plasmid DNA, host cell proteins, and for virus clearance in polishing steps (Knudsen et al., 2001; Tennikov et al., 1998; Zhou et al., 2006). Membranes are particularly useful for the separation of large protein molecules ($M_w > 250$ kDa) where better access to the binding sites is essential (Endres et al., 2003). The potential of working at high flow rates also allows to process larger volumes and, hence, membrane chromatography can be employed for volume reduction before expensive unit operations, such as Protein A affinity steps.

Membrane chromatography capsules are available in different configurations on the market (Zhou et al., 2006). The flat sheet arrangement with axial flow, in which the membranes are stacked in multiple layers in a small capsule, is usually available for lab scale applications and meant to provide a convenient scale-down approach for designing specific separation problems. In typical capsules for large-scale purification with radial flow, the membranes are either spirally wound or pleated around a core. As membrane chromatography has diverse applications and is increasingly accepted in biopharmaceutical industry, accurate models for different configurations become important for rational process analysis and design.

In the present contribution the previously published ZRM is extended from axial to radial flow configurations and applied for describing breakthrough data of both configurations under binding and non-binding conditions. A simultaneous analysis and evaluation strategy across scales and conditions is presented, and the potential of the proposed modeling approach for model-assisted scale-up is evaluated.

Theory

Chromatography with stacked membranes has been modeled for many years (Boi, 2007; Boi et al., 2007; Roper and Lightfoot, 1995; Wang et al., 2008). In most studies the membranes are described in one spatial dimension along the axial coordinate, and external hold-up volumes are accounted for by a plug flow region (PFR) and one or two continuously stirred tank regions (CSTR) in series with the membrane (Fig. 1). Such models assume homogeneity over membrane cross-sections, which is practically hard to achieve in membrane capsules due to large length-to-width ratios. In fact, the external hold-up volumes of membrane chromatography capsules are typically in the same order of magnitude as the membrane volume, and therefore these volumes contribute significantly to solute dispersion apart from the membrane stacks. Thus, a linear sequence of interconnected PFR and CSTR is insufficient for describing the effect of these hold-up volumes (Montesinos-Cisneros et al., 2007; Sarfert and Etzel, 1997; Vicente et al., 2008).

In axial flow configurations several membrane sheets are stacked in capsules whose diameter is several orders of magnitude larger than the bed length. At such extreme length-to-diameter ratios the path lengths traversed by solute molecules that are passing through the outer radial region are much longer than the path lengths traversed by solute molecules that are passing through the central region (Ghosh and Wong, 2006) (Fig. 2). A similar situation is found in radial flow configurations where the feed stream is split into different fractions before reaching the membrane that is either spirally wound or pleated around a cylindrical core.

ZRM (Francis et al., 2011, 2012) has been developed for quantitatively analyzing the impact of radially inhomogeneous flow distributions on measured chromatograms under non-binding and binding conditions for axial flow configurations. The concept of the ZRM is to virtually partition the hold-up volumes before and behind the membrane as well as the membrane stack itself into different zones. Each zone is considered homogenous but of different size and subjected to different boundary conditions depending on its relative position in the given arrangement.

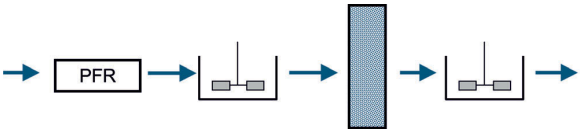

Figure 1. Traditional modeling of external hold-up volumes by a linear PFR and CSTR sequence Roper and Lightfoot model (Roper and Lightfoot, 1995).

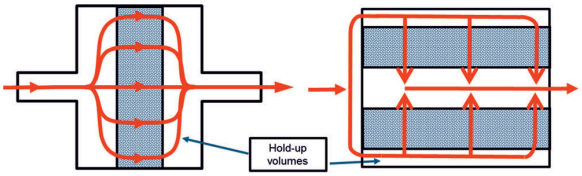

Figure 2. Different flow paths in axial and radial flow configurations.

The interconnected virtual zones for the hold-up volumes are modeled as a network of CSTRs. The virtual zones of the membrane stack are described by several instances of a conventional membrane chromatography model. The inflows of these identical instances are connected to different CSTRs in the network and, hence, subject to different boundary conditions. A PFR is connected in series with the CSTR and membrane model network in order to account for possible time lags that are not associated with system dispersion. The ZRM is a semi-empirical approach for independently quantifying the impacts of binding kinetics and internal flow distributions in membrane chromatography units without knowing the internal capsule geometry.

In this work the ZRM is further extended to radial flow configurations. The radial flow configuration has a different flow pattern as the axial flow configuration and therefore requires a different set-up and interconnection of virtual zones. In the following sections the differences in setting up the ZRM for axial and radial flow configurations are highlighted.

Zonal Rate Model for Axial Flow Configuration

A detailed description of the ZRM for different axial flow configurations has been published earlier (Francis et al., 2011, 2012; von Lieres et al., 2009). Figure 3a illustrates the modeling approach for a configuration with three virtual zones for the hold-up volumes before and behind the membrane stack as well as for the membrane stack itself. Solute molecules that cross the outermost zone of the membrane stack are sequentially passed through tanks 1a, 2a, and 3a; the respective membrane zone, and tanks 3b, 2b, and 1b. Solute molecules that cross the central zone of the membrane stack are only passed through tank 1a, the respective membrane zone, and tank 1b. Average residence times of solute molecules that pass the capsule along different paths are calculated as the sum of residence times of the passed tanks and of a PFR in series with the CSTR network plus the residence time in the respective membrane zone.

Zonal Rate Model for Radial Flow Configuration

Different capsules with radial flow configuration are available on the market. The ZRM has been developed

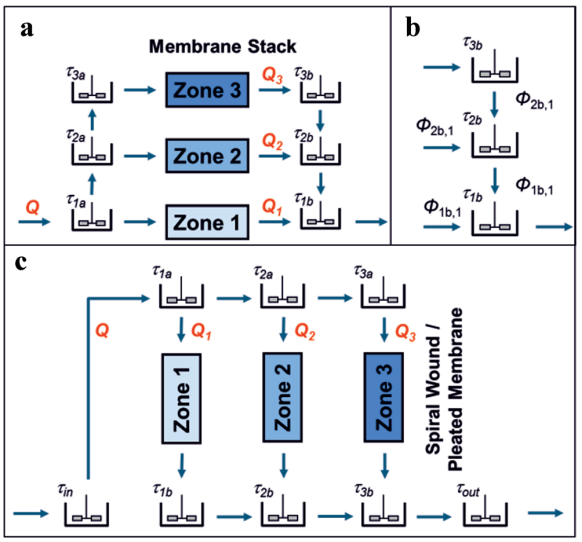

Figure 3. **a**: Virtual partitioning of hold-up volumes and of the membrane for an axial flow configuration with three membrane zones, (**b**) flow fractions for tanks downstream of the membrane, and (**c**) virtual partitioning of hold-up volumes and of the membrane for a radial flow configuration with three membrane zones.

as a flexible tool for individually studying the effects of inhomogeneous flow and of solute molecule binding in different design types of membrane chromatography capsules. The radial flow configuration of the ZRM is derived for capsules in which the solute molecules pass through the membrane from the periphery to the center of the capsule (Fig. 2), but a similar configuration can be derived for the opposite flow direction. As illustrated in Figure 3c, the feed flow is redirected and distributed over an outer peripheral channel, then perpendicularly crosses the membrane and is collected in a central cylindrical channel before exiting the capsule. Extra tanks are incorporated at the inlet and outlet of the capsule in order to account for the hold-up volumes of the distributor and collector regions. The Roper and Lightfoot model (Fig. 1) is also a special case of the radial flow configuration with only one membrane zone. However, this model must be set-up with non-identical CSTR regions upstream and downstream of the membrane in order to account for the inherent asymmetry of radial flow capsules.

The solute molecules can be sequentially passed through the inlet zone and zone 1a, the inlet zone, zone 1a and zone 2a, or through the inlet zone, zones 1a, 2a, and zone 3a before reaching the outer side of the membrane. The fractions of the overall volumetric flow that pass through the individual membrane zones are given by Q_1, Q_2, and Q_3. In contrast to the axial flow configuration, all solute molecules pass though the same number of tanks, independent of their individual flow paths, but the residence times of the central tanks are significantly smaller than those of the

corresponding tanks in the periphery. Hence, the average residence time, which is the sum of the residence times of the passed tanks plus of the crossed membrane zone, does depend on the flow path. The individual PFR and CSTR equations are set-up identical as for the axial flow configuration, but differently interconnected with each other and with the model instances for the membrane zones.

Transport Equations

Each virtual zone of the membrane stack is described by an instance of the same mass-balance equation (Eq. 1).

$$\frac{\partial c}{\partial t} + \nu \frac{\partial c}{\partial z} = D_a \frac{\partial^2 c}{\partial z^2} + \frac{(1-\varepsilon)}{\varepsilon} \frac{\partial q}{\partial t} \tag{1}$$

In Equation (1), c and q are the solute concentrations in the mobile and stationary phases, respectively, ν is the flow velocity, D_a is the dispersion coefficient, and $\partial q/\partial t$ denotes the rate of adsorption or desorption of solute molecules to or from the membrane surface. The stationary phase concentration is accounted for per unit volume of solid membrane, and the dispersion coefficient has been shown earlier to contribute negligibly to the total system dispersion (Francis et al., 2011, 2012). The binding of solute molecules will be discussed in Binding Kinetics Section. A PFR is added in series with the CSTR network for modeling the time-lag in the breakthrough curve that is caused in the system dead volume and not associated with system (Eq. 2).

$$c_{\text{out}}^{\text{PFR}}(t) = \begin{cases} 0 & t < t_{\text{lag}} \\ c_o & t \geq t_{\text{lag}} \end{cases} \tag{2}$$

In Equation (2), t_{log} is the ratio of the PFR volume to the volumetric feed flow rate, V_{PFR}/Q. Several CSTR models are connected for describing solute dispersion in the hold-up volumes upstream and downstream of the membrane stack. Equation (3) is used for tanks with one feed stream, where $c_{\text{in}}^{\text{CSTR}}$ and c^{CSTR} are the solute concentrations at the tank inlet and outlet, respectively, $\tau = V/Q$ is the average residence time of solute molecules, V is the tank volume, and Q is the volumetric flow rate.

$$\frac{\partial c^{\text{CSTR}}}{\partial t} = \frac{c_{\text{in}}^{\text{CSTR}} - c^{\text{CSTR}}}{\tau} \tag{3}$$

Tanks with two or more feed stream, that are required downstream of the membrane, are described by Equation (4), where j is the number of tank inlets.

$$\frac{\partial c^{\text{CSTR}}}{\partial t} = \sum_{j=1}^{m} \frac{c_{\text{in},j}^{\text{CSTR}}}{\tau_j} - c^{\text{CSTR}} \sum_{j=1}^{m} \frac{1}{\tau_j} \tag{4}$$

The ZRM also includes a set of flow fractions, Φ_k, which define the fraction of the total volumetric flow, Q that passes through each of the membrane zones. Figure 3b illustrates this for an example with three membrane zones. Let Φ_1, Φ_2, and Φ_3 denote the fractions of the total volumetric flow that pass through the membrane zones. Due to mass conservation, the sum of these flow fractions must equal one ($\Phi_1 + \Phi_2 + \Phi_3 = 1$). Moreover, let $\Phi_{1b,1}$ and $\Phi_{1b,2}$ denote the flow fractions of the two inlets of the first tank, and $\Phi_{2b,1}$ and $\Phi_{2b,2}$ the same for the second tank. The sum of these flow fractions of individual tanks also equals one ($\Phi_{1b,1} + \Phi_{1b,2} = 1$ and $\Phi_{2b,1} + \Phi_{2b,2} = 1$). In the given scenario, Equation (4) is set up for each of these tanks with residence time $1/\tau_{1b,1} + 1/\tau_{1b,2} = 1/\tau_{1b}$ and $1/\tau_{2b,1} + 1/\tau_{2b,2} = 1/\tau_{2b}$. The corresponding flow fractions are $\Phi_{1b,i} = \tau_{1b}/\tau_{1b,i}$ and $\Phi_{2b,i} = \tau_{2b}/\tau_{2b,i}$ for $1 \leq i \leq 2$. The flow fractions through the membrane zones are then determined by $\Phi_1 = \Phi_{1b,1}$, $\Phi_2 = \Phi_{1b,2}\Phi_{2b,1}$, and $\Phi_3 = \Phi_{1b,2}\Phi_{2b,2}$. Similar relations can be analogously derived for more complex networks.

Binding Kinetics

Several models have been published for describing the binding of solute molecules to functionalized surfaces. Protein adsorption is a complex process, and the variety of involved physical mechanisms can hardly be included in binding isotherms that are used for practical applications. The rather simple Langmuir kinetic (Eq. 5) is often applied for modeling protein adsorption and desorption to and from ion-exchange membranes (Gebauer et al., 1997; Suen and Etzel, 1994).

$$\frac{\partial q}{\partial t} = k_a c(q_m - q) - k_d q \tag{5}$$

In Equation (5), k_a and k_d are the adsorption and desorption rate constants and q_m is the maximum binding capacity. The Langmuir model assumes single-component interaction with one type of binding sites of solute molecules that do not interact with each other.

Several more complex modeling approaches have been developed for describing adsorption and desorption of proteins and other biomolecules. For instance, large molecules can cause steric hindrance and pore blocking can entirely prevent the adsorption of further molecules. The adsorbate molecules can also interact with each other and form dimers and other aggregates, and the aggregate species interact differently with the adsorption sites. Furthermore, adsorbent materials can provide more than one binding mechanism. It can also be assumed that since adsorption is an energetically driven process, the adsorbate molecules can undergo conformation or orientation changes in order to minimize the free energy during adsorption. The latter is described by the spreading model (Clark et al., 2007), which is used in the present study for overcoming the limitations of the Langmuir model.

Etzel and coworkers have successfully applied the spreading model for describing the asymmetric breakthrough behavior of protein loading on membrane surfaces (Yang and Etzel, 2003). A recent study of the Hubbuch group provides evidence for the existence of different binding orientations of lysozyme on ion-exchange beads (Florian Dismer, 2007). In a comparative study of different binding models in membrane chromatography (Francis et al., 2011), the spreading model has been found to be most suitable for quantitatively describing the adsorption of ovalbumin on a modified polyethersulfone (PES) membrane with cationic groups. The shape of BSA, which is used in the present study, has been reported as a cigar shaped ellipsoid (7 nm × 4 nm× 4 nm) (Kim, 2002). Hence BSA can physically absorb to the membrane surface in two different orientations, at the end or sideways. The most general form of the spreading model for two orientations of the molecules is given by Equations (6)–(8). The protein molecules can be bound and released in both orientations but with different rate constants and also change their orientation in the bound state (Fig. 4). The total amount of bound protein is given by the sum of both orientations. In contrast to the bi-Langmuir model, both orientations compete for the same binding sites.

$$\frac{\partial q}{\partial t} = \frac{\partial q_1}{\partial t} + \frac{\partial q_2}{\partial t} \tag{6}$$

$$\frac{\partial q_1}{\partial t} = (k_{a,1}c - k_{12}q_1)(q_m - q_1 - \beta q_2) - k_{d,1}q_1 + k_{21}q_2 \tag{7}$$

$$\frac{\partial q_2}{\partial t} = (k_{a,2}c + k_{12}q_1)(q_m - q_1 - \beta q_2) - (k_{21} - k_{d,2})q_2 \tag{8}$$

In Equations (6)–(8), q_1 and q_2 represent the concentrations of bound protein in orientation 1 and 2, respectively, β is the ratio of the sorbent surface area occupied by a bound protein in state 2 relative to that in state 1, the binding rate constants $k_{a,1}$, $k_{d,1}$, $k_{a,2}$, and $k_{d,2}$ are defined in analogy to the Langmuir model, and the constants k_{12} and k_{21} describe the rates of the orientation change.

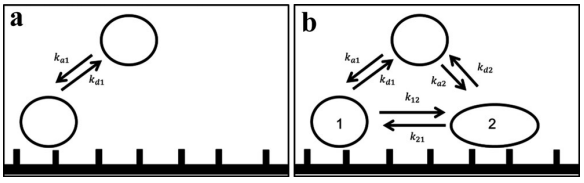

Figure 4. Adsorption schemes in the (**a**) Langmuir and (**b**) spreading models.

Materials and Methods

Bovine serum albumin (BSA) (A 7638, Sigma–Aldrich Corp., St. Louis, MO) was used in breakthrough experiments at a concentration of 1 g/L and flow rates of 12 CV/min for both the axial and radial flow membrane chromatography capsules. The protein was dissolved in 25 mM Tris buffer at pH 8.0 (Sigma–Aldrich) for the loading step. Loading was followed by a washing step with 25 mM Tris buffer at pH 8.0. Then, 1 M NaCl in 25 mM Tris buffer pH 8.0 was used to elute the bound BSA from the membranes. The units were cleaned with 1 N NaOH as specified by the manufacturer after each run. In a revised protocol the cleaning step was performed with 1 M NaCl instead of 1 N NaOH.

Mustang Q XT5 anion-exchange membrane chromatography capsules (axial flow) and Mustang Q XT140 anion-exchange membrane chromatography capsules (radial flow) were purchased from Pall, Inc. (East Hills, NY). Both capsules contain modified hydrophilic polyethersulfone (PES) membranes whose surfaces are coated with an irreversibly cross-linked polymer that contains pendant Q groups. In the XT5 capsules 15 layers of flat membrane sheets are stacked with a bed height of 2.20 mm and a frontal area of 22.06 cm^2. In the XT140 capsules membrane pleats are arranged in a radial flow configuration with a pleat length of 7.6 cm and a pleat width of 2.8 cm. The effective bed height of the membrane stacks in the XT140 capsule is also 2.20 mm. The pore size and porosity ε of the membrane are 0.8 μm and 0.70 ± 0.05, respectively (manufacturer data).

The total membrane volume in the XT5 capsule is 5 mL, and the hold-up volumes upstream and downstream of the membrane stack are 3.21 mL each. The XT5 capsule was attached to a ÄKTAexplorer system that was controlled by the Unicorn software (GE Healthcare, Uppsala, Sweden). The total membrane volume in the XT140 capsule is 140 mL, and the hold-up volumes upstream and downstream of the pleated membrane are 105 and 45 mL, respectively. The XT140 capsule was attached to a ÄKTAprocess system that was controlled by the Unicorn software (GE Healthcare). An experimental 9.4 T magnetic resonance tomography device (MRT) was used for visualizing the internal geometry of both capsules.

The model equations for the virtual membrane zones, continuously stirred tank and PFR were coupled together, resulting in a large set of differential equations. The space derivatives in the membrane model instances were first discretized with a finite difference method. The MATLAB solver *ode15s* was then used for integrating the forward problem for given parameter values over time. A highly efficient computational algorithm has been implemented that solves typical set-ups of the ZRM in 2–3 s on a standard

desktop computer with 2 GHz. The inverse problem, that is estimating unknown model parameters from breakthrough data, is iteratively solved using the MATLAB optimizer *lsqnonlin*. A multi-start strategy is employed for avoiding local optima in the parameter space.

Results and Discussion

The Pall XT5 and XT140 capsules were studied by analyzing breakthrough curves that have been measured under binding and non-binding conditions. A flow rate of 12 CV/min was chosen for studying the capsules under industrially relevant conditions. The effects of different flow rates in the axial flow configuration have been described in a previous publication (Francis et al., 2011).

Axial Flow Configuration at Non-Binding Conditions

Breakthrough experiments performed under non-binding conditions provide insights into solute dispersion within the studied membrane chromatography capsules. Non-binding conditions are obtained by adding 1 M NaCl to the protein solution. The analysis of non-binding data is crucial for quantifying the effect of system non-idealities that are caused by inhomogeneous flow separately from non-ideal binding mechanisms.

Breakthrough experiments under non-binding conditions provide information on the sum of the hold-up volumes in the Äkta system and in the studied chromatography capsule. The chromatography system was primed with load material up to the column switch valve in order to effectively remove the impact of the hold-up volumes before that point, as the corresponding system components, that is pumps, mixer and tubing, are already filled with protein solution when the valve is switched from bypass to the capsule. Consequently, the dispersion in the measured breakthrough curve (Fig. 5a) is caused only by the chromatography capsule and by the hold-up volumes behind that capsule that is the tubing and the detection chamber. However, the hold-up volumes behind the capsule sum up to only 18 μL and, hence, their contribution to system dispersion can be neglected.

After an initial lag of 6 s the signal rapidly increases to half of the inlet concentration in 4 s but then gradually flattens out and takes approximately 20 more seconds for reaching the full inlet concentration. The observed tailing is far from the ideal system response but rather typical for membrane chromatography units with extreme length-to-with ratios, even though the dispersion of solute molecules on their short path through the membrane stack itself can often be neglected. Francis et al.(2011, 2012) have studied the same capsule and shown that the dispersion coefficient in the model for the membrane stack can be replaced by the molecular diffusion coefficient when the hold-up volumes are properly described. The same approach is followed in the present study. The membrane stack in the analyzed XT5 capsule has a volume of 5 mL while the hold-up volumes on the either side of the stack are 3.21 m. The membrane stack has a porosity of 0.7 (Pall XT5, which implies that the capsule contains only 1.5 mL of solid membrane. Hence, the total hold-up volume of the capsule actually exceeds the membrane volume.

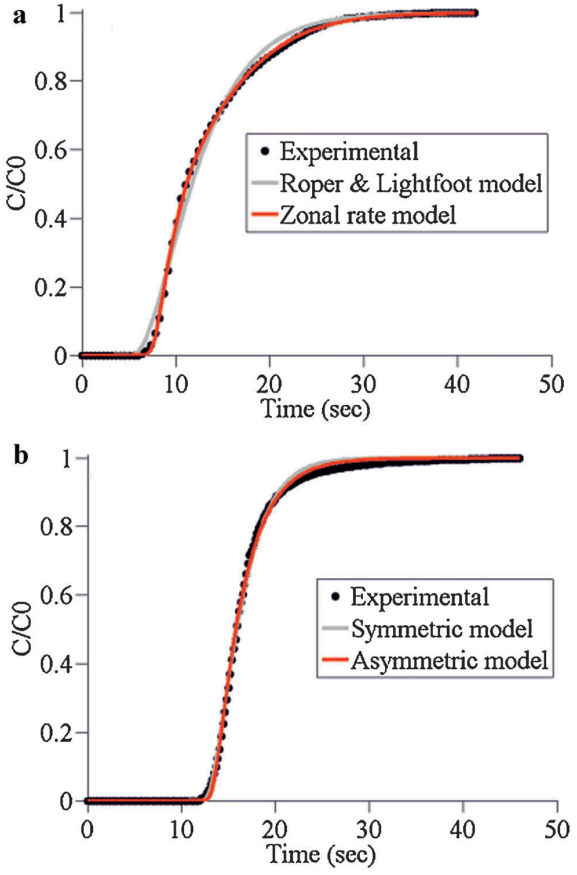

Figure 5. Measured breakthrough curve of the axial flow XT5 capsule under non-binding conditions. **a**: Best fit of the symmetric Roper and Lightfoot model and of the symmetric zonal rate model (ZRM) with two membrane zones for XT5 capsule, (**b**): best fit of the symmetric and asymmetric ZRM with one membrane zone (Roper and Lightfoot model) for XT140 capsule.

As a reference, the Roper and Lightfoot model with a linear sequence of PFR and two CSTRs, one before and one after the membrane stack, is fitted to the measured breakthrough curve (see Fig. 5a). The residence times for the tanks on either side of the membrane stack are chosen identical in order to account for the respective symmetry of the studied XT5 capsule. Hence, two parameters of the Roper and Light foot model are estimated from measurement data, namely the residence times of the PFR and of the CSTRs (see Table I). The Roper and Lightfoot model can

Table I. Hold-up volumes and volumetric flow fractions as determined by fitting the zonal rate model (ZRM) with one membrane zone (Roper and Lightfoot model) and with two membrane zones to a non-binding breakthrough curve of the axial flow XT5 capsule ($V_{PFR} = Qt_{PFR}$, $V_{inner} = Q\tau_1$, $V_{outer} = Q\Phi_2\tau_2$).

Parameter	One membrane zone (mL)	Two membrane zones (mL)
V_{PFR}	2.22	3.91
V_{inner}	3.64	1.24
V_{outer}	—	1.69
Φ_2	—	0.43

only coarsely approximate the measured breakthrough curve. The simulated curve not only shows a delay of the initial breakthrough but also a reduced tailing as compared to the measurement data.

The ZRM was set-up with differently many membrane zones, also assuming symmetry of the tanks before and behind the membrane stack. Each of these configurations was fitted to the data in order to determine the minimal number of membrane zones that is required for quantitatively reproducing the measured breakthrough curve. In full agreement with previous results for the same capsule (Francis et al., 2011), a set-up with two membrane zones was found to be optimal. This set-up has four parameters, namely the PFR volume, the different volumes of two CSTRs for describing the hold-up zones before the membrane stack (the hold-up zones behind the stack are symmetrically modeled), and the volumetric flow fraction between the two membrane zones. The values of these parameters (see Table I) are completely determined by the internal geometry of the studied capsule. Although the inner tank has a smaller volume, 57% of the volumetric flow passes through the central region. The determined total hold-up volume of the capsule of 2.91 mL is reasonably close to the manufacturer specification of 3.21 mL. The ZRM is a semi-empirical approach that is based on the physical geometry, but a good reproduction of the experimental data is preferred over a perfect match of the physical volumes. A restriction of the total hold-up volume in the ZRM would remove one degree of freedom from the parameter estimation. However, the entire breakthrough curve would be shifted to the right, and this effect could not be compensated for by taking more zones, as the total hold-up volume is proportional to the area over the breakthrough curve. Computational fluid dynamics allows for a more stringent description of the internal capsule geometry, however, this would require much higher modeling and computing efforts and goes beyond the scope of the present study.

Radial Flow Configuration at Non-Binding Conditions

Non-binding breakthrough data of the radial flow XT140 capsule were also analyzed with different set-ups of the ZRM. Similar to the XT5 capsule, the impact of the system hold-up volumes is reduced by priming the chromatography system with load material up to the column-switching valve. The remaining hold-up volumes in the tubing before and behind the XT140 capsule and in the detection chamber add up to 100 mL and cannot be completely neglected. However, the analysis in the following paragraph indicates that these external hold-up volumes mainly contribute to the PFR volume and not to the CSTR volumes in the ZRM. The resulting shift of the breakthrough curve does not affect the observed performance of the XT140 capsule.

Although the internal geometry of the XT140 capsule is more complex than of the XT5 capsule, a ZRM set-up with just one membrane zone was found to be sufficient for quantitatively reproducing breakthrough curves at the studied flow rate. However, an asymmetric model with unequal volumes before and behind the membrane is required (see Fig. 5b). A second membrane zone increases the number of regression parameters, but does not significantly improve the fit (data not shown). Hence, the asymmetric model with one membrane zone is used in the following sections. The sufficiency of one membrane zone indicates that the flow is distributed more homogeneously in the XT140 capsule than in the XT5 capsule. The substantially different tank volumes upstream and downstream of the membrane stack (see Table II) reflect the fact that, in contrast to the XT5 capsule, the peripheral distribution region with 105 mL and central collection region with 45 mL in the XT140 capsule are actually not symmetric. The fitted CSTR volumes in the ZRM are smaller, which indicates that a fraction of the rather complex shaped hold-up volumes within the XT140 capsule can be modeled as a PFR. The external hold-up volumes in the tubing and in the detector chamber are much more streamlined and will, consequently, predominantly contribute to the PFR volume in the ZRM, which does not contribute to system dispersion.

Axial Flow Configuration at Binding Conditions

In the previous two sections the impacts of flow non-idealities within the studied membrane chromatography capsules on experimentally measured breakthrough curves were individually analyzed under non-binding conditions. The internal geometry of the studied capsules was characterized by parameter values that represent residence times in virtual zones and flow fractions between these

Table II. Hold-up volumes as determined by fitting the symmetric and the asymmetric ZRM with one membrane zone (Roper and Lightfoot model) to a non-binding breakthrough curve of the radial flow XT140 capsule ($V_{PFR} = Qt_{PFR}$, $V_{upstream} = Q\tau_1$, $V_{downstream} = Q\tau_2$).

Parameter	Symmetric model (mL)	Asymmetric model
V_{PFR}	259	269.93
$V_{upstream}$	55.16	82.88
$V_{downstream}$	Same as $V_{upstream}$	19.32

zones. These parameters are now fixed in order to independently analyze the impact of protein binding on the observed breakthrough curves with the Langmuir and spreading models.

In the first binding experiments, the capsule was cleaned using 1 N NaOH after each run as specified by manufacturer. The cleaning step was followed by a regeneration step with 1 M NaCl. However, this protocol resulted in a very poor reproducibility (see Fig. 6a). Huge variations are observed for subsequent runs that were performed with the same capsule and under the same conditions. The exact reasons for the observed variations between measured breakthrough curves under the same conditions cannot be cogently explained, which poses a challenge in developing a coherent model. A possible explanation could be based on the fact that individual sheets of the membrane stack can slightly move within the XT5 capsule, and that swelling and de-swelling during treatment with NaOH might cause changes in the membrane position and shape. An MRI image of the membrane capsule after repeated cleaning with 1 N NaOH (see Fig. 7a) shows an uneven membrane surface with several wedges that could potentially cause preferential flow. The MRI investigation of membrane chromatography capsules will be continued in a separate study.

This study was continued with a fresh capsule and with a revised cleaning protocol in which 20 CV of 1 M NaCl were passed through the capsule after each completed cycle of load, wash and elution. Moreover, the time between two experiments was minimized by performing all runs immediately one after another. The revised protocol resulted in a much improved reproducibility of the breakthrough curve shapes (see Fig. 6b).

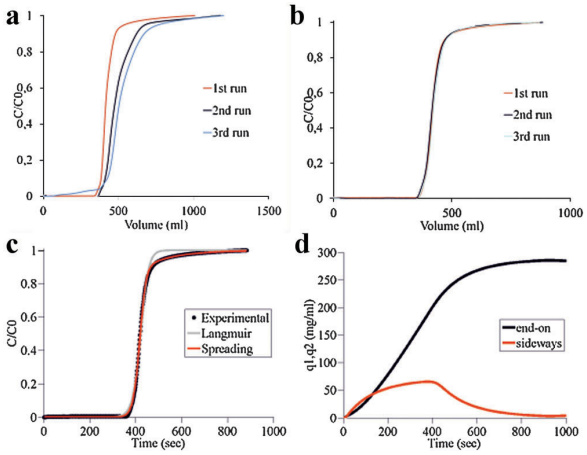

Figure 6. Measured breakthrough curve of the axial flow XT5 capsule under binding conditions. **a**: Using 1 N NaOH for cleaning after each run, (**b**): using 1 M NaCl for cleaning after each run, (**c**): best fit of the ZRM combined with the Langmuir binding model and the spreading model, and (**d**): simulated concentrations of bound molecules in the end-on orientation (q1: red line) and in the sideways orientation (q2: black line) during the loading process over time.

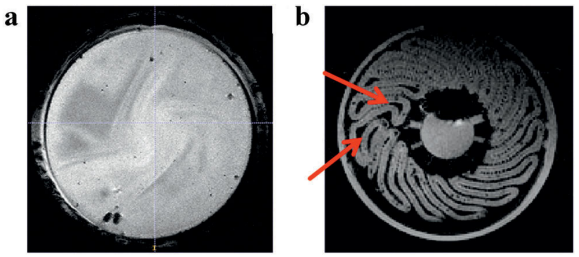

Figure 7. **a**: Cross-sectional MRI scan through the center of the membrane stack of an axial flow XT5 capsule that has been cleaned using 1 N NaOH, (**b**): Cross-sectional MRI scan of the XT140 capsule. The membrane pleats are clearly visible in gray, due to their water content.

Rapid execution of the experiments was observed to be crucial, as the breakthrough curves were shifted to the right after the membrane was stored in the cleaning buffer (1 N NaOH) for several hours (data not shown). Similar shifts of the breakthrough curves are observed for the radial flow XT140 capsule that contains the same type of membrane (Radial Flow Configuration at Binding Conditions Section). These shifts, which are also observed in industrial applications of the same capsules, indicate that the overall binding capacity increases with storage time in the cleaning buffer. The cause is unclear, but the capacity would increase if the polyethylene sulfone (PES) backbone of the membrane had an inherent binding capacity for BSA and if the storage in NaCl would expose more of this backbone to the protein. Alternatively, more of the Q ligands could be exposed after storage in the cleaning buffer.

The measured breakthrough curves in Figure 6b are asymmetric and show a sharp increase from the initial breakthrough point to ca. 90 percent of the inlet concentration, which is followed by a very slow rise towards 100% of the inlet concentration. Without further analysis, the experimental data does not reveal the origin of the observed tailing. The tailing could be exclusively caused by non-ideal flow in the hold-up volumes, but the binding process can also influence the breakthrough curve in a non-ideal way. Hence, a model-based data analysis is proposed for separately quantifying the impact of flow non-idealities and binding non-idealities. The ZRM was combined with the Langmuir model and the spreading model for analyzing the binding data.

The complexity of the spreading model was reduced by assuming that BSA cannot directly adsorb or desorb from or to the sideways orientation. The resulting model reproduces the measurements equally well (data not shown) with a lower number of regressed parameters and is hence preferred in order to avoid over-parameterization and over-fitting.

Table III. Parameters of the Langmuir model for the axial flow configuration as determined by fitting the ZRM to a binding breakthrough curve of the axial flow XT5 capsule.

Parameter	Value
k_a (L/(g s))	6.4×10^{-2}
k_d (L/s)	6×10^{-3}
q_m (g/L)	284.04

Figure 6c shows the best fit of the ZRM with the Langmuir model, and the estimated parameters are summarized in Table III. The Langmuir model can reproduce the initial breakthrough but not the tailing. The spreading model reproduces the entire breakthrough curve much better than the Langmuir model (see Fig. 6c), even with neglected adsorption and desorption of the second bound state. The spreading model involves six parameters, k_{a1}, k_{d1}, k_{12}, k_{21}, $q_{m,}$ and β, that are also estimated from binding breakthrough data (see Table IV).

The spreading factor β is larger than one and, hence, the molecules that are bound in the first orientation require less space as in the second orientation. This indicates that the first orientation is with one end towards the surface, whereas the second bound state is in a sideways orientation. However, the fact that the spreading model fits the experimental data very well cannot be taken as final proof for the underlying hypothesis of different binding orientations, and conformational changes of the bound molecule might also be involved.

The initial adsorption rate of solute molecules to the unsaturated membrane in the end-on orientation is $1/(k_{a1} \times q_m) = 0.042$ s and the reorientation rate to the sideways orientation is $1/(k_{12} \times q_m) = 4.69$ s. Both rates are quite fast, but the desorption rate is $1/k_{d1} = 157$ min, which indicates almost irreversible binding under the observed conditions with an overall loading time of 15 min. However, the reorientation rate from the sideways to the end-on orientation is $1/k_{21} = 106$ s and, consequently, both directions of the reorientation process are relevant during the loading process. Figure 6d shows the simulated amounts of bound molecules in both orientations over time. The BSA molecules are first bound in end-on orientation but rapidly transferred to the sideways orientation, which requires more space. Hence the surface is quickly saturated within 20 s.

Table IV. Parameters of the spreading model for the axial flow configuration as determined by fitting the ZRM to a binding breakthrough curve of the axial flow XT5 capsule.

Parameter	Value
k_{a1} (L/(g s))	8.08×10^{-2}
k_{d1} (L/s)	1.06×10^{-5}
k_{12} L/(g s))	7.37×10^{-4}
k_{21} (L/s)	9.41×10^{-3}
q_m (g/L)	289.003
β	1.144

Then bound molecules in sideways orientation are more slowly transferred back to the end-on orientation, making room for further binding in end-on state. More than 15 min are required for reaching the complete equilibrium between both bound states. These two phases can also be seen in the measured breakthrough curves. The first phase corresponds with the initial sharp increase and the second phase with the long tail of the experimental curve. The maximum in the sideways orientation curve occurs at the inflection point in the breakthrough curve at 420 s where approximately 90% of the inlet concentration is reached (compare with Fig. 6b).

Radial Flow Configuration at Binding Conditions

With the manufacturer protocol for cleaning, the slopes of the measured breakthrough curves of the radial flow XT140 capsule were found to be better reproducible as compared to the XT5 capsule (see Fig. 8a). This might be due to the fact that in the XT140 capsule the membrane is not stacked but tightly arranged in fixed pleats, which effectively prevent position and shape changes. However, the breakthrough curves are also shifted to the right with increasing cycle numbers. Hence, the XT140 experiments were also performed with a fresh capsule and the revised cleaning protocol using 1 M NaCl instead of 1 N NaOH. The resulting breakthrough curves are not shifted but have similar shapes as compared to the original cleaning protocol (see Fig. 8b). The breakthrough curve in Figure 8b shows a sharply increasing section after the initial breakthrough point at 380 s in which 70% of the inlet concentration is reached within 420 s. The curve then gradually flattens out and reaches the full inlet concentration after approximately 850 more seconds.

In Radial Flow Configuration at Non-Binding Conditions Section, the flow non-idealities in the XT140 capsule were described by an asymmetric ZRM with one membrane zone, and in Radial Flow Configuration at Binding Conditions Section, the kinetic parameters of the spreading model were determined independently from the flow configuration. Hence, the flow related parameters of the XT140 capsule (Table II) could be combined with the binding related parameters (Table IV) that have been determined for the same membrane type in the XT5 capsule. With this information, the ZRM can be applied for predicting breakthrough curves of the XT140 capsule under binding conditions. The result of this model-based prediction is compared to the corresponding measurement data in Figure 9. The simulated breakthrough curve closely matches the breakthrough point and the initial slope of the measured data. The model also correctly predicts the flattening of the breakthrough curve after 420 s, however, the predicted tail starts at 90% of the inlet concentration whereas the measured tail starts at 70% of the inlet concentration.

The ZRM quantitatively accounts for non-ideal flow in the void volumes of the XT140 capsule, and the binding parameters are determined independently from the flow

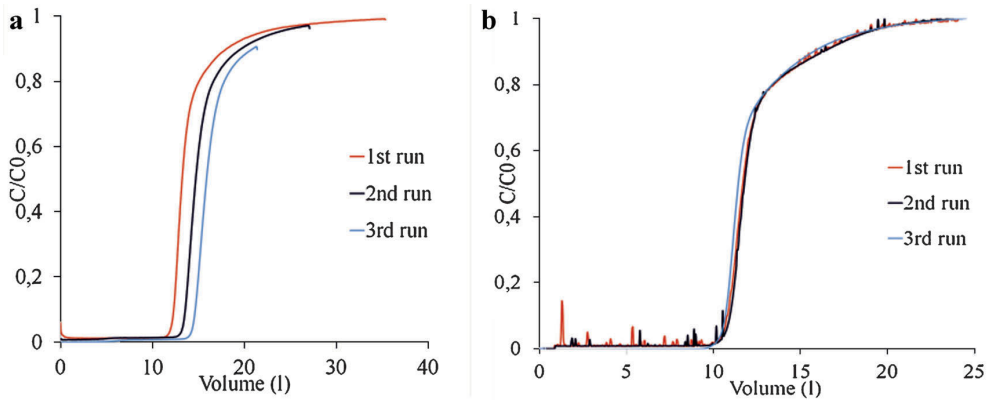

Figure 8. Measured breakthrough curve of the axial flow XT140 capsule under binding conditions. **a**: Using 1 N NaOH and (**b**): using 1 M NaCl for cleaning after each run.

regime. Hence, the observed deviations must be caused by capsule specific issues that are negligible under non-binding conditions. An MRI scan reveals that the membrane pleats are not perfectly arranged in the used XT140 capsule. The red arrows in Figure 7b indicate irregular pleats with varying membrane areas. These variations can cause local deviations in the linear velocity that are not accounted by the ZRM, as configured according to Figure 3c. Hence, the data is re-analyzed with a novel configuration of the ZRM in which the axial membrane zone is splitted into several angular sectors with different linear velocities (see Fig. 10a).

The configurations in Figures 3c and Figure 10a can be combined for a ZRM with more than one membrane zone and several sectors with different linear velocities. However, one axial membrane zone has been shown already to accurately describe the XT140 capsule under non-binding conditions (Radial Flow Configuration at Non-Binding Conditions Section), and a second axial membrane zone does not improve the model-based prediction of the XT140 binding data in Figure 9 (data not shown). Varying linear velocities in different sectors of the membrane zone are negligible under non-binding conditions, because the membrane stack is very thin and, consequently, the residence time of the solute molecules in the membrane stack is much shorter as in the hold-up volumes. Nonetheless, varying linear velocities do significantly impact on the loading of the membrane sectors, as the solute molecules are supplied at different rates. The ZRM has two additional parameters for each angular section, the volumetric flow through this section and the linear velocity within this section. However, the overall model has one degree of freedom less when the total volumetric flow rate is given, for example in a three sector model, the relation $Q_1 + Q_2 + Q_3 = Q$ allows to compute Q_3 from Q_1 and Q_2.

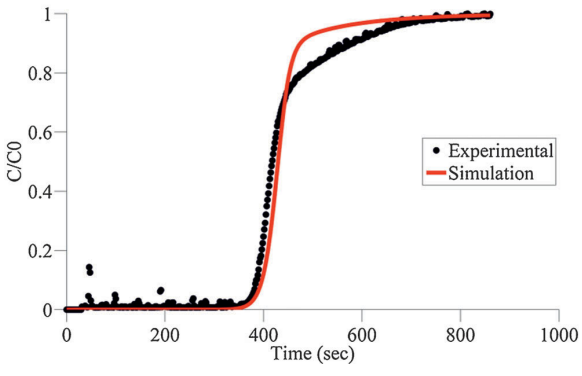

Figure 9. Predicted and measured breakthrough curve of the axial flow XT140 capsule under binding conditions. The asymmetric ZRM with one membrane zone was solved with the flow related parameters from Table III and the binding related parameters from Table V.

The measured breakthrough data is first re-analyzed with ZRM configurations with one axial membrane zone and two to four angular sectors (see Fig. 11a–c). Table V shows the fitted volumetric flow through the angular sectors relative to the overall volumetric flow and the linear velocities in these sectors relative to the average linear velocity. Figure 11a–c illustrates that the revised configuration of the ZRM can quantitatively reproduce the measured breakthrough curve. The simulated breakthrough curve increasingly adapts to the measurement data with increasing numbers of sectors. The visible steps in Figure 11a,b are due to the fact, that the ZRM with two and three sectors only coarsely approximates the true velocity distribution. The fitted parameters in Table V reveal that more than 85% of the overall volumetric flow has only a slightly increased linear velocity, whereas the remaining fraction of the volumetric flow has significantly decreased linear velocities. This coincides with the observation that most of the pleats in the used XT140 capsule are quite regular (see Fig. 7b).

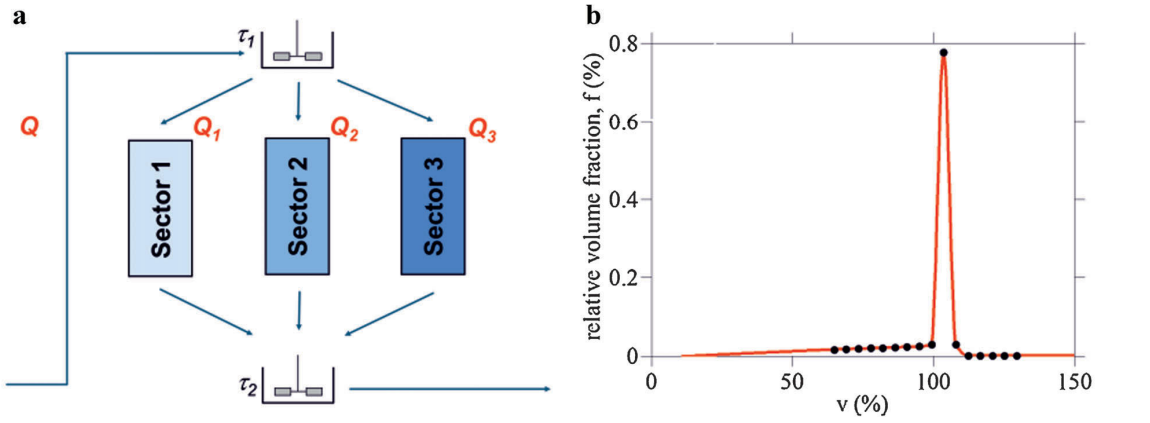

Figure 10. **a**: Virtual partitioning of hold-up volumes and of the membrane for a radial flow configuration in which one axial membrane zone is splitted into three angular sectors with different linear velocities, (**b**): distribution of the volumetric flow relative to the total volumetric flow, *f*, over the linear velocity relative to the average linear velocity, *v*, in the respective sector.

The ZRM with four sectors describes the measurement data very well but comprises too many parameters that need to be estimated from experimental data. The following approach is applied for reducing the number of parameters and at the same time to account for the fact, that the true velocity distribution is a continuous function: The ZRM is configured with 16 sectors, and a series of equidistantly spaced linear velocities is assigned to these sectors. The distribution of the total volumetric flow through these sections is approximated by a function that depends on only three parameters (see Fig. 10b). The first two parameters describe the position and the width of the main peak, which is modeled by a Gaussian distribution. The third parameter describes the slope of a linear increase starting at the origin. On the left hand side of the peak, the maximum of these curves is taken. The area under the curve is normalized such as to maintain the total volumetric flow rate. The parameters for the sectors are simultaneously estimated by fitting the ZRM to the measured breakthrough curve.

Figure 11d shows an excellent fit with only three additional parameters. The volumetric flow rate and the linear velocity in the sectors are expressed in relation to their total or average values, respectively. The peak in Figure 10b is slightly shifted to the right, because the average is decreased by the existence of smaller velocities. As before, approximately 85% of the total volumetric flow has almost the same linear velocity, whereas the remaining 15% have significantly different linear velocities.

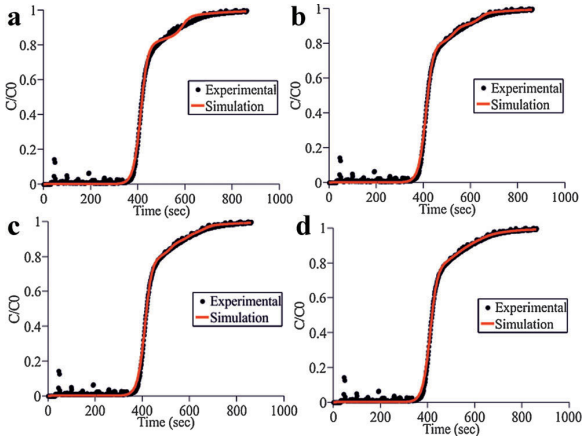

Figure 11. Measured breakthrough curve of the axial flow XT140 capsule under binding conditions. Best fit of the ZRM with one axial membrane zone and (**a**) two, (**b**) three, (**c**) four, and (**d**) sixteen angular sectors.

Conclusions

The ZRM has previously been applied for analyzing the performance of axial flow membrane chromatography capsules by independently determining the impacts of flow and binding related non-idealities on measured breakthrough curves. In the present study, the ZRM was extended to radial flow configurations and applied for a rigorous analysis of the axial flow XT5 capsule and the radial flow XT140 capsule from Pall. For both capsules, the residence times of the CSTR network were first determined from non-binding data. A symmetric configuration with two membrane zones and four model parameters was required for quantitatively reproducing breakthrough curves of the XT5 capsule, whereas an asymmetric

Table V. Volumetric flow relative to the total volumetric flow and linear velocity relative to the average linear velocity for the asymmetric ZRM with one axial membrane zone and one to four angular membrane sectors as determined by fitting the ZRM to a binding breakthrough curve of the radial flow XT140 capsule.

	ZRM with 1 sectors		ZRM with 2 sectors		ZRM with 3 sectors		ZRM with 4 sectors	
Sectors	Volumetric velocity (%)	Linear velocity (%)	Volumetric velocity (%)	Linear velocity (%)	Volumetric velocity (%)	Linear velocity (%)	Volumetric velocity (%)	Linear velocity (%)
1	100	100%	88	103	87	103	86	104
2	—	—	12	72	8	83	6.6	82
3	—	—	—	—	5	70	3.5	72
4	—	—	—	—	—	—	3.9	64

configuration with one membrane zone and three parameters was sufficient for the XT140 capsule. This indicated that the flow is distributed more homogeneously in the XT140 capsule than in the XT5 capsule. Hence, the transfer of binding parameters from one capsule to the other must be accompanied by quantitative modeling of the different flow geometries. Binding data of the XT5 capsule was used for identifying a suitable binding model and determining the corresponding model parameters. The spreading model with six parameters was found to be both physically meaningful and able to reproduce the measurement data much better than the Langmuir model with three parameters. The spreading model is based on the hypothesis of different binding orientations, which might still oversimplify the physical reality of the binding mechanism. However, the model was found to be the best compromise between the number of model parameters and the quality of data fits.

Quantitative reproductions of the individual breakthrough curves in both the simulations and the measurements are essential for a consistent analysis across flow configurations and operating conditions. A revised cleaning protocol with 1 M NaCl instead of 1 N NaOH and the minimization of storage times between the experiments was found to be important for getting reproducible measurement data. A first attempt for model-based scale-up was made by combining the binding related parameters of the XT5 capsule with the flow related parameters of the XT140 capsule. This approach technically allows the prediction of the XT140 performance under binding conditions, as the ZRM makes the binding parameters independent from the flow non-idealities in both capsules. Such predictions can potentially save much money, since the predicted XT140 experiments at binding conditions require significantly more material than the other three experiments together, which are required for calibrating the ZRM namely XT5 experiments at binding and non-binding conditions and XT140 experiments at non-binding conditions.

Unfortunately, the attempt of model-based scale-up from the XT5 capsule to the XT140 capsule was not successful. Irregular pleat structures in the XT140 capsule that can lead to local variations in the linear velocity have been identified as potential cause in an MRI analysis. However, more than 85% of the total volumetric flow was found to be transported with the standard velocity, and only the remaining less than 15% were transported with much lower velocities. These variations in the linear velocity could be described by a distribution with only three parameters. The resulting model can consistently and quantitatively reproduces the studied configurations and operating conditions (compare Figs. 5a and b, 6c, and 11d) with only 16 parameters, that is four parameters per data set. Such an integrative analysis would not have been possible either with the Roper and Lightfoot model for external dispersion or with the Langmuir binding model. The novel results once again highlight the universality and potency of the ZRM.

Future work will be focused on performing similar analyses with capsules of different vendors, in particular analyzing the potential of model-based scale-up, different solute molecules, and different operating conditions that include binding and elution steps.

This presented work is supported by the Cluster Industrial Biotechnology (CLIB) with a doctoral scholarship for Pranay Ghosh. The authors wish to thank Anil Salgotra, Jennifer Tom, and Dr. Tim Herrmann, Downstream Technologies, Bayer Healthcare, Berkeley for their valuable inputs and help throughout the project.

References

Boi C. 2007. Membrane adsorbers as purification tools for monoclonal antibody purification. J Chromatogr B 848(1):19–27.

Boi C, Dimartino S, et al. 2007. Modelling and simulation of affinity membrane adsorption. J Chromatogr A 1162(1):24–33.

Clark AJ, K A, Haynes CA, Whitehead LA. 2007. A new model of protein adsorption kinetics derived from simultaneous measurement of mass loading and changes in surface energy. Langmuir 23:5591–5600.

Dimartino S, Boi C. et al. 2011. A validated model for the simulation of protein purification through affinity membrane chromatography. J Chromatogr A 1218(13):1677–1690.

Endres HN, Johnson JA. et al. 2003. Evaluation of an ion-exchange membrane for the purification of plasmid DNA. Biotechnol Appl Biochem 37(Pt 3):259–266.

Florian Dismer JH. 2007. A novel approach to characterize the binding orientation of lysozyme on ion-exchange resins. J Chromatogr A(1149): 312–320.

Francis P, von Lieres E. et al. 2011. Zonal rate model for stacked membrane chromatography part II: Characterizing ion-exchange membrane chromatography under protein retention conditions. Biotechnol Bioeng.

Francis P, von Lieres E. et al. 2012. Zonal rate model for stacked membrane chromatography. I: Characterizing solute dispersion under flow-through conditions. J Chromatogr A 1218(31):5071–5078.

Frey DD, Vandewater R. et al. 1992. Dispersion in stacked-membrane chromatography. J Chromatogr 603(1–2):43–47.

Gebauer KH, Thommes J. et al. 1997. Plasma protein fractionation with advanced membrane adsorbents. Biotechnol Bioeng 54(2):181–189.

Gerstner JA, Hamilton R. et al. 1992. Membrane chromatographic systems for high-throughput protein separations. J Chromatogr 596(2):173–180.

Ghosh R. 2001. Separation of proteins using hydrophobic interaction membrane chromatography. J Chromatogr A 923(1–2):59–64.

Ghosh R, Wong T. 2006. Effect of module design on the efficiency of membrane chromatographic separation processes. J Membr Sci 281(1–2):532–540.

Levine HL. 2002. Economic analysis of biopharmaceutical manufacturing. 2002 BIO International Biotechnology convention and Exhibition, 9–12 June, Toronto, Ontario, Canada.

Kim JSGA. 2002. Molecular packing of lysozyme, fibrinogen, and bovine serum albumin on hydrophilic and hydrophobic surfaces studied by infrared-visible sum frequency generation and flrescence microscopy. JACS Articles 125(10):3150–3158.

Klein E. 2000. Affinity membranes: A 10 year review. J Membr Sci 179(1–2):1–27.

Knudsen HL, Fahrner RL. et al. 2001. Membrane ion-exchange chromatography for process-scale antibody purification. J Chromatogr A 907(1–2):145–154.

Montesinos-Cisneros RM, Lucero-Acuna A. et al. 2007. Breakthrough performance of large proteins on ion-exchange membrane columns. Biotechnol Appl Biochem 48:117–125.

Przybycien TM, Pujar NS. 2004. Alternative bioseparation operations: Life beyond packed-bed chromatography. Curr Opin Biotechnol 15(5):469–478.

Roper DK, Lightfoot NE. 1995. Estimating plate heights in stacked-membrane chromatography by flow reversal. J Chromatogr A 702(1–2):69–80.

Sarfert FT, Etzel MR. 1997. Mass transfer limitations in protein separations using ion-exchange membranes. J Chromatogr A 764(1):3–20.

Saxena A, Tripathi BP. et al. 2009. Membrane-based techniques for the separation and purification of proteins: An overview. Adv Colloid Interface Sci 145(1–2):1–22.

Shiosaki A, Goto M. et al. 1994. Frontal analysis of protein adsorption on a membrane adsorber. J Chromatogr A 679(1):1–9.

Suen SY, Etzel MR. 1994. Sorption kinetics and breakthrough curves for pepsin and chymosin using pepstatin A affinity membranes. J Chromatogr A 686(2):179–192.

Teeters MA, Conrardy SE. et al. 2003. Adsorptive membrane chromatography for purification of plasmid DNA. J Chromatogr A 989(1):165–173.

Tennikov MB, Gazdina NV. et al. 1998. Effect of porous structure of macroporous polymer supports on resolution in high-performance membrane chromatography of proteins. J Chromatogr A 798(1–2):55–64.

Vicente T, Sousa MFQ. et al. 2008. Anion-exchange membrane chromatography for purification of rotavirus-like particles. J Membr Sci 311(1–2):270–283.

Vogel JH, Nguyen H, et al. 2012. A new large-scale manufacturing platform for complex biopharmaceuticals. Biotechnol Bioeng 108(12):3049–3058.

von Lieres E, Wang J, Ulbricht M. 2010. Model based quantification of internal flow distributions from breakthrough curves of coin-shaped membrane chromatography modules. Chem Eng Technol 33(6):690–968.

Wang J, Dismer F. et al. 2008. Detailed analysis of membrane adsorber pore structure and protein binding by advanced microscopy. J Membr Sci 320(1–2):456–467.

Yang H, Etzel MR. 2003. Evaluation of three kinetic equations in models of protein purification using ion-exchange membranes. Ind Eng Chem Res 42(4):890–896.

Zhou JX, Tressel T. 2006. Basic concepts in Q membrane chromatography for large-scale antibody production. Biotechnol Prog 22(2):341–349.

Zhou JX, Tressel T, et al. 2006. New Q membrane scale-down model for process-scale antibody purification. J Chromatogr A 1134(1–2):66–73.

2.2 Publication II

"Zonal Rate Model for Axial and Radial Membrane Chromatography. Part II: Model based scale-up."

(Biotechnology and Bioengineering, 111 (2014) 1587-1594)

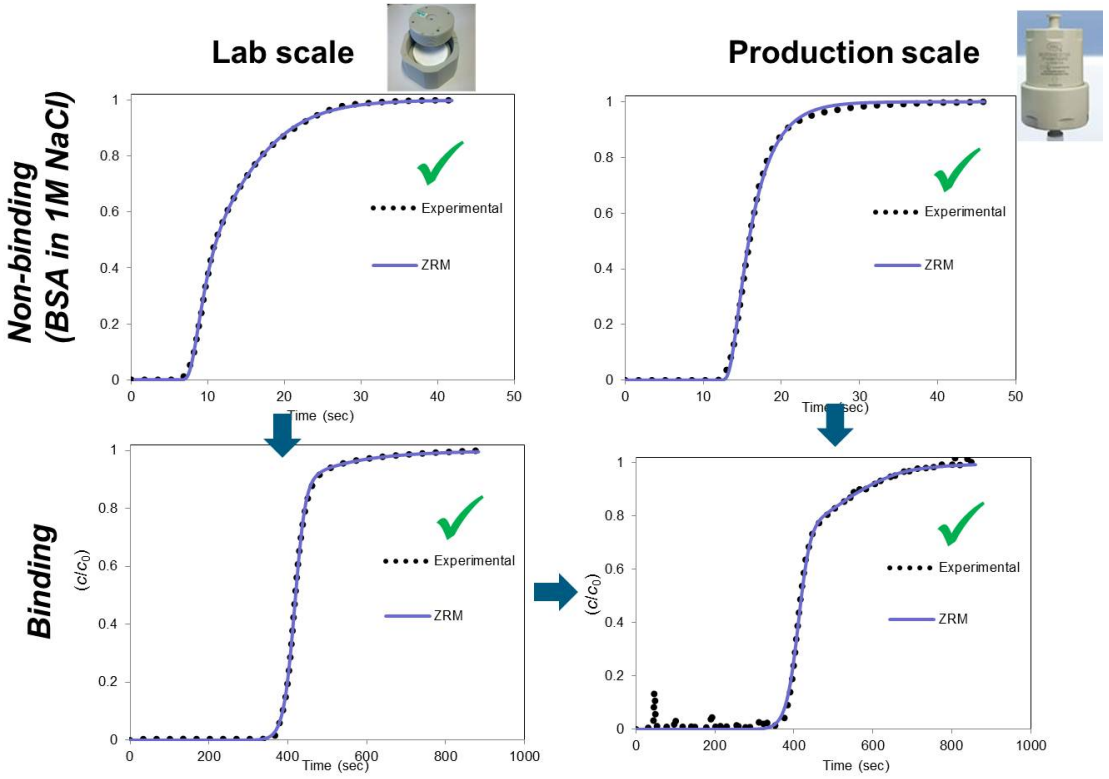

Pranay Ghosh, Min Lin, Jens H. Vogel, Derek Choy, Charles Haynes, Eric von Lieres

ARTICLE

BIOTECHNOLOGY and BIOENGINEERING

Zonal Rate Model for Axial and Radial Flow Membrane Chromatography, Part II: Model-Based Scale-Up

Pranay Ghosh,[1] Min Lin,[2] Jens H. Vogel,[2] Derek Choy,[3] Charles Haynes,[3] Eric von Lieres[1]

[1]IBG-1: Biotechnology, Forschungszentrum Jülich, Wilhelm-Johnen-Straße 1 52425, Jülich, Germany; telephone: +49-2461-61-2168; fax: +49-2461-61-3870; e-mail: e.von.lieres@fz-juelich.de

[2]Isolation and Purification Department, Global Biologics Development, Bayer Healthcare, Berkeley, CA

[3]Michael Smith Laboratories, University of British Columbia, Vancouver, Canada

Boehringer Ingelheim, Fremont, CA

ABSTRACT: Membrane chromatography (MC) systems are finding increasing use in downstream processing trains for therapeutic proteins due to the unique mass-transfer characteristics they provide. As a result, there is increased need for model-based methods to scale-up MC units using data collected on a scaled-down unit. Here, a strategy is presented for MC unit scale-up using the zonal rate model (ZRM). The ZRM partitions an MC unit into virtual flow zones to account for deviations from ideal plug-flow behavior. To permit scale-up, it is first configured for the specific device geometry and flow profiles within the scaled-down unit so as to achieve decoupling of flow and binding related non-idealities. The ZRM is then configured for the preparative-scale unit, which typically utilizes markedly different flow manifolds and membrane architecture. Breakthrough is first analyzed in both units under non-binding conditions using an inexpensive tracer to independently determine unit geometry related parameters of the ZRM. Binding related parameters are then determined from breakthrough data on the scaled-down MC capsule to minimize sample requirements. Model-based scale-up may then be performed to predict band broadening and breakthrough curves on the preparative-scale unit. Here, the approach is shown to be valid when the Pall XT140 and XT5 capsules serve as the preparative and scaled-down units, respectively. In this case, scale-up is facilitated by our finding that the distribution of linear velocities through the membrane in the XT140 capsule is independent of the feed flow rate and the type of protein transmitted. Introduction of this finding into the ZRM permits quantitative predictions of breakthrough over a range of industrially relevant operating conditions.

Biotechnol. Bioeng. 2014;9999: 1–8.

KEYWORDS: membrane chromatography; scale-up; modeling

The present address of Pranay Ghosh is Hoffmann-La-Roche AG, Basel, Switzerland
The present address of Jens H. Vogel is Boehringer Ingelheim, Fremont, CA
Correspondence to: E. von Lieres
Contract grant sponsor: Cluster for Industrial Biotechnology (CLIB)
Contract grant sponsor: NSERC, the Natural Sciences and Engineering Research Council of Canada
Received 13 December 2013; Revision received 31 January 2014; Accepted 3 February 2014
Accepted manuscript online xx Month 2014;
Article first published online in Wiley Online Library (wileyonlinelibrary.com).
DOI 10.1002/bit.25217

Introduction

Membrane chromatography (MC) is increasingly used in industry as an alternative purification platform to packed bed chromatography (Boi et al., 2007; Ghosh, 2001; Ghosh and Wong, 2006; Vogel et al., 2012). Due to larger pore sizes, slow pore diffusion processes are essentially eliminated, leading to higher mass-transfer rates, and reduced overall operational times. The rate of column loading in a MC system is mainly governed by protein convection and either the thermodynamics or the rates of protein–sorbent complex formation (Briefs and Kula, 1992; Charcosset, 2006; Suen and Etzel, 1994). However, it is known that column-loading profiles of MC systems can deviate from the desired plug-flow behavior and can be strongly asymmetrical in nature under certain operating conditions (Montesinos-Cisneros et al., 2007; Sarfert and Etzel, 1997; Yang and Etzel, 2003). Experimental breakthrough curves (BTCs) typically show a sharp initial breakthrough that is followed by a slow approach to saturation. Such non-ideal behavior has been subject to active research for many years.

In the past, the asymmetric band broadening has been attributed mainly to complex protein binding mechanisms. These mechanisms have been modeled by many groups using different hypotheses such as multi-site, spreading, random-sequential adsorption, and steric mass-action/hindrance isotherm or rate models (Boi et al., 2007; Briefs and Kula, 1992; Brooks and Cramer, 1992; Clark et al., 2007; Lundstrom, 1985; Suen and Etzel, 1992; Talbot et al., 2000). In previous publications, we have shown that the spreading model, which hypothesizes different binding orientations of protein, can accurately describe the adsorption of bovine serum albumin (BSA) and ovalbumin on polyethersulfone membrane (PES) membranes coated with a cross-linked polymer containing pendant Q groups (Francis et al., 2011, 2012; Ghosh et al., 2013a). As well, Sarti and co-workers have shown that the bi-Langmuir model can accurately reproduce BTC data of BSA on cellulose acetate surfaces (Dimartino et al., 2011).

In addition to non-ideal binding, it has been observed that hold-up volumes within MC capsules, which are often as large as the membrane volume itself, can contribute significantly to system dispersion. This particularly holds for low-volume lab-scale MC capsules with an axial flow configuration, where solute molecules break through the central membrane area much earlier than through outer radial regions, and the resulting elution profiles can appear highly dispersed (Ghosh and Wong, 2006). However, the magnitude of these hold-up-volume related non-idealities does not necessarily scale due to the often vastly different manifold and membrane geometries used in scaled-down and preparative-scale units. Indeed, we have previously reported pronounced differences in band broadening within lab-scale (Pall Mustang XT5 with 5 mL membrane volume), and preparative-scale (Pall Mustang XT140 with 140 mL membrane volume) MC capsules containing the same membrane and operated at the same mean linear velocities (Fig. 1) (Ghosh et al., 2013a). Variations in the manifold design of the two MC capsules were identified as the major cause of the observed non-linear scaling between these capsules. Hence, any mathematical approach for model-based analysis and scale-up of MC units must carefully decouple the impacts of different non-idealities, including those caused by protein binding and by manifold and membrane architecture, on breakthrough performance.

We have previously developed a semi-empirical modeling approach, the zonal rate model (ZRM) (Francis et al., 2011, 2012; Ghosh et al., 2013a; von Lieres et al., 2009), for decoupling the contributions to band broadening of non-ideal hydrodynamics and binding in MC capsules. In the first paper of this series, the ZRM was thereby applied to systematically analyze lab-scale Mustang XT5 capsules. A more limited study of the preparative-scale XT140 capsule was also reported. Variations in protein residence times within the inlet and elution manifolds of both units were recorded, with the nature of the non-idealities unit-specific due the different flow geometries employed. In addition, variations in the linear velocity through the membrane stack were recorded in the preparative-scale capsule due in part to the radial-flow pleated membrane geometry employed. Those latter variations were shown to impact BTCs under binding conditions, while making relatively little contribution to band broadening under non-binding conditions. Here, we show that the relative distribution of linear velocities is independent of both the volumetric flow rate and the characteristics of the transmitted protein. When this knowledge is introduced into the ZRM, quantitative prediction of protein BTCs within production-scale MC capsules is then demonstrated over a range of industrially relevant operating conditions. Predictions are based on binding parameters determined in the scaled-down unit yielding a new cost-effective model-based method for scale-up and simulation of production-scale MC units.

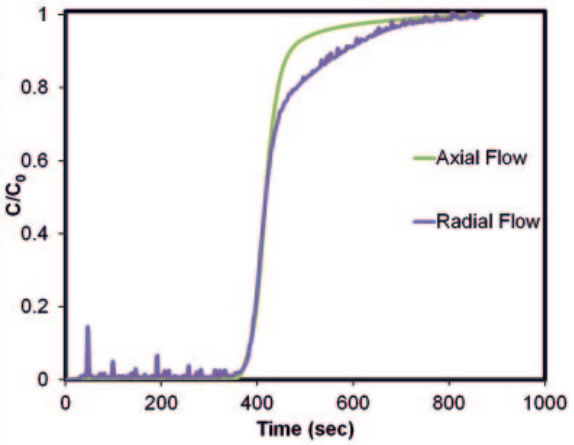

Figure 1. Breakthrough curves obtained under binding conditions for lab-scale axial-flow and production-scale radial-flow MC capsules with 1 mg/mL BSA at a flow rate of 12 MV/min.

Theory

Traditionally, MC has been modeled assuming flow homogeneity (linear velocities and mean residence times) within hold-up volumes upstream and downstream of the membrane stack and also over membrane cross sections. The hold-up volumes are therefore usually modeled by a linear combination of one or two continuously stirred tank regions (CSTR) and a plug flow region (PFR). The Roper and Lightfoot model (RLM) captures system dispersion by differently sized CSTRs on each side of the membrane (Roper and Lightfoot, 1995). The RLM, although adequate for modeling some cases, is based on a rather simplified representation of the true physical geometry of these systems.

Zonal Rate Model

The ZRM is designed to quantitatively capture the impact of inhomogeneous flow in MC capsules. To predict BTCs under

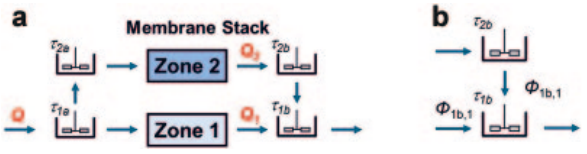

Figure 2. **a**: Virtual partitioning of hold-up volumes and membrane for the lab-scale axial-flow capsule, and (**b**) flow fractions of the collecting tank downstream of the membrane.

binding conditions, it requires a binding model, and the Langmuir, steric mass action (SMA), and spreading models have previously been integrated into the ZRM. A detailed mathematical description of the ZRM can be found in previous publications (Francis et al., 2011, 2012; von Lieres et al., 2009). Here, we therefore only describe configurations of the ZRM for the lab-scale Pall Mustang XT5 capsule (axial flow, see Fig. 2a) and the production-scale Pall Mustang XT140 capsule (radial flow, see Fig. 3a). Detailed information on the internal geometry of both capsules has been reported in a previous publication (Ghosh et al., 2013a). For the lab-scale capsule, the ZRM conceptually partitions the hold-up volumes before and after the membrane into two virtual flow zones. The membrane stack is also partitioned into two virtual zones having the same physical properties but subject to different boundary conditions. The inter-connected virtual zones for the hold-up volumes are modeled as a CSTR network, while each of those within the membrane stack are described by the one-dimensional mass continuity equation of chromatography:

$$\frac{\partial c}{\partial t} = -v\frac{\partial c}{\partial z} + D_a\frac{\partial^2 c}{\partial z^2} - \frac{1-\varepsilon}{\varepsilon}\frac{\partial q}{\partial t} \tag{1}$$

Here c and q are the solute concentrations in the mobile and stationary phases, respectively, z is the axial coordinate, v is the interstitial fluid velocity, D_a is the axial dispersion coefficient, and ε is the membrane porosity. We have previously shown with the help of infrared spectroscopy that the bulk porosity is rather homogeneous across the entire cross-section and thickness of the membranes used in this study (Johannes Kiefer et al., 2014). As is typical for chromatography modeling, solution of Equation (1) requires coupling to an appropriate protein-binding rate or isotherm model (see Binding Kinetics). Finally, the ZRM adds a plug flow region (PFR) in series with the CSTR network to model any time lag that is not associated with system dispersion (the time lag $t_{lag} = V_{PFR}/Q$ is the ratio of the PFR volume V_{PFR} to the volumetric feed flow rate Q):

$$c_{out}(t) = c_{in}(t - t_{lag}) \tag{2}$$

Due to its partitioning of the system into virtual zones, the ZRM requires a set of flow fractions, Φ_k, which define the fraction of the total volumetric flow passing through each of the membrane zones (Fig. 2b). Solute dispersion in the virtual zones upstream and downstream of the membrane stack is described by a conventional CSTR equation ($\tau = V_{CSTR}/Q$ is the average residence time, and j is the number of inflows of the respective CSTR):

$$\frac{\partial c_{out}}{\partial t} = \sum_{j=1}^{m}\frac{c_{in,j} - c_{out}}{\tau_j} \tag{3}$$

For the production-scale capsule, one virtual zone was found to be sufficient for capturing the flow behavior in the hold-up volumes before and behind the membrane region (Fig. 3a) (Ghosh et al., 2013a). However, the membrane zone had to be divided into several sectors with different linear velocities (Fig. 3a, only three sectors are shown for clarity of the sketch). These sectors represent specific regions of the pleated membrane, each characterized by unique structural attributes such as bed height and frontal area. Protein transport in each sector of the membrane is computed by solution of Equation (1) with the boundary conditions remaining constant across sectors and the distribution of linear velocities varying as a Gaussian-type function reported in Figure 3b.

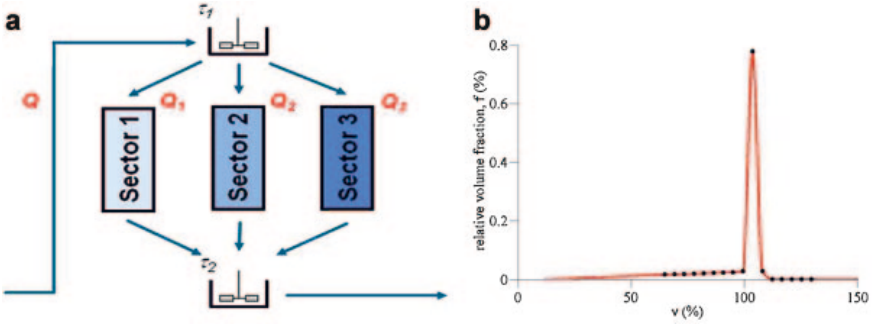

Figure 3. **a**: Virtual partitioning of hold-up volumes and membrane for the production-scale radial-flow capsule, where the membrane zone is split into sectors with varying linear velocities, and (**b**) distribution of the relative volumetric flow, *f*, over the relative linear velocity, *v*, in the respective sector.

Binding Kinetics

The kinetic form of the spreading model has been previously shown to accurately correlate BTC data for BSA eluting from a XT5 capsule (Francis et al., 2011, 2012; Ghosh et al., 2013a). That model assumes two different bound states, yielding rate equations of the form (Clark et al., 2007; Yang and Etzel, 2003):

$$\frac{\partial q}{\partial t} = \frac{\partial q_1}{\partial t} + \frac{\partial q_2}{\partial t} \quad (4)$$

$$\frac{\partial q_1}{\partial t} = (k_{a,1}c - k_{12}q_1)(q_m - q_1 - \beta q_2) - k_{d,1}q_1 + k_{21}q_2 \quad (5)$$

$$\frac{\partial q_2}{\partial t} = (k_{a,2}c + k_{12}q_1)(q_m - q_1 - \beta q_2) - (k_{21} - k_{d,2})q_2 \quad (6)$$

Here q_1 and q_2 are the concentrations of bound states 1 and 2, respectively, β is the ratio of the sorbent surface area occupied by state 2 relative to state 1, $k_{a,1}$, $k_{d,1}$, $k_{a,2}$, and $k_{d,2}$ are binding rate constants defined in analogy to the Langmuir model, and k_{12} and k_{21} describe the rates of bound-state changes.

Materials and Methods

Bovine serum albumin (BSA, A 7638, Sigma–Aldrich Corp., St. Louis, MO) and ovalbumin (A 2512, Sigma–Aldrich Corp.) were used for breakthrough experiments at a feed concentration of 1 g/L. The protein was dissolved in 25 mM Tris buffer at pH 8.0 (Sigma–Aldrich Corp.) for the loading step. Loading was followed by a 5–10 column-volume (CV) washing step with 25 mM Tris buffer at pH 8.0. Then, 1 M NaCl in 25 mM Tris buffer pH 8.0 was used to elute the bound protein from the membranes. The capsules were cleaned with 1 M NaCl after each run.

Mustang Q XT5 (axial flow, 5 mL membrane volume) and Mustang Q XT140 (radial flow, 140 mL membrane volume) anion-exchange membrane chromatography capsules were purchased from Pall Inc. (East Hills, NY). Both capsules contain modified hydrophilic polyethersulfone (PES) membranes whose surfaces are coated with an irreversibly cross-linked polymer that contains pendant Q groups. The average effective bed height of the membrane stacks in the XT5 and XT140 capsules is 2.20 mm. The pore size and porosity ε of the membrane are 0.8 μm and 0.70 ± 0.05, respectively (manufacturer data). More details on the internal capsule geometries, including a comprehensive MRI analysis, can be found in a previous publication (Ghosh et al., 2013a). The XT5 capsule was attached to an ÄKTAexplorer system that was controlled by the Unicorn software (GE Healthcare, Uppsala, Sweden). The XT140 capsule was attached to an ÄKTAprocess system that was controlled by the Unicorn software.

Results

In the first paper of this series, lab-scale MC capsules with an axial flow configuration and production-scale MC capsules with a radial flow configuration were comparatively analyzed using 1 mg/mL BSA at a flow rate of 12 CV/min. Non-ideal flow in the lab-scale capsule was effectively captured using a two-zone configuration of the ZRM to describe BTC data obtained under non-binding conditions. The membrane was modeled using the same linear velocity in each zone, as validated by an independent study employing computational fluid dynamics (CFD) (Ghosh et al., 2013b). In contrast, magnetic resonance imaging (MRI) data and CFD simulation both revealed variations in the linear velocity within the membrane stack in the production-scale capsule, and the ZRM was correspondingly configured for describing this capsule (Fig. 3). Several binding models were evaluated. A simplified version of the spreading model, without adsorption/desorption from/to the second bound state, was found to reproduce measured BTCs very well, and provides a coherent explanation of the binding mechanism. Notably, this binding model, combined with different configurations of the ZRM, quantitatively describes BTC data at lab and production scales with the same model parameters. However, model-based scale-up (i.e., prediction of binding BTC data of the production-scale capsule using parameters of the binding model determined at lab scale) was not possible, in part due to the fact that the linear velocity distribution in the production-scale capsule could not be determined from non-binding data.

Here, the linear velocity distribution in the membrane stack of the XT140 capsule is studied as a function of the volumetric flow rate (in membrane volumes per minute, the XT5 and XT140 capsules contain 5 and 140 mL of membrane, respectively). Figure 3b shows that distribution at a flow rate of 12 MV/min. The validity of that distribution is demonstrated through the fact that it was also predicted by CFD simulations in an independent study (Ghosh et al., 2013b). CFD simulations of the same capsule at flow rates of 1.2, 4, and 5.7 MV/min further reveal that the relative distribution of linear flow rates through the membrane is independent of the volumetric flow rate (data not shown). Figure 4 shows

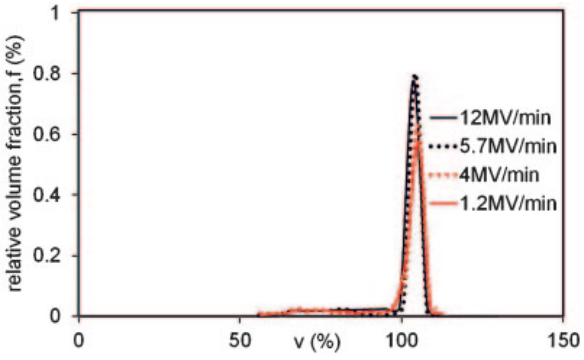

Figure 4. Relative frequency, *f*, of linear velocities, *v*, through the membrane stack at different volumetric flow rates through the production-scale capsule, as determined by fitting a 16-sector ZRM to BTC data measured using BSA (1.2, 4, and 12 MV/min) and ovalbumin (5.7 MV/min) under binding conditions.

that the observed flow-rate-independent velocity distribution, in this case as determined experimentally from BTC data measured under protein binding conditions, can be accurately modeled using a ZRM configured with 16 sectors. The experiments at 1.2 and 4 MV/min were performed with BSA as tracer molecule, while ovalbumin was used at 5.7 MV/min. As predicted by the CFD simulations, the experimentally determined distributions are nearly super imposable, though the width was seen to increase very slightly with decreasing flow rate, likely due to measurement uncertainty. As the effect is indeed quite small, the velocity distribution measured at 12 MV/min was used for all subsequent model calculations, irrespective of the flow rate.

Model-Based Scale-Up for BSA

With the linear velocity distributions known, we asked whether the ZRM could now be used to predict BTC data in the production-scale XT140 capsule. To do this, BTC data for BSA were collected in both the lab and production-scale capsules as a function of feed flow rates.

With the ZRM configured using two membrane zones with the same linear velocity for the lab-scale capsule (Fig. 2), and using one membrane zone and 16 sectors with different linear velocities for the production-scale capsule (Fig. 3), inhomogeneous flow in the hold-up volumes of each capsule was analyzed by regressing the required PFR and CSTR parameters to BTC data measured under non-binding conditions at 1.2 MV/min (Fig. 5a and b) and 4 MV/min (Fig. 6a and b). For both capsules, the configured ZRM reproduces the BTC measured at both flow rates very well. The regressed PFR and CSTR parameters, which are related to the capsule geometry and independent of the binding mechanism, are reported in Tables I and II. Notably, the

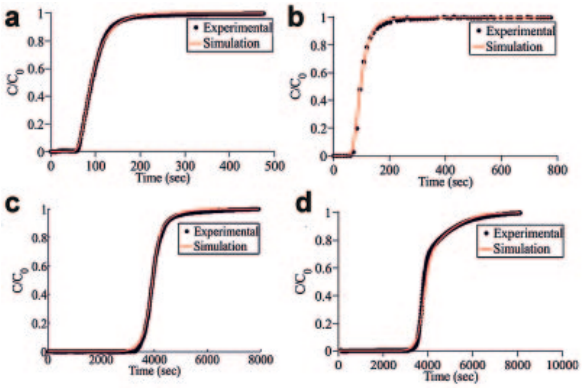

Figure 5. Model-based scale-up for 1 mg/mL BSA at 1.2 MV/min: (**a**) best fit of two-zone ZRM to non-binding BTC of lab-scale capsule, (**b**) best fit of one-zone ZRM with given velocity distribution to non-binding BTC of production-scale capsule, (**c**) best fit to of spreading model combined with two-zone ZRM with fixed PFR and CSTR parameters to binding BTC of lab-scale capsule, and (**d**) predicted and measured binding BTC of production-scale capsule.

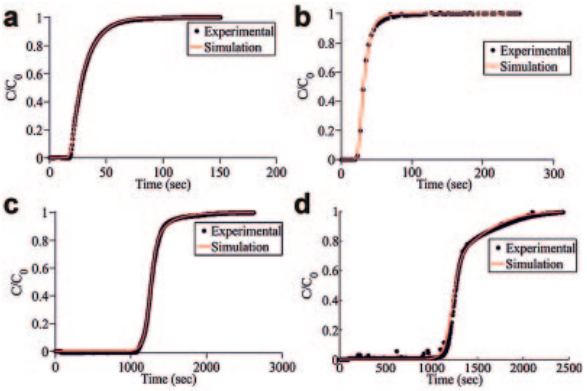

Figure 6. Model-based scale-up for 1 mg/mL BSA at 4 MV/min: (**a**) best fit of two-zone ZRM to non-binding BTC of lab-scale capsule, (**b**) best fit of one-zone ZRM with given velocity distribution to non-binding BTC of production-scale capsule, (**c**) best fit to of spreading model combined with two-zone ZRM with fixed PFR and CSTR parameters to binding BTC of lab-scale capsule, and (**d**) predicted and measured binding BTC of production-scale capsule.

inverse values of the determined residence times approximately follow linear trends over flow rate. This could technically be utilized for predicting these parameters at different flow rates. However, individual determination of these parameters from measurement data at the studied flow rate has been found to yield more accurate results. With these parameters known, the impact of protein binding on BTC behavior in the lab-scale capsule could next be evaluated.

The spreading model was therefore combined with the two-zone ZRM describing flow within the XT5 capsule. Spreading model parameters for BSA binding were then estimated from BTC data measured in that capsule under binding conditions at flow rates of 1.2 MV/min (Fig. 5c) and 4 MV/min (Fig. 6c) and 12 MV/min (Ghosh et al., 2013a). By properly capturing the effects of flow non-idealities in the XT5 capsule, the ZRM configured for that capsule accurately reproduces the BTC at each flow condition. In Table III, the estimated spreading model parameters are reported as a function of flow rate. Each parameter is practically flow rate independent, except for the binding constant $k_{a,1}$. Taking averages of the k_{21} and q_m values observed across flow rates would cause negligible changes in model predictions (data not shown). The initial adsorption rate $1/(k_{a,1} \cdot Q_m) = 0.37$ s (1.2 MV/min), 0.13 s (4 MV/min), and 0.042 s (12 MV/min) is always fast, but increases with flow rate, suggesting either that the protein's surface energy (e.g., conformation) changes with flow, or that the regressed parameter is not intrinsic in nature but contains a small contribution from protein mass-transfer effects.

The goal of this work, however, is not to understand that dependence further, but rather to determine if the ZRM configured for the production-scale capsule with geometry parameters from Table II can be used to predict BTCs in that

Table I. Geometry parameters of symmetric two-zone ZRM of lab-scale capsule operated at different flow rates, as regressed from BTC data measured using 1 mg/mL BSA under non-binding conditions.

Parameter	1.2 MV/min	4 MV/min	12 MV/min
t_{lag} (s)	31.38	7.38	3.91
τ_{inner} (s)	12.02	5.78	1.24
τ_{outer} (s)	22.54	6.60	1.69

preparative-scale unit using parameters for the spreading model (Table III) determined using the scaled-down system. Using that approach, we applied the ZRM configured for the XT140 capsule to predict breakthrough curves for BSA under binding conditions at flow rates of 1.2 MV/min (Fig. 5d) and 4 MV/min (Fig. 6d) within that capsule. Both predictions are in excellent quantitative agreement with experiment. The preparative-scale ZRM not only predicts the point of breakthrough, but also the complex tailing of the BTC as membrane saturation is approached. These predictive results for the full-scale system using binding parameters collected in a scaled-down system are highly relevant for industrial process development, as they prove that binding and breakthrough studies at preparative or pilot scales using potentially scarce and likely expensive pure product are not needed for model development. Instead, any convenient and inexpensive tracer molecule can be applied to define the precise flow non-idealities and thereby configure the ZRM for each scaled unit. Product binding studies conducted in the small-scale unit may then be used to determine all remaining model parameters.

The success of the presented method absolutely depends on the ability of the ZRM to quantitatively decouple band-broadening effects caused by non-ideal flow and non-ideal binding, which are both unavoidable in MC capsules. Binding parameters can only be transferred across scales if this condition is met by the ZRMs configured at the two scales. Finally, the results obtained validate our finding that the linear velocity distribution through membrane in the production-scale capsule is indeed independent of the applied volumetric flow rate.

Model-Based Scale-Up for Ovalbumin

To determine if the scale-up approach described is generally applicable, we next applied it to the same capsules but using a different protein, ovalbumin, at a flow rate of 5.7 MV/min. The ZRM configurations, binding parameter determination and scale-up methodology remained the same as described above. The resulting PFR and CSTR parameters, as shown in Table IV, are in accordance with those obtained with BSA. Moreover, BTCs under non-binding conditions are again reproduced with high accuracy (Fig. 7a and b).

Table II. Geometry parameters of one-zone ZRM of production-scale capsule operated at different flow rates, as regressed from BTC data measured using 1 mg/mL BSA under non-binding conditions.

Parameter	1.2 MV/min	4 MV/min	12 MV/min
t_{lag} (s)	90.50	29.22	9.70
$\tau_{upstream}$ (s)	27.89	9.02	2.99
$\tau_{downstream}$ (s)	4.85	1.56	0.52

Table III. Binding parameters, as estimated by fitting spreading model combined with two-zone ZRM to BTC data of lab-scale capsule measured using 1 mg/mL BSA under binding conditions.

Parameter	1.2 MV/min	4 MV/min	12 MV/min
k_{a1} (1/(g s))	0.90×10^{-2}	2.67×10^{-2}	8.08×10^{-2}
k_{d1} (1/s)	1.06×10^{-5}	1.06×10^{-5}	1.06×10^{-5}
k_{12} (1/(g s))	7.37×10^{-4}	7.37×10^{-4}	7.37×10^{-4}
k_{21} (1/s)	8.02×10^{-3}	9.41×10^{-3}	9.41×10^{-3}
q_m (g/L)	288.8	290.3	289.0
β (−)	1.14	1.14	1.14

The 12 MV/min data are taken from the first paper of this series (Ghosh et al., 2012).

As for BSA, binding of ovalbumin on the PES membrane was quantitatively reproduced and most coherently described by the spreading model (Francis et al., 2011, 2012). Table V shows the binding parameters for ovalbumin determined in the scaled-down unit at a flow rate of 5.7 MV/min. Using those parameters, the ZRM for the XT5 capsule accurately represents ovalbumin breakthrough behavior in that scaled-down system (Fig. 7c).

The ZRM for the production-scale capsule, with the geometric parameters from Table IV, was then combined with the spreading model and binding parameters from Table V to predict the binding BTC of ovalbumin at 5.7 MV/min. As with BSA, the model prediction and measured BTC data are in excellent agreement (Fig. 7d). Both the initial breakthrough point and the approach to saturation of the BTC are quantitatively predicted by the model. The results obtained therefore validate the potential generality of our proposed scale-up method, as well as, our finding that the linear velocity distribution through membrane in the production-scale capsule is not only independent of the applied volumetric flow rate but also of the tracer molecule.

Discussion and Conclusions

The use of scaled-down models of preparative units is a proven strategy for saving material and time in process development. However, few resources are currently available to apply that strategy to MC scale-up. In general, manufacturers of preparative-scale MC units also sell low-volume units that utilize the same membrane chemistry, but

Table IV. Geometry parameters of symmetric two-zone ZRM of lab-scale capsule and of one-zone ZRM of production-scale capsule operated at a flow rate of 5.7 MV/min, as regressed from BTC data measured using 1 mg/mL ovalbumin under non-binding conditions.

Parameter	Lab-scale	Parameter	Production-scale
t_{lag} (s)	4.40	t_{lag} (s)	23.90
τ_{inner} (s)	3.08	$\tau_{upstream}$ (s)	5.80
τ_{outer} (s)	3.31	$\tau_{downstream}$ (s)	0.89

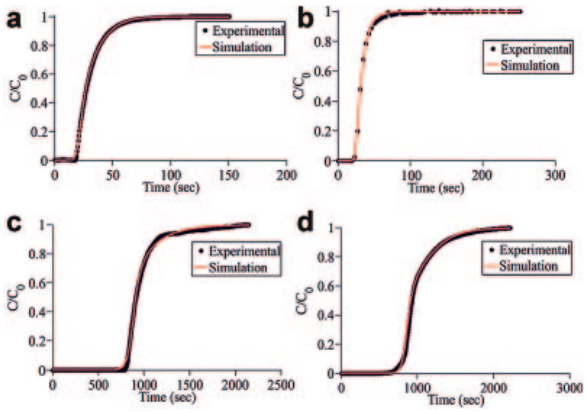

Figure 7. Model-based scale-up for 1 mg/mL ovalbumin at 5.7 MV/min: (**a**) best fit of two-zone ZRM to non-binding BTC of lab-scale capsule, (**b**) best fit of one-zone ZRM with given velocity distribution to non-binding BTC of production-scale capsule, (**c**) best fit to of spreading model combined with two-zone ZRM with fixed PFR and CSTR parameters to binding BTC of lab-scale capsule, and (**d**) predicted and measured binding BTC of production-scale capsule.

not the same membrane arrangement nor the same inlet and outlet flow manifold design. For example, the lab-scale Pall Mustang XT5 capsule utilizes an axial flow design and a 5 mL stack of flat-sheet membranes, while the preparative Pall Mustang XT140 capsule utilizes a radial flow design and a 140 mL membrane stack presented in a pleated-sheet arrangement. Thus, while the low-volume XT5 capsule is well suited for routine laboratory separation needs, it is not designed specifically for process scale-up studies. This fact is demonstrated in Figure 1, which shows that normalized BTCs measured at the two scales differ, notably above ca. 60% saturation.

Here, however, we have shown that results obtained on the geometrically and operationally distinct lab-scale XT5 MC unit can nevertheless be used to accurately predict expected performance in a preparative XT140 unit through application of the ZRM. This is achieved by precisely configuring the ZRM to each unit, thereby permitting contributions to band broadening related to the unique flow non-idealities within each device to be estimated. Those contributions in the scaled-down unit can then be subtracted from overall breakthrough behavior in that unit. The residual defines intrinsic binding non-idealities common to both units, allowing binding parameters obtained from low-cost studies on the scaled-down unit to be directly applied in the ZRM configured for the preparative unit. The present contribution therefore provides proof of concept that the ZRM enables model-based scale-up by conceptually decoupling and independently quantifying the mechanisms of inhomogeneous flow and non-ideal binding in MC capsules at different scales and operating conditions.

Table V. Binding parameters, as estimated by fitting spreading model combined with two-zone ZRM to BTC data of lab-scale capsule measured using 1 mg/mL ovalbumin under binding conditions.

Parameter	5.7 MV/min
k_{a1} (1/(g s))	3.60×10^{-2}
k_{d1} (1/s)	1.40×10^{-5}
k_{12} (1/(g s))	3.20×10^{-3}
k_{21} (1/s)	6.07×10^{-2}
q_m (g/L)	313.6
β	1.55

In a separate publication, we have shown that CFD provides an alternative means to achieve this required decoupling of non-idealities (Ghosh et al., 2013b). However, CFD simulations are computationally expensive and require detailed information on the internal capsule geometry, which can be difficult to acquire. The ZRM is a semi-empirical approach with the same predictive power. It requires estimation of geometry parameters from BTC data for an inexpensive tracer loaded under non-binding conditions. That same information can instead be obtained using CFD models. However, the ZRM approach offers the clear advantage that it is computationally very fast and does not require precise information on internal capsule geometries. Unlike CFD modeling, the ZRM cannot estimate the distribution of linear velocities through the membrane of a given preparative MC unit. However, we show here for the XT140 unit that this distribution is independent of the applied flow rate and tracer molecule used. Consequently, the required distribution can be determined once and for all from only one production scale experiment at binding conditions using a cheap tracer molecule.

The presented work was supported by the Cluster for Industrial Biotechnology (CLIB) with a doctoral scholarship for Pranay Ghosh, as well as by NSERC, the Natural Sciences and Engineering Research Council of Canada.

References

Boi C, Dimartino S, Sarti GC. 2007. Modelling and simulation of affinity membrane adsorption. J Chromatogr A 1162(1):24–33.

Briefs KG, Kula MR. 1992. Fast protein chromatography on analytical and preparative scale using modified microporous membranes. Chem Eng Sci 47(1):141–149.

Brooks CA, Cramer SM. 1992. Steric mass-action ion-exchange—Displacement profiles and induced salt gradients. Aiche J 38(12):1969–1978.

Charcosset C. 2006. Membrane processes in biotechnology: An overview. Biotechnol Adv 24(5):482–492.

Clark AJ, Kotlicki A, Haynes CA, Whitehead AL. 2007. A new model of protein adsorption kinetics derived from simultaneous measurement of mass loading and changes in surface energy. Langmuir 23(10):5591–5600.

Dimartino S, Boi C, Sarti, GC. 2011. A validated model for the simulation of protein purification through affinity membrane chromatography. J Chromatogr A 1218(13):1677–1690.

Francis P, von Lieres E, Haynes C. 2011. Zonal rate model for stacked membrane chromatography. I: Characterizing solute dispersion under flow-through conditions. J Chromatogr A 1218(31):5071–5078.

Francis P, von Lieres E, Haynes C. 2012. Zonal rate model for stacked membrane chromatography part II: Characterizing ion-exchange

membrane chromatography under protein retention conditions. Biotechnol Bioeng 109(3):615–629.

Ghosh R. 2001. Separation of proteins using hydrophobic interaction membrane chromatography. J Chromatogr A 923(1–2):59–64.

Ghosh P, Vahedipour K, Lin M, Vogel JH, Haynes CA, von Lieres E. 2013a. Zonal rate model for axial and radial flow membrane chromatography. Part I: Knowledge transfer across operating conditions and scales. Biotechnol Bioeng 110(4):1129–1141.

Ghosh P, Vahedipour K, Lin M, Vogel JH, Haynes CA, von Lieres E. 2013b. Computational fluid dynamic simulation of axial and radial flow membrane chromatography: Mechanisms of non-ideality and validation of the zonal rate model. J Chromatogr A 1305:114–122.

Ghosh R, Wong T. 2006. Effect of module design on the efficiency of membrane chromatographic separation processes. J Membr Sci 281(1–2):532–540.

Johannes Kiefer, Rasul Nadia H, Ghosh Pranay K, von Lieres Eric. 2014. Surface and bulk porosity mapping of polymer membranes using infrared spectroscopy. J Membr Sci 452:152–156.

Lundstrom I. 1985. Models of protein adsorption on solid-surfaces. Prog Colloid Polym Sci 70:76–82.

Montesinos-Cisneros RM, Lucero-Acuña A, Ortega J, Guzmán R, Tejeda-Mansir A. 2007. Breakthrough performance of large proteins on ion-exchange membrane columns. Biotechnol Appl Biochem 48(Pt 2): 117–125.

Roper DK, Lightfoot EN. 1995. Estimating plate heights in stacked-membrane chromatography by flow reversal. J Chromatogr A 702(1–2): 69–80.

Sarfert FT, Etzel MR. 1997. Mass transfer limitations in protein separations using ion-exchange membranes. J Chromatogr A 764(1): 3–20.

Suen SY, Etzel MR. 1992. A mathematical-analysis of affinity membrane bioseparations. Chem Eng Sci 47(6):1355–1364.

Suen SY, Etzel MR. 1994. Sorption kinetics and breakthrough curves for pepsin and chymosin using pepstatin A affinity membranes. J Chromatogr A 686(2):179–192.

Talbot J, Tarjus G, Van Tassel PR, Viot P. 2000. From car parking to protein adsorption: An overview of sequential adsorption processes. Colloid Surf A-Physicochem Eng Aspects 165(1–3):287–324.

Vogel JH, Nguyen H, Giovannini R, Ignowski J, Garger S, Salgotra A, Tom J. 2012. A new large-scale manufacturing platform for complex biopharmaceuticals. Biotechnol Bioeng 108(12):3049–3058.

von Lieres E, Wang J, Ulbricht M. 2009. Model based quantification of internal flow distributions from breakthrough curves of coin-shaped membrane chromatography modules. Chem Eng Technol 33(6):690–968.

Yang H, Etzel MR. 2003. Evaluation of three kinetic equations in models of protein purification using ion-exchange membranes. Ind Eng Chem Res 42(4):890–896.

Chapter 3

Computational fluid dynamics (CFD)

3.1 Publication III

"Computational fluid dynamic simulation of axial and radial flow membrane chromatography: Mechanisms of non-ideality and validation of the zonal rate model"

(Journal of Chromatography A. 1305 (2013) 114-122)

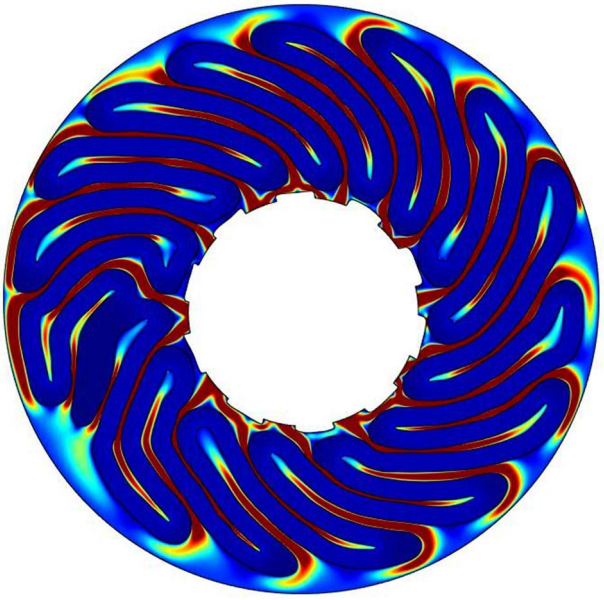

Pranay Ghosh, Kaveh Vahedipour, Min Lin, Jens H. Vogel, Charles Haynes, Eric von Lieres

Journal of Chromatography A, 1305 (2013) 114–122

Contents lists available at SciVerse ScienceDirect

Journal of Chromatography A

journal homepage: www.elsevier.com/locate/chroma

Computational fluid dynamic simulation of axial and radial flow membrane chromatography: Mechanisms of non-ideality and validation of the zonal rate model

Pranay Ghosh[a], Kaveh Vahedipour[b], Min Lin[c], Jens H. Vogel[c,1], Charles Haynes[d], Eric von Lieres[a,*]

[a] *IBG-1: Biotechnology, Forschungszentrum Jülich, Germany*
[b] *INM-4: Medical Imaging Physics, Forschungszentrum Jülich, Germany*
[c] *Isolation and Purification Department, Global Biologics Development, Bayer Healthcare, Berkeley, USA*
[d] *Michael Smith Laboratories, University of British Columbia, Vancouver, Canada*

ARTICLE INFO

Article history:
Received 1 April 2013
Received in revised form 28 June 2013
Accepted 1 July 2013
Available online 4 July 2013

Keywords:
Membrane chromatography
Computational fluid dynamics
Flow distribution
Zonal rate model
Model-based scale-up

ABSTRACT

Membrane chromatography (MC) is increasingly being used as a purification platform for large biomolecules due to higher operational flow rates. The zonal rate model (ZRM) has previously been applied to accurately characterize the hydrodynamic behavior in commercial MC capsules at different configurations and scales. Explorations of capsule size, geometry and operating conditions using the model and experiment were used to identify possible causes of inhomogeneous flow and their contributions to band broadening. In the present study, the hydrodynamics within membrane chromatography capsules are more rigorously investigated by computational fluid dynamics (CFD). The CFD models are defined according to precisely measured capsule geometries in order to avoid the estimation of geometry related model parameters. In addition to validating the assumptions and hypotheses regarding non-ideal flow mechanisms encoded in the ZRM, we show that CFD simulations can be used to mechanistically understand and predict non-binding breakthrough curves without need for estimation of any parameters. When applied to a small-scale axial flow MC capsules, CFD simulations identify non-ideal flows in the distribution (hold-up) volumes upstream and downstream of the membrane stack as the major source of band broadening. For the large-scale radial flow capsule, the CFD model quantitatively predicts breakthrough data using binding parameters independently determined using the small-scale axial flow capsule, identifying structural irregularities within the membrane pleats as an important source of band broadening. The modeling and parameter determination scheme described here therefore facilitates a holistic mechanistic-based method for model based scale-up, obviating the need of performing expensive large-scale experiments under binding conditions. As the CFD model described provides a rich mechanistic analysis of membrane chromatography systems and the ability to explore operational space, but requires detailed knowledge of internal capsule geometries and has much greater computational requirements, it is complementary to the previously described strengths and uses of the ZRM for process analysis and design.

1. Introduction

Membrane chromatography (MC) is widely used as a purification platform for virus clearance and polishing. Larger pore sizes in membranes (1–1.2 μm) make the mass transfer predominantly convective and permit higher flow rates to be realized at lower pressure drops [1–3]. Recent improvements in membrane surface chemistries have led to higher binding capacities and, consequently, MC is also finding traction in industry as an alternative platform to conventional packed bed chromatography for the purification of complex biomolecules such as, e.g. glycoproteins [4]. In a recent study, Bayer Healthcare has demonstrated a first commercial-scale application of MC in bind and elute mode for blood coagulation factors and has reported a yield improvement of 40% while maintaining high product quality as compared to packed bed chromatography [4]. As MC is becoming increasingly accepted in the biopharmaceutical industry, accurate modeling strategies

* Corresponding author at: IBG-1: Biotechnology, Forschungszentrum Jülich, Wilhelm-Johnen-Straße 1, 52425 Jülich, Germany. Tel.: +49 2461 61 2168; fax: +49 2461 61 3870.
E-mail address: e.von.lieres@fz-juelich.de (E. von Lieres).
[1] Current address: Boehringer Ingelheim, Fremont, USA.

0021-9673/$ – see front matter © 2013 Elsevier B.V. All rights reserved.
http://dx.doi.org/10.1016/j.chroma.2013.07.004

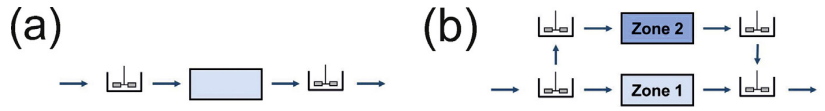

Fig. 1. Representations of (a) the classical one-dimensional Roper and Lightfoot model, and (b) a two zone ZRM configuration for axial flow MC capsules.

have become important for rational process analysis, simulation and design.

MC has traditionally been modeled by only considering the axial coordinate [5–8]. In most of these classic studies, the effects of external hold-up volumes on elution band broadening are accounted for by coupling a plug flow model (PFR) for transport within the membrane stack with one or two continuously stirred tank regions (CSTR) in series to account for mixing and residence times within the extra-column spaces (see Fig. 1a). These one-dimensional models assume flow homogeneity over the entire membrane cross-section, which in practice is hard to achieve due to device design constraints. Lab scale MC capsules often have axial flow configurations, employing a stack of flat membrane sheets. Preparative or pilot-scale capsules usually have radial flow configurations with various winding schemes such as spiral wound, hollow fibers, or pleats. Manifold design is long known to significantly impact on the breakthrough performance of MC capsules [9,10]. In a recent report, we showed that the assumption of flow homogeneity over the entire membrane cross-sections does not necessarily hold for commercially available capsules, and that the resulting inhomogeneous mass flows can cause unwanted tailing of breakthrough curves [11]. The zonal rate model (ZRM), which treats this problem, uniquely de-couples the effects of hydrodynamics and binding on the resulting chromatograms by partitioning the entrance and elution hold-up volumes, as well as the membrane stack, into virtual zones that are modeled as a network of inter-connected CSTRs and PFRs [12,13]. The ZRM is thereby able to quantify non-ideal flows, as well as binding non-idealities, and their contributions to band-broadening, and illustrations of these capabilities were provided through application to the Pall Mustang XT5 (axial flow) and Mustang XT140 (radial flow) capsules. Both capsules exhibit admirable performance attributes, but nevertheless exhibit non-idealities at standard operating conditions. ZRM analysis of the axial-flow XT5 capsule suggested that non-ideal flow in the external hold-up volumes upstream and downstream of the membrane stack, which is consistent with the high aspect ratio of the XT5 capsule, contribute to band broadening. In contrast, the ZRM suggested that structural irregularities in the membrane pleats are the primary source of flow non-idealities in the radial flow XT140 capsule. For both studies, the ZRM was able to quantitatively reproduce breakthrough data, a result that cannot be achieved using traditional membrane chromatography models. Moreover, the existence of varying linear velocities in the radial-flow capsule, as suggested by the ZRM, was consistent with magnetic resonance tomography (MRT) images of the internal capsule, which provided evidence of structural irregularities in the membrane pleats. However, direct evidence of linear flow variations within either capsule was not acquired, making it unclear if the ZRM structure and predictions are correct at the mechanistic level. The current study aims to address this shortcoming through the creation and solution of computational fluid dynamic (CFD) models of the axial and radial membrane chromatography modules described above. Although not widely employed in MC modeling, CFD provides a scale-neutral modeling strategy that is able to independently predict hydrodynamic behavior. Linear velocities as a function of position and breakthrough curves under non-binding conditions may therefore be accurately predicted using only knowledge of internal capsule geometries and basic membrane properties. Moreover, when applied to column loading, CFD simulations provide precise hydrodynamics and thereby allow for unambiguous analysis of the ability of different binding models to reproduce measured breakthrough curves. CFD may therefore be used as a powerful tool for gaining a richer and more accurate understanding of mechanisms contributing to band broadening and their relative importance in different MC devices.

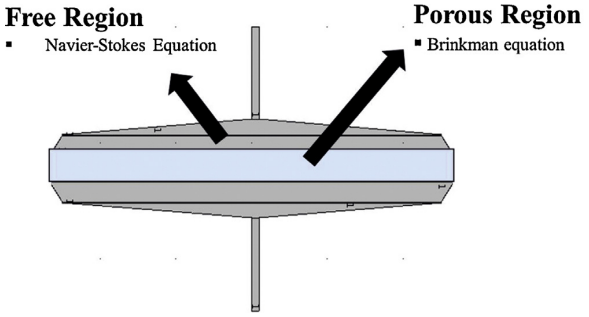

Fig. 2. Longitudinal cross-section of the Pall Mustang XT5 capsule, showing free and porous regions as implemented in the CFD model.

2. Theory

2.1. Computational fluid dynamics

CFD models are based on solution of the fundamental conservation laws of mass, momentum and (sometimes) energy. Mathematically, these laws are described by a set of partial differential equations (PDEs) that have analytical solutions only in a few cases, usually described by rather simple boundary conditions. Hence, numerical methods are required in most applications. In CFD the collective set of PDEs and initial and boundary conditions (the model) is solved to compute fluid flow and related phenomena, such as transport and adsorption of solute molecules.

The system boundaries are defined by the physical geometries of the system, in this case the MC capsules. For example, Fig. 2 shows the internal geometry of a Pall Mustang XT5 capsule. In this capsule, spacer meshes are placed at either sides of the membrane stack. The geometry shown is simplified by omitting these spacer meshes and by considering the membrane stack as one homogeneous region. The model therefore considers the internal geometry as two free regions and one porous region with rotational symmetry. The capsule hold-up volumes before and after the membrane stack constitute the free regions, and the Navier–Stokes equations describe fluid flow in these two regions. The peak Reynolds number within the capsule remains below 5, clearly indicating laminar flow. The incompressible Navier–Stokes equations without external forces are given by Eq. (1) (v denotes the fluid velocity, p the pressure, and μ the kinematic viscosity).

$$\rho\left(\frac{\partial v}{\partial t}+v\cdot\nabla v\right)=-\nabla pI+\nabla\left(\mu(\nabla v+(\nabla v)^T)-\frac{2}{3}\mu(\nabla\cdot v)I\right)+F \tag{1a}$$

$$\nabla\cdot v=0 \tag{1b}$$

The fluid flow within the porous membrane is modeled using Brinkman's equations, considering the membrane stack as a single porous domain with porosity ε and permeability K. Brinkman's equations for this region are given by Eq. (2).

$$\rho\left(\frac{\partial v^*}{\partial t} + v^* \cdot \nabla v^*\right) = -\nabla pI + \nabla\left(\mu(\nabla v^* + (\nabla v^*)^T) - \frac{2}{3}\mu(\nabla \cdot v^*)I\right) - \frac{\mu}{K}v^* + F \tag{2a}$$

$$\nabla \cdot v^* = 0 \tag{2b}$$

The above equations include momentum loss due to shear stress. Here, v^* is the interstitial velocity given by v/ε. No slip conditions, i.e. $v = 0$, are applied at the inner capsule boundaries. A given linear flow rate is specified at the inlet, and vanishing viscous stress is used as the boundary condition at the outlet of the capsule. The velocity field and the pressure profile are continuous, resulting in a stress discontinuity at the interface between the void and porous regions. Membrane movements that might be caused by this stress are not considered this study.

The transport of solute molecules is described by a classic continuity (mass balance) equation, given by Eq. (3).

$$\frac{dc}{dt} = -v\nabla c + D\nabla^2 c - \frac{1-\varepsilon}{\varepsilon}\frac{dq}{dt} \tag{3}$$

In Eq. (3), c and q denote the solute concentrations in the mobile and stationary phases, respectively, v the flow velocity, and D the dispersion coefficient. The velocity vector v in Eq. (3) is taken from the solution of Eq. (1) or Eq. (2), depending on the region (free or porous). The stationary phase concentration, q, is accounted for per unit volume of solid membrane. Possible binding models used to compute q are described in the next section. We have previously shown that axial dispersion within the membrane stack makes a negligible contribution to the total system dispersion [12,14]. D is therefore set to the molecular diffusivity of the protein molecule in water at column operating temperature.

The CFD model is solved in two steps. In the first step, the velocity field and the pressure profile, which are both stationary, are computed by solving the coupled Navier–Stokes and Brinkman equations. In the second step, time-dependent concentration profiles are computed by solving the mass balance equation, based on the previously computed velocity field.

For CFD modeling, the geometry of the XT140 capsule was re-constructed from MRT data using the commercial image processing software CorelDRAW graphics suite. The CFD model is implemented in the commercial software COMSOL multiphysics. COMSOL spatially discretizes the PDE with finite elements and uses a BDF method for time integration. The CFD geometries of both capsules are finely meshed with unstructured triangular elements at a minimum and maximum element size of 0.0001 m and 0.001 m, respectively. Zero solute concentration within the entire system was provided as initial condition, and vanishing viscous stress was used as outlet boundary condition. The direct PARDISO solver is chosen for solving the resulting large linear-equation systems.

2.2. Binding models

Protein adsorption on functionalized membrane is a complex process and several models, accounting for different physical mechanisms, have been published [2]. A review of the general performance of different kinetic models (Langmuir, bi-Langmuir, steric mass action, spreading) can be found in a previous publication [14]. In another publication [11], we compared a ZRM utilizing the kinetic Langmuir model and with one utilizing the spreading model [15,16] to evaluate their ability to reproduce breakthrough data. These same two models will be used in this work. The Langmuir binding kinetics model is given by.

$$\frac{\partial q}{\partial t} = k_a c(q_m - q) - k_d q \tag{4}$$

In Eq. (4), k_a and k_d are the adsorption and desorption rate constants, and q_m is the maximum binding capacity. The Langmuir model assumes single-component interaction with one type of binding site for solute molecules that do not interact with each other.

The spreading model (Eq. (5)) assumes two different bound states due to a re-orientation or re-conformation of the bound molecules. It is given by

$$\frac{\partial \mathrm{q}}{\partial \mathrm{t}} = \frac{\partial \mathrm{q}_1}{\partial \mathrm{t}} + \frac{\partial \mathrm{q}_2}{\partial \mathrm{t}} \tag{5a}$$

$$\frac{\partial q_1}{\partial t} = (k_{a,1}c - k_{12}q_1)(q_m - q_1 - \beta q_2) - k_{d,1}q_1 + k_{21}q_2 \tag{5b}$$

$$\frac{\partial q_2}{\partial t} = (k_{a,2}c + k_{12}q_1)(q_m - q_1 - \beta q_2) - (k_{21} - k_{d,2})q_2 \tag{5c}$$

Here, q_1 and q_2 are the concentrations in bound states 1 and 2, respectively, β is the ratio of the sorbent surface area occupied in state 2 relative to state 1, $k_{a,1}$, $k_{d,1}$, $k_{a,2}$ and $k_{d,2}$ are binding constants, that are defined in analogy to the Langmuir model, and k_{12} and k_{21} describe the rates of state changes.

3. Materials and methods

Bovine serum albumin (A 7638, Sigma–Aldrich Corp, St. Louis, MO, USA) was used in breakthrough experiments at a concentration of 1 g/l and a flow rate of 12 CV/min for both the axial and radial flow MC capsules. The protein was dissolved in 25 mM Tris buffer at pH 8.0 (Sigma–Aldrich, USA) for the loading step. Loading was followed by a washing step with 25 mM Tris buffer at pH 8.0. Then, 1 M NaCl in 25 mM Tris buffer pH 8.0 was used to elute the bound BSA from the membranes. The units were cleaned with 1 N NaOH after each run, as specified by the manufacturer. In a revised protocol, the cleaning step was performed with 1 M NaCl instead of 1 N NaOH.

Mustang Q XT5 anion-exchange membrane chromatography capsules (axial flow) and Mustang Q XT140 anion-exchange membrane chromatography capsules (radial flow) were purchased from Pall Inc. (East Hills, NY, USA) (see Fig. 12). Both capsules contain modified hydrophilic polyethersulfone (PES) membranes whose surfaces are coated with a cross-linked polymer that contains pendant Q groups. The effective bed height of the membrane stack in either capsule is 2.20 mm. The pore size and porosity ε of the membrane are 0.8 μm and 0.70 ± 0.05, respectively (manufacturer data). Internal dimensions were manually measured by opening the capsules. The total hold-up volume of the XT5 capsule was calculated to be 6 ml from the weight difference between a dry capsule and a capsule filled with water. Due to the symmetry of the capsule, the hold-up volumes before and behind the membrane are assumed to be 3 ml each. The XT140 capsule has hold-up volumes of 105 ml before and 45 ml after the membrane (manufacturer data). In addition, an experimental 9.4 T magnetic resonance tomography (MRT) device was used to measure internal geometries.

The XT5 capsule was attached to an ÄKTAexplorer system that was controlled by the Unicorn software (GE Healthcare, Uppsala, Sweden). The XT140 capsule was attached to an ÄKTAprocess system that was controlled by the Unicorn software (GE Healthcare, Uppsala, Sweden).

Table 1
Model parameters employed in the CFD simulations.

Parameter	Value
Density, ρ [kg/m^3]	1×10^3
Viscosity, μ [Pa·s]	1×10^{-3}
Permeability, k [m^2]	1×10^{-13}
Porosity, ε	0.7
Dispersion coefficient, D [m^2/s]	7.13×10^{-9}

4. Results and discussion

4.1. Model assumptions and parameters

Strict mechanistic CFD simulations require one to model the entire physical dimensions of the membrane chromatography capsules under study. A full 3D simulation, including all physical complexities, with the available hardware and software (COMSOL on a shared memory machine with 16 compute cores and 128 GB memory) would therefore be a challenging endeavor due to the expense and long duration. Hence, judicious modeling assumptions were made to reduce the computational effort with minimal impact on the accuracy of the model in reflecting the real device:

1. For the XT5 capsule, rotational symmetry was assumed, allowing the CFD model to be transformed into cylindrical co-ordinates, which reduces the model to 2D. This simplification effectively assumes that the small capsule spacers do not contribute significantly to band broadening.
2. For the XT140 capsule, we previously showed that a single virtual zone along the axial coordinate was sufficient to quantitatively predict breakthrough performance with the ZRM. Hence, the CFD model is set-up for a 2D cross-section, perpendicular to the axial coordinate, which again reduces the model to 2D.
3. For either capsule, the membranes were considered static, and possible movements under dynamic conditions were not considered.

We will show below that these assumptions are reasonable for their respective capsule, so that quantitative predictions of experimental behavior are achieved. The physical parameters of the CFD model are provided in Table 1.

4.2. Analysis of an axial-flow MC system

CFD model results were compared to experimental breakthrough curves and to ZRM results reported previously [11] with the aims of both identifying the hydrodynamic and binding mechanisms leading to band broadening, and determining if the ZRM properly captures those non-idealities and their underlying causes. For these studies, replacement of 1 N NaOH with 1 M NaCl in the cleaning protocol and reducing exposure to the storage buffer was found to be crucial for achieving reproducible well-behaved experimental breakthrough curves.

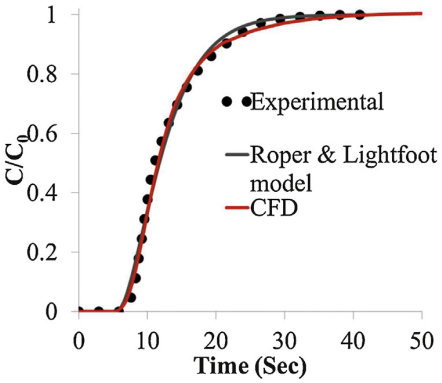

Fig. 3. Comparison of simulation using the Roper and Lightfoot model, CFD simulated and measured breakthrough curve for bovine serum albumin loaded under non-binding conditions on the XT5 capsule.

4.2.1. Non-binding conditions

First, a forward simulation was performed with the CFD model of the XT5 capsule, assuming no adsorption in the porous domain. This ab initio simulation was solely based on the capsule geometry and parameters in Table 1. A dead time of 3 s was added to the solution in order to account for a combined plug-flow dead time in the tubing and in the Äkta system. The CFD simulated breakthrough curve closely matches experiment (see Fig. 3), which illustrates the accuracy of the CFD model, including the aforementioned assumptions that reduced the order to a 2D geometry, we observed in predicting breakthrough for non-binding conditions.

Our CFD simulations of the velocity field in the membrane stack of the XT5 capsule (Fig. 4b) show a near constant linear velocity throughout the membrane stack, which implies ideal flow in this region. Non-ideal flow leading to a distribution of residence times is predicted in the hold-up volumes before and behind the membrane stack, and the CFD simulations reveal that this non-ideality is caused by the geometry and high aspect ratio of the capsule.

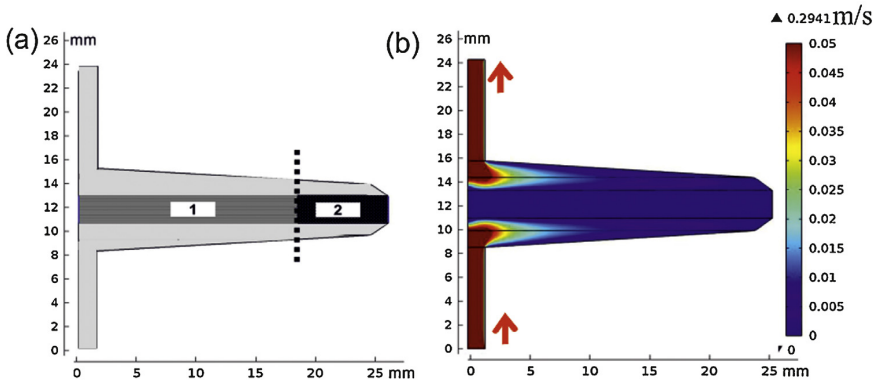

Fig. 4. (a) Definition of central region (1) and outer region (2) in the CFD geometry of the XT5 capsule. Each region occupies 50 percent of the frontal surface area of the membrane stack. (b) CFD simulation of the magnitude of the velocity field inside the XT5 capsule.

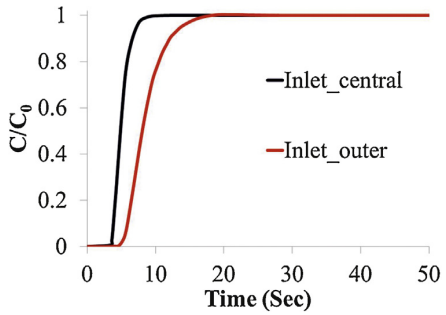

Fig. 5. Averaged inlet side boundary concentration at the central and outer regions of the membrane (as defined in Fig. 4a) in the CFD simulation of the XT5 capsule under non-binding conditions.

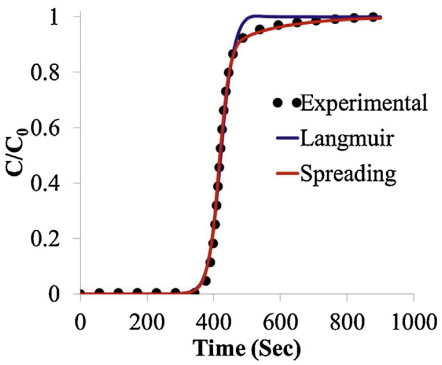

Fig. 6. Best fit of various forms of the CFD model to breakthrough curves for bovine serum albumin loaded onto the XT5 capsule. CFD results are shown when either the Langmuir or spreading model for protein binding is employed.

Fig. 4a shows a virtual segmentation of the XT5 capsule into two regions, each of which occupies 50% of the frontal surface area of the membrane stack, and Fig. 5 shows the CFD simulated average boundary concentrations at the inlet side of the membrane in these two regions. One can clearly see that the inner and outer boundary concentration profiles differ not only in the time when the concentration front initially reaches the membrane, but also in the initial slope and in the subsequent tailing. The flux through the outer region is delayed and more dispersive, due to an increased residence time in a larger fraction of the hold-up volume on the inlet side of the membrane, and the same mechanism is active in the hold-up volume on the outlet side. The CFD simulations therefore provide a detailed snapshot of flow patterns and sources of non-uniform solute residence times at resolutions that cannot be achieved by standard MC modeling approaches.

Flow non-idealities in the extra-membrane volumes are specifically addressed by the ZRM, and in accordance with CFD results a symmetric two-zone configuration of the ZRM (Fig. 1b) was required to accurately reproduce measured breakthrough data for the XT5 capsule. The validity of the ZRM at the mechanistic level can be further evaluated by comparing the CFD computed and ZRM predicted hold-up volumes and mass flows through each of the outer and central regions. In the CFD simulations, the hold-up volumes upstream of the central membrane region (1) and outer membrane region (2) sum to the total upstream distributor volume (they are 1.90 ml and 1.10 ml, respectively), as shown in Fig. 4a. The corresponding upstream inner and outer CSTR volumes used in the ZRM are best-fit values (1.69 ml and 1.24 ml, respectively). While not required or expected to be identical to the partitioning of the XT5 capsule in the CFD analysis shown in Figs. 4a and 5, the ZRM CSTR volumes are similar to those volumes. They reflect the sizes of corresponding CSTRs needed to match both the mass flows and average solute residence times through each zone of the device. In the CFD simulation, 57% of the total mass passes though the central membrane zone, while the remaining 43% passes through the outer region. The ZRM predicts this result essentially exactly (57% and 43%, respectively).

These results therefore show that ZRM analysis of the XT5 capsule, though not as rigorous as CFD, does not just provide a good correlative fit, but reveals real and important properties of the physical system without requiring knowledge of the actual system geometry. In particular, the ZRM provides reliable information on the percentage of the entering mass flow that cannot be treated as an ideal plug passing through the stack (and thus whose breakthrough would not obey classic MC models). It likewise provides a reliable estimate of the elution band broadening caused by the increased residence times of mass elements passing through the outer zone(s). The more rigorous CFD simulations obviously provide this and more information as well, but with considerably more computational effort and time.

4.2.2. Binding conditions

The CFD model was next combined with either the Langmuir or spreading model to simulate breakthrough under load (binding) conditions. The parameters of either binding model were estimated by fitting CFD simulations to measured breakthrough curves for BSA (Tables 2 and 3). Fig. 6 shows the best fit of each CFD model to a breakthrough curve for BSA loaded at a flow rate of 12 CV/min.

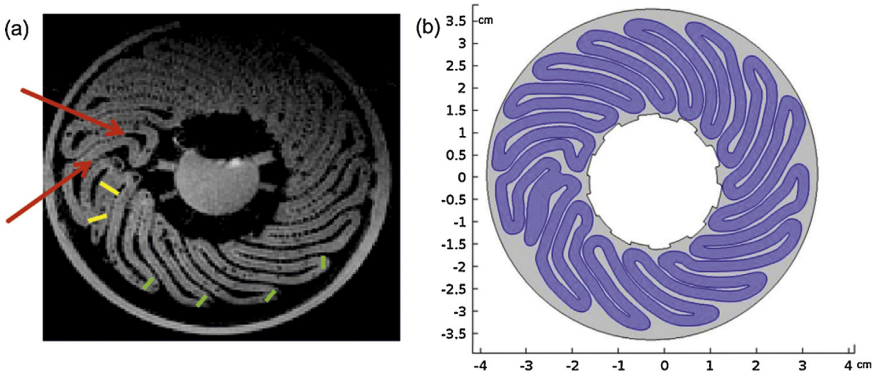

Fig. 7. (a) cross-sectional MRT scan of the XT140 capsule. The membrane pleats are clearly visible in gray, due to their water content and irregularities shown in different colors, (b) 2D CFD geometry reconstructed from the MRT image.

Table 2
Parameters of the Langmuir model, as determined by fitting the corresponding Roper and Lightfoot model (RLM), CFD and ZRM simulations to a binding breakthrough curve of the XT5 capsule. The ZRM related parameter values are taken from a previous publication [11].

Parameter	CFD	ZRM	RLM
k_a [l/(g·s)]	6.434×10^{-2}	6.4×10^{-2}	6.13×10^{-2}
k_d [1/s]	6×10^{-3}	6×10^{-3}	7.2×10^{-4}
q_m [g/l]	278.19	284.04	284.83

Table 3
Parameters of the spreading model, as determined by fitting the corresponding Roper and Lightfoot model (RLM), CFD and ZRM simulations to a binding breakthrough curve of the XT5 capsule. The ZRM related parameter values are taken from a previous publication [11].

Parameter	CFD	ZRM	RLM
k_{a1} [l/(g·s)]	8.073×10^{-2}	8.08×10^{-2}	8.37×10^{-2}
k_{d1} [1/s]	1.06×10^{-5}	1.06×10^{-5}	0.82×10^{-5}
k_{12} [l/(g·s)]	11.08×10^{-4}	7.37×10^{-4}	10.67×10^{-4}
k_{21} [1/s]	10.01×10^{-3}	9.41×10^{-3}	13.45×10^{-3}
q_m [g/l]	286.56	289.003	289
β	1.15617	1.144	1.166

CFD simulations using the Langmuir model fail to reproduce the observed tailing of the breakthrough curve near sorbent saturation, indicating non-ideal binding mechanisms contribute to broadening of BSA breakthrough, even though the CFD model accurately describes the hydrodynamics in the XT5 capsule. The spreading model accurately captures these non-idealities, and when combined with the accurate hydrodynamics provided by CFD results in an excellent representation of the true breakthrough curve.

It is important to note here that using the classical Roper and Lightfoot model along with the spreading isotherm also regresses to the binding breakthrough curve well (data not shown). However, the parameters of the binding models are different when estimated using the Roper and Lightfoot model, because the description of non-ideal flow is then lumped into the binding model. Hence, these parameters cannot be used for predicting the performance of different capsules with the same membrane but changed hydrodynamics (model-based scale-up), as will be further discussed in Section 4.3.2. The binding parameters obtained through CFD-based parameter estimation are summarized in Tables 2 and 3. The parameters previously obtained through ZRM analysis and using the classical Roper and Lightfoot model are also tabulated for comparison. The binding parameter sets are quite similar in both cases, even though different flow models and independent optimization algorithms have been used.

The same set of initial parameters was used for the CFD and ZRM models. However, the CFD based optimization of the spreading model took 2 weeks on 4 compute cores, whereas the ZRM based optimization took only 10 min on one compute core. Hence, though the CFD method is more information rich, the reduced computational complexity of the ZRM can be a big advantage when different binding models need to be evaluated for suitability.

4.3. Analysis of an radial-flow MC system

A similar analysis was conducted on the larger radial-flow MC device to identify differences in hydrodynamics and sources of flow non-ideality, and to assess the fundamental value of the ZRM when applied to this configuration [11].

4.3.1. Non-binding conditions

Fig. 7a shows an MRT image at an internal axial position of the XT140 capsule. Although most pleats are similarly structured, certain differences in folded pleat can be observed; some specific structural irregularities are marked in the figure. The pleats indicated by red arrows have larger cross-sectional areas as compared to average pleats. The sealing region, which is the start and end point of the winding process (yellow bars), is thicker than the rest of the pleats. Finally, some pleats are broadened at the outer loops (green bars). A CFD geometry that accounts for all of these structural irregularities was reconstructed from the MRT image using COREL draw, as shown in Fig. 7b. The porosity in the membrane region was increased within the outer loops in order to maintain a constant average membrane volume (however, no impact of these porosity variations on the simulated chromatograms could be observed, data not shown). A two-dimensional CFD model was thereby achieved with the hold-up volumes upstream and downstream of the membrane set at their experimental values of 62 ml and 36 ml, respectively. Due to additional channels, the XT140 capsule has total hold-up volumes of 105 ml and 45 ml. The residual hold-up volume upstream of the membrane is accounted for by a CSTR before the CFD model with average residence time $\tau = (105–65)/28 = 1.53$ s. The protein concentration $C_{CFD,in}$ at the model capsule inlet is then given by

$$C_{CFD,in} = C(1 - e^{-t/\tau}) \quad (6)$$

Similarly the output of the CFD simulation is connected with a second CSTR in order to model the remaining downstream hold-up volume with average residence time $\tau = (45–36)/28 = 0.32$ s:

$$\frac{dc}{dt} = \frac{C_{CFD,out} - c}{\tau} \quad (7)$$

First, a forward simulation was performed with this CFD model of the XT140 capsule, assuming no binding in the porous domain. A dead time of 7.5 s was added to the solution in order to account for a plug flow in the tubing of the Äkta system. Fig. 8 shows the predicted breakthrough curve, which closely matches the experimental data. The stationary velocity profile in the XT140 capsule will be discussed in next section, as the solute residence times in the membrane are very small under non-binding conditions. Hence, structural irregularities hardly impact on the simulated breakthrough curves. This was also observed in the ZRM analysis of the same capsule [11], where a one-zone configuration was able to accurately correlate with the experimental non-binding curve. However, below we show that the widely accepted practice of using non-binding breakthrough data, alone, is not sufficient to quantify flow inhomogeneities and then predict breakthrough in large-scale MC capsules.

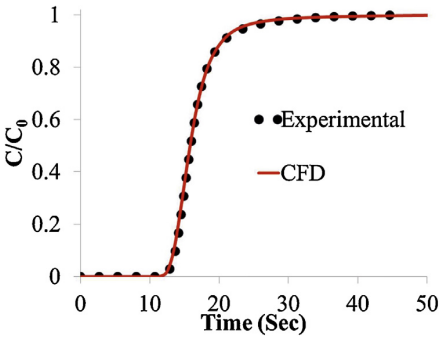

Fig. 8. Comparison of CFD simulation to measured breakthrough curve of XT140 capsule under non-binding conditions.

4.3.2. Binding conditions

In Section 4.2.2, we showed that CFD simulations employing the spreading model accurately reproduce BSA breakthrough from the axial-flow XT5 capsule. As a more powerful illustration of the

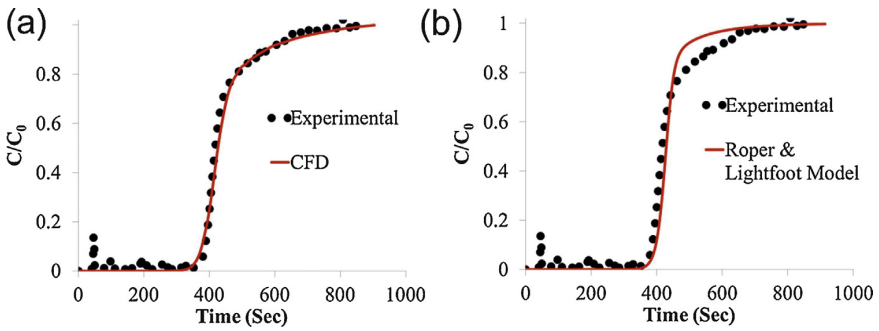

Fig. 9. Comparison of measured breakthrough data of the XT140 capsule under binding conditions and of model-based predictions, computed with parameters of the spreading model that have been estimated from breakthrough data of the XT5 capsule. The hydrodynamics in both capsules was modeled using (a) the CFD model, and (b) the classical Roper and Lightfoot model.

value of CFD modeling, truly predictive simulation of breakthrough from the larger scale and altered geometry (radial flow) XT140 MC capsule was performed by transferring the binding parameters estimated from data for the XT5 capsule to a CFD model of the XT140 capsule; an attempt to predict the breakthrough curve under binding conditions was then made. As shown in Fig. 9a, the result of this simulation, for which no model parameters measured directly on the XT140 device (basic device geometry values excepted) were used, matches the experimental data very well. Due to the careful decomposition of scale-dependent flow non-idealities and scale-independent binding non-idealities, both the initial increase and the tailing of the breakthrough curve are accurately predicted. For comparison, the same model-based scale-up was attempted using the Roper and Lightfoot model. As shown in Fig. 9b, this approach fails to quantitatively predict the experimental data, which further underlies the importance of carefully separating the impact of non-idealities that are related to binding and hydrodynamics.

In addition to its predictive power, the CFD model provides a wealth of mechanistic information related to causes of band-broadening as well. For example, Fig. 10 reports magnitudes of the velocity field within the cross-section of the XT140 capsule. The fluid enters radially at the outer boundary of the capsule, passes through the curved membrane pleats, and exits through channels at the inner capsule boundary. Variations in fluid velocity are predicted in the void regions upstream and downstream of the membrane, with the largest gradients occurring upstream of the folded regions of the membrane. This suggests the added membrane surface area and throughput provided by the pleat design may come at the expense of non-ideal fluid hydrodynamics. Moreover, in contrast to the XT5 capsule, the fluid velocity is not constant within the porous membrane. Instead, based on velocities,

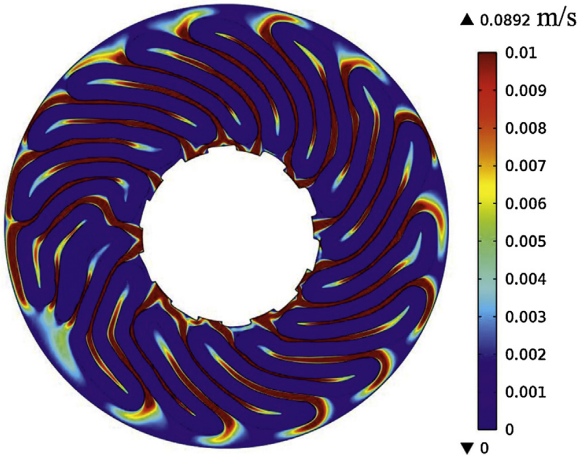

Fig. 10. CFD simulation of the magnitude of the velocity field inside the XT140 capsule.

the membrane volume can by roughly split into two sub-regions (Fig. 11a). The first sub-region, which covers approximately 15% of the total membrane area and mainly comprises the sealing (inner) and the outer membrane bends, is characterized by fluid velocities less than 85% of the average. In the larger sub-region, mainly covering the linearly configured pleat centers, velocities are more uniform and close to (within 15% of) the average.

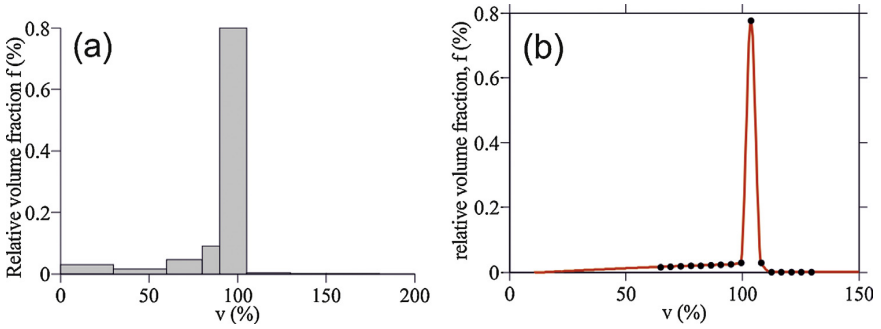

Fig. 11. Distribution of the volumetric flow relative to the total volumetric flow, *f*, over the corresponding linear velocity relative to the average linear velocity, *v*: (a) velocity distribution obtained from the CFD analysis of the XT140 capsule, (b) velocity distribution obtained from the ZRM analysis of the XT140 capsule, taken from previous publication [11].

Fig. 12. The XT5 and XT140 capsules as bought from the vendor. A 2 Euro coin is included for size comparison.

In contrast, we recently reported that direct application of the ZRM to model-based scale-up failed for the Pall Mustang XT140 capsule [11] because, unlike with the CFD model, linear velocity variations within the membrane pleats could not be determined from non-binding data. Instead, the velocity distribution used in the ZRM was calibrated to breakthrough data collected under binding conditions. That distribution is shown in Fig. 11b and can be approximated and parameterized by an initial linear increase with given slope and a Gaussian peak with given center and width. Based on that distribution, we were able to define a multi-zone configuration of the ZRM capable of modeling breakthrough curve shape with good accuracy [11]. Notably, the velocity distribution estimated by best fit of the ZRM to breakthrough data under binding conditions is nearly identical to that predicted from first principles by our CFD analysis of the XT140 capsule (see Fig. 11a). Thus, the ZRM, once calibrated, can be employed to properly understand hydrodynamics and predict the breakthrough performance at different operating conditions and for different molecules in much shorter compute times, as compared to the CFD approach. Knowledge of the internal capsule geometry is not required. The two modeling approaches are therefore complementary, with the CFD model serving to provide a comprehensive analysis of system hydrodynamics and sources of band broadening, and thus a rational basis for improving capsule design, and the ZRM providing a reliable and rapid method for simulating process operation and screening for optimal operating conditions.

5. Conclusions and outlook

Ideal hydrodynamics behavior is hard to achieve in membrane chromatography capsules at all scales for various reasons, and traditional modeling approaches cannot capture non-ideal flow. The zonal rate model (ZRM) has been originally developed as a semi-empirical approach for independently quantifying the impacts of non-ideal flow and non-ideal binding in membrane chromatography capsules. In the ZRM, the physical capsule geometry is virtually partitioned into zones that are approximately homogeneous. In a previous publication [11], the ZRM was applied for analyzing Pall Mustang XT5 and Mustang XT140 capsules. The high length-to-width ratio of the XT5 capsule was concluded to cause non-ideal flow due to flow paths of different lengths, while irregular pleats in the XT140 capsule were hypothesized to cause non-ideal flow due to different linear velocities though the membrane stack.

In the current contribution, mechanistic CFD models are employed to independently validate and confirm the assumptions and hypotheses, which were developed in the previous ZRM analyses. CFD modeling is based on the exact capsule geometries. Both models, for the XT5 and XT140 capsules, could be reduced to 2 spatial dimensions, in order reduce computation requirements. The stationary velocity profile, computed for the XT5 geometry, shows that the central membrane region receives a different inflow than the peripheral membrane region, due to the great width of the capsule. Hence, the assumption of two parallel zones in the corresponding ZRM configuration is not only reasonable, but also required. In full agreement with ZRM results, the spreading model for protein binding was found to describe the experimental binding breakthrough curve much better than the traditional Langmuir model. The stationary velocity profile, computed for the XT140 geometry, shows that a small fraction of the membrane area, mainly the sealing and bend regions, have significantly reduced velocity magnitudes. This velocity reduction explains the strong tailing observed in the experimental breakthrough curves of this capsule. The distribution of flow magnitudes throughout the membrane can be described and parameterized by a combination of linear and Gaussian functions. The ZRM configuration with varying linear velocities, introduced in a previous publication [11], is therefore proven to be most adequate to capture the impact of hydrodynamics in the XT140 capsule.

The CFD simulations in this contribution do not only provide a quantitative validation of the ZRM, but can also accurately predict non-binding breakthrough curves of the XT5 and XT140 capsules. Moreover, a CFD model of the XT140 capsule was able to precisely predict the measured binding breakthrough curve, based on binding parameters obtained from an analysis of the XT5 capsule, thereby providing a method for model-based scale-up. The fundamental knowledge obtained about hydrodynamics can also potentially lead to improvement in capsule design. On the other hand, CFD simulations are computationally expensive and time consuming, which hinders their routine application in dynamic process analysis and design of experiments. The ZRM, conversely, provides a much faster modeling approach and, as substantiated by the present contribution, not only accurately describes the impact of hydrodynamics, but also reflects physical properties of the studied capsules. Therefore, both the ZRM and CFD modeling approaches have great potentials to be used as tools in process analysis and capsule design. Future work will address ZRM and CFD analyses of different capsules from other vendors, and of different molecules and operating conditions.

Acknowledgements

The presented work was supported by the Cluster for Industrial Biotechnology (CLIB) with a doctoral scholarship for Pranay Ghosh, as well as by NSERC, the Natural Sciences and Engineering Research Council of Canada. The authors wish to thank Birgit Stute, Andreas Püttmann and Sebastian Schnittert for their valuable inputs and help throughout this work.

References

[1] F.T. Sarfert, M.R. Etzel, J. Chromatogr. A 764 (2000) 1.
[2] S.Y. Suen, M.R. Etzel, J. Chromatogr. A 686 (1994) 2.
[3] E. Klein, J. Membr. Sci. 179 (2000) 1.
[4] J.H. Vogel, H. Nguyen, R. Giovannini, J. Ignowski, S. Garger, A. Salgotra, Biotechnol. Bioeng. 109 (2012) 12.
[5] D.K. Roper, E.N. Lightfoot, J. Chromatogr. A 702 (1995) 1.
[6] C. Boi, J. Chromatogr. B 848 (2007) 1.
[7] S. Dimartino, C. Boi, G.C. Sarti, J. Chromatogr. A 1218 (2011) 13.

[8] J. Wang, F. Dismer, J. Hubbuch, M. Ulbricht, J. Membr. Sci. 320 (2008) 1.
[9] R. Ghosh, T. Wong, J. Membr. Sci. 281 (2006) 1.
[10] A. Tejeda, J. Ortega, I. Magaña, R. Guzmán, J. Chromatogr. A 830 (1999) 293.
[11] P. Ghosh, K. Vahedipour, M. Lin, J.H. Vogel, C.A. Haynes, E. von Lieres, Biotechnol. Bioeng. 110 (2013) 4.
[12] P. Francis, E. von Lieres, C.A. Haynes, J. Chromatogr. A 1218 (2011) 31.
[13] E. von Lieres, J. Wang, M. Ulbricht, Chem. Eng. Technol. 33 (2010) 6.
[14] P. Francis, E. von Lieres, C.A. Haynes, Biotechnol. Bioeng. 109 (2012) 3.
[15] H. Yang, M.R. Etzel, Ind. Eng. Chem. Res. 42 (2003) 4.
[16] A.J. Clark, A. Kotlicki, C.A. Haynes, A.L. Whitehead, Langmuir 23 (2007) 10.

3.2 Publication IV

"Model-based analysis and quantitative prediction of membrane chromatography: Extreme scale-up from 0.08ml to 1200 ml"

(Journal of Chromatography A, 1332 (2014) 8–13)

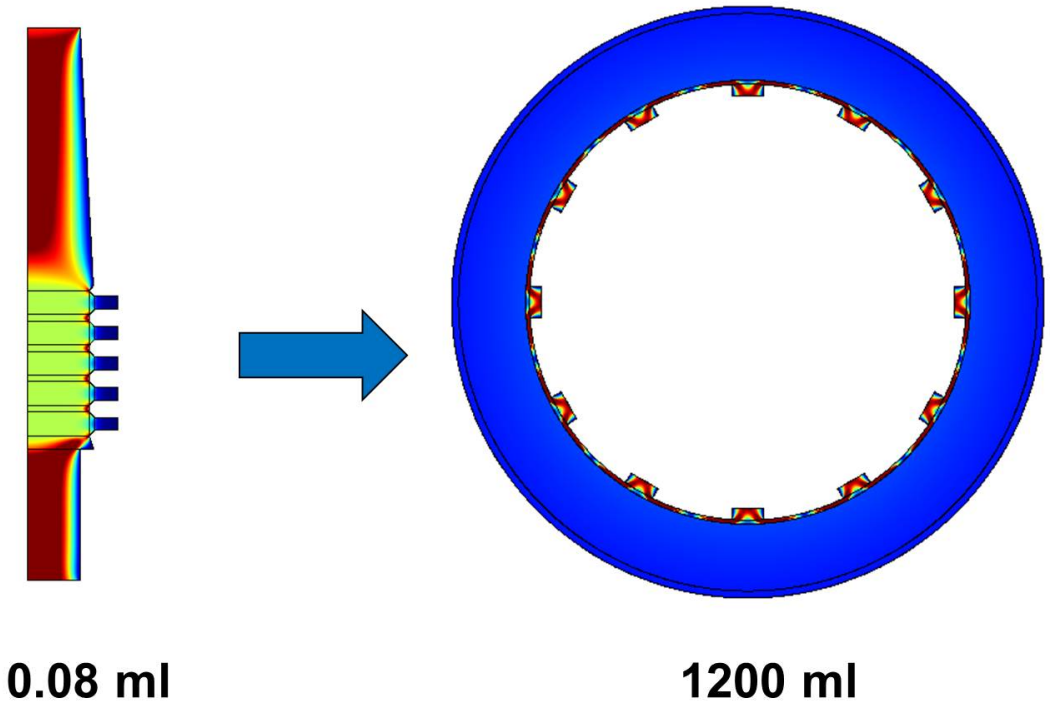

Pranay Ghosh, Kaveh Vahedipour, Martin Leuthold, Eric von Lieres

Journal of Chromatography A, 1332 (2014) 8–13

Contents lists available at ScienceDirect

Journal of Chromatography A

journal homepage: www.elsevier.com/locate/chroma

Model-based analysis and quantitative prediction of membrane chromatography: Extreme scale-up from 0.08 ml to 1200 ml

Pranay Ghosh[a], Kaveh Vahedipour[b], Martin Leuthold[c], Eric von Lieres[a,*]

[a] *IBG-1: Biotechnology, Forschungszentrum Jülich, Germany*
[b] *INM-4: Medical Imaging, Forschungszentrum Jülich, Germany*
[c] *Sartorius Stedim Biotech GmbH, Göttingen, Germany*

ARTICLE INFO

Article history:
Received 25 November 2013
Received in revised form 14 January 2014
Accepted 16 January 2014
Available online 24 January 2014

Keywords:
Membrane chromatography (MC)
Scale-up
Modeling
Prediction
Computational fluid dynamics (CFD)

ABSTRACT

A model-based approach is presented for quantitatively decoupling the impacts of non-ideal flow and non-ideal binding in membrane chromatography (MC) capsules at different scales. The internal geometry of Sartobind® capsules with 0.08 ml and 1200 ml membrane volume is reconstructed from MRI measurements and manufacturer data. Based on this information, computational fluid dynamics (CFD) simulations are used for computing internal flow patterns of both capsules. Measured breakthrough curves (BTC) under non-binding conditions are used for calibrating PFR and CSTR models of the holdup volumes in the Äkta systems. A suitable binding model is determined and the binding parameters are estimated from binding BTC data of the 0.08 ml capsule. Due to the decoupling of non-idealities, the binding parameters can be directly transferred between the CFD models of both capsules. This advantage is used for quantitatively predicting BTC data of the 1200 ml capsule under binding conditions. The model-based prediction excellently matches with independently measured BTC data, facilitating an extreme scale-up factor of 15,000. The presented approach has previously been shown to be universally applicable to capsules from other vendors with different flow configurations and membrane types.

1. Introduction

Biopharmaceutical Industry, today, faces a formidable challenge in catering to the ever increasing worldwide demand of therapeutic drugs. There is an immense pressure on manufacturing facilities to increase production capacities. Currently, bioreactors with capacities of 10,000 l and higher are in operation to meet demands, and consequently, large quantities of culture harvest are produced in batch operations. Therapeutic drugs, such as proteins and enzymes, usually have rather low titers in the culture harvest. For recombinant products such as glycoproteins, product concentrations are usually in the order of μg/l [1]. Furthermore, biomolecules tend to loose activity when kept longer in the culture harvest environment. Hence, the design of downstream processes faces a two-fold challenge, namely (a) reduction of the large process volume and, (b) fast isolation of the product.

In the past decade, membrane chromatography (MC) was commercialized for facing these challenges. MC devices exhibit lower pressure drops and can be operated at higher flow-rates, as compared to packed bed chromatography. MC allows to process more culture harvest at reduced mass transfer limitations, leading to faster product removal [2–4]. Today, MC has found usage in capture as well as polishing steps [5–9].

MC devices are often characterized by the shape of their breakthrough curves (BTC). Generally, BTC shapes are not only governed by adsorption kinetics within the functionalized membranes but also by fluid hydrodynamics in the holdup volumes of the MC capsules [10]. Manufacturers are today optimizing the design of MC capsules such as to obtain BTC that are as sharp as possible, in order to minimize buffer consumption and to maximize utilized membrane capacity. This requires in-depth understanding of both protein adsorption and fluid flow mechanisms. Model-based approaches have been shown to be helpful in analyzing and optimizing equipment design. We have previously developed a computational fluid dynamics (CFD) based modeling approach that was able to aid in fundamental understanding and quantitative prediction of fluid flow within membrane chromatography capsules [11]. A mechanistic decoupling from the impact of non-ideal fluid flow on observed BTC allowed the independent selection and calibration of appropriate binding models for describing protein adsorption on the studied membranes. Consequently, the binding parameters determined from BTC analysis of lab scale MC capsules could be successfully transferred into different CFD models for quantitatively predicting the BTC of production scale MC capsules.

* Corresponding author at: IBG-1: Biotechnology, Forschungszentrum Jülich, Wilhelm-Johnen-Straße 1, 52425 Jülich, Germany. Tel.: +49 2461 61 2168; fax: +49 2461 61 3870.
E-mail address: e.von.lieres@fz-juelich.de (E. von Lieres).

0021-9673/$ – see front matter © 2014 Elsevier B.V. All rights reserved.
http://dx.doi.org/10.1016/j.chroma.2014.01.047

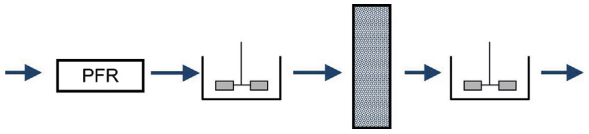

Fig. 1. Traditional modeling approach, based on a serial arrangement of PFR, CSTR and functionalized membrane.

Previous work allowed to scale-up the behavior of different proteins from 5 ml to 140 ml MC capsules, i.e. scale-up factors of 28 [11,12]. However, MC devices are further miniaturized in order to save valuable material and time in process development. Hence, in this study the same model-based approach is applied for comprehensively analyzing MC at an extremely small scale, Sartorius Pico capsule with 0.08 ml bed volume, and directly transferring the identified binding mechanism and parameters for quantitatively predicting the performance of a commercial scale purification platform with 1.2 l bed volume, notably, with a scale-up factor of 15,000.

2. Theory

2.1. Traditional model

Traditionally, mass transfer in MC devices has been modeled by semi-empirical approaches, based on a serial arrangement of a plug flow region (PFR), continuously stirred tank regions (CSTR) and a membrane region, as illustrated by Fig. 1 [13–16]. This model is introduced to compare our CFD simulations with. The fluid flow is considered perfectly homogeneously distributed over the inlet side of the membrane, whose interior is described by a customary mass balance equation, Eq. (1):

$$\frac{\partial c}{\partial t} + v\frac{\partial c}{\partial z} = D_a\frac{\partial^2 c}{\partial z^2} + \frac{(1-\varepsilon)}{\varepsilon}\frac{\partial q}{\partial t} \tag{1}$$

Here, c and q are the solute concentrations in the mobile and stationary phases, respectively, v is the flow velocity, D_a is the axial dispersion coefficient, and $\partial q/\partial t$ denotes the rate of adsorption or desorption of solute molecules to or from the membrane surface. Axial dispersion in the membrane stack has been earlier shown to contribute negligibly to overall system dispersion [17,18] and, hence, D_a can be replaced by the molecular diffusion coefficient. System dispersion is mainly caused by holdup volumes in the MC capsules upstream and downstream of the membrane stack. These regions are described by CSTR, Eq. (2):

$$\frac{\partial c^{CSTR}}{\partial t} = \frac{c_{in}^{CSTR} - c^{CSTR}}{\tau} \tag{2}$$

Here c_{in}^{CSTR} and c^{CSTR} are the solute concentrations at the CSTR inlet and outlet, respectively, $\tau_{CSTR} = V_{CSTR}/Q$ is the average residence time of solute molecules, V_{CSTR} is the CSTR volume, and Q is the volumetric flow rate. An additional time lag, not associated with system dispersion, for example due to the tubing, is described by a PFR, Eq. (3):

$$c_{out}^{PFR}(t) = \begin{cases} 0 & t < \tau_{PFR} \\ c_0 & t \geq \tau_{PFR} \end{cases} \tag{3}$$

Here, $\tau_{PFR} = V_{PFR}/Q$ is the ratio of the PFR volume to the volumetric feed flow rate. The traditional model was implemented in MATLAB, using finite volumes and the time integrator *ode15s* for solving the differential equations and the optimizer *lsqnonlin* for estimating model parameters from BTC data.

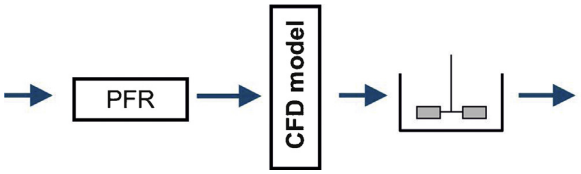

Fig. 2. CFD model combined with PFR and CSTR for describing system dispersion caused by holdup volumes that are external to the MC capsule.

2.2. CFD model

The CFD based modeling approach has been previously described in [11]. Fluid flow in the holdup volumes upstream and downstream of the membrane stack is described by the classical Naviers-Stokes equations, Eqs. (4)–(5), under the conditions of laminar, incompressible flow and without external forces:

$$\rho\left(\frac{\partial v}{\partial t} + v\cdot\nabla v\right) = -\nabla p + \nabla(\mu(\nabla v + (\nabla v)^{\mathrm{T}})) \tag{4}$$

$$\nabla\cdot v = 0 \tag{5}$$

Here, v denotes the fluid velocity, p the pressure, ρ is the fluid density and μ the kinematic viscosity. The Brinkman equations, Eqs. (6)–(7), under the conditions of laminar, incompressible flow and without external forces, describe fluid flow through the membrane stack, accounting for a loss of momentum in the porous domain:

$$\rho\left(\frac{\partial v^*}{\partial t} + v^*\cdot\nabla v^*\right) = -\nabla p + \nabla(\mu(\nabla v^* + (\nabla v^*)^{\mathrm{T}})) - \frac{\mu}{K}v^* \tag{6}$$

$$\nabla\cdot v^* = 0 \tag{7}$$

Here, $v^* = v/\varepsilon$ is the interstitial velocity, ε is the membrane porosity, and K is the membrane permeability. No slip conditions, i.e. $v = 0$, are applied at the inner capsule boundaries. A given linear flow rate is specified at the inlet, and vanishing viscous stress is used as the boundary condition at the outlet of the capsule.

The transport of solute molecules is described by mass balance equations in the free holdup volumes by, Eq. (8), and in the porous membrane domain, Eq. (9):

$$\frac{\partial c}{\partial t} = -v\nabla c + D\nabla^2 c \tag{8}$$

$$\varepsilon\frac{\partial c}{\partial t} = -\varepsilon v\nabla c + \varepsilon D\nabla^2 c - (1-\varepsilon)\frac{\partial q}{\partial t} \tag{9}$$

Here, v and v^* are the velocity fields computed by solving Eqs. (6)–(7) in the membrane stack together with Eqs. (4)–(5) in the holdup volumes. The CFD model describes fluid flow and mass transport only in the MC capsule. Additional time-lag and dispersion due to the tubing and holdup volumes of the Äkta system are described by a PFR and CSTR combination, as illustrated by Fig. 2. The CFD model was implemented and solved using the multiphysics software COMSOL.

2.3. Binding models

The Langmuir model, Eq. (10), and the spreading model, Eq. (11), are compared with respect to their ability of quantitatively describing the binding of bovine serum albumin (BSA) on the studied membrane.

$$\frac{\partial q}{\partial t} = k_a c(q_m - q) - k_d q \tag{10}$$

In the Langmuir model, k_a and k_d are the adsorption and desorption rate constants, and q_m is the maximum binding capacity. The

spreading model [17,19,20] assumes two binding orientations of the protein on the membrane surface.

$$\frac{\partial q}{\partial t} = \frac{\partial q_1}{\partial t} + \frac{\partial q_2}{\partial t} \tag{11a}$$

$$\frac{\partial q_1}{\partial t} = (k_{a,1}c - k_{12}q_1)(q_m - q_1 - \beta q_2) - k_{d,1}q_1 + k_{21}q_2 \tag{11b}$$

$$\frac{\partial q_2}{\partial t} = (k_{a,2}c + k_{12}q_1)(q_m - q_1 - \beta q_2) - (k_{21} - k_{d,2})q_2 \tag{11c}$$

In the spreading model, q_1 and q_2 are the concentrations of adsorbed molecules in bound states 1 and 2, respectively, β is the ratio of the sorbent surface area occupied in state 2 relative to state 1, $k_{a,1}$, $k_{d,1}$, $k_{a,2}$ and $k_{d,2}$ are binding constants, that are defined in analogy to the Langmuir model, and k_{12} and k_{21} describe the exchange rates between the bound states. The spreading model can be further simplified by assuming that adsorption/desorption only occur to/from the first bound state, i.e. by setting the parameters $k_{a,2}$ and $k_{d,2}$ to zero.

3. Materials and methods

Breakthrough experiments were performed with bovine serum albumin (BSA, A 7638, Sigma Aldrich Corp, St. Louis, MO, USA) at two scales, using a Sartobind Pico MC capsule with 0.08 ml bed volume and 4 mm bed height, and a Sartobind 1.2 l MC capsule with 8 mm bed height which was recently introduced to the market and features optimized holdup volumes and fluid channel design. Both capsules contain the same membrane, a strong anion exchanger functionalized with quaternary ammonium groups on a stabilized reinforced cellulose matrix. The Pico device has a flat sheet axial flow configuration. It has been developed as a scale down tool for polishing applications, particularly for expensive virus spiking studies and early development stages when product is available at low quantities. The 1200 ml device has a spiral wound radial flow configuration and is mainly used for commercial scale capture and polishing steps. Notably, the studied capsules are from separate product lines, differing not only in size but also in the intended applications. The Pico device was not developed as a scale-down model of the 1.2 l device. Breakthrough experiments are performed at a concentration of 2 g/l BSA and a flow rate of 4 MV/min for both the axial and radial flow MC capsules. Here, MV denotes membrane volumes, i.e. 0.08 ml and 1200 ml, respectively. The protein was dissolved in 20 mM Tris buffer at pH 8.2 (Sigma Aldrich, USA) for the loading step. Loading was followed by a washing step with 25 mM Tris buffer at pH 8.2. Then, 1 M NaCl in 20 mM Tris buffer at pH 8.2 was used to elute the bound BSA from the membrane. The protein was dissolved in 20 mM Tris buffer pH 8.2 and 1 M NaCl for obtaining breakthrough curves under non-binding conditions. Subsequently, a wash step was performed by 25 mM Tris buffer plus 1 M NaCl at pH 8.2.

The porosity ε of the membrane is 0.80 ± 0.05 (manufacturer data). Internal capsule dimensions were provided by the manufacturer. In addition, an experimental 9.4 tesla magnetic resonance imaging (MRI) device was used to precisely measure the internal geometry of the assembled Pico device.

The 0.08 ml capsule was attached to an ÄKTAbasic system that was controlled by the Unicorn software (GE Healthcare, Uppsala, Sweden). The 1200 ml capsule was attached to a custom made chromatography skid system that was controlled by custom made software.

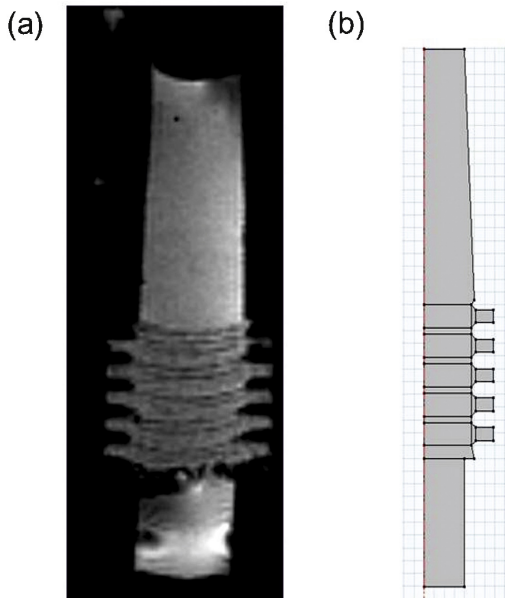

Fig. 3. (a) Internal geometry of the Sartobind Pico capsule as visualized by MRI (light grey: water in void region, dark grey: water in porous region, black: dry solid, MRI image is disturbed by artifacts in the void region below the membrane stack), (b) the same geometry reconstructed in COMSOL (assuming rotational symmetry).

4. Results and discussion

A model without abstraction and simplification of the real process would be as useful as a street map in the scale 1:1. Hence, the modeling of both studied capsules is based on the following assumptions, which are verified *a posteriori* by quantitative agreements of model prediction and experiment.

1. The role of fleece layer over the membrane for fluid distribution is neglected.
2. The Pico device is considered rotationally symmetric, which effectively reduces the CFD model to 2D.
3. The membrane stack is modeled as a single porous domain and is not allowed to move under dynamic conditions.
4. An axial 2D cross section is considered representative for the 1200 ml capsule.

4.1. Analysis of 0.08 ml capsule

The Pico capsule was filled with water and placed in the MRI device for measuring its interior geometry. Fig. 3a shows an axial cross section of the MRI data, in which five separately clamped stacks of membrane are clearly visible. In the central part of the capsule, each of these stacks has a thickness of 0.83–0.87 mm. In the clamping region the membrane stacks are separated by O-rings and compressed by a factor of two. The measured geometry is reconstructed in COMSOL, assuming rotational symmetry, as shown in Fig. 3b. The CFD geometry includes three membrane regions with different porosities. The central region, which is aligned with the free region above and below the membrane stack, has a porosity of 0.8. Due to compression, the clamped region and the intermediate region between the clamped and the central regions have reduced porosities. These porosities are calculated on the basis of a constant amount of solid membrane volume in the compressed and uncompressed regions. This results in average porosities of 0.74 in the intermediate region and 0.565 in the clamped region.

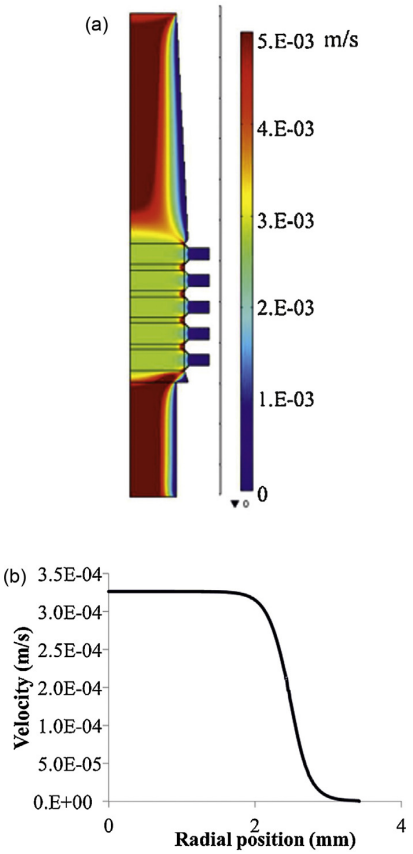

Fig. 4. (a) Computed velocity field magnitude in the Sartobind Pico capsule, (b) velocity magnitude in the central plane of a membrane stack (differences between the five stacks are negligible).

The velocity profile in the Pico capsule is computed by solving the coupled Navier-Stokes and Brinkman equations in the reconstructed geometry. Fig. 4a shows the resulting velocity field magnitude in the entire capsule. Fig. 4b shows the magnitude of the velocity field across each of the five membrane stacks. The velocity magnitude is almost constant throughout the central region and slightly decreases towards the intermediate region, in which it rapidly decreases. Even the clamped region exhibits non-zero velocities, but the flow is much slower there as in the central region.

The determined velocity field enters the mass balance equations, which are combined with different binding models for computing BTC under varying operating conditions. First, binding is neglected, $\partial q/\partial t = 0$, for simulating non-binding conditions. The

Table 1
External holdup volumes as determined by estimating the volumes of PFR and CSTR in series with the CFD model of both studied capsules from non-binding BTC.

Parameter	0.08 ml capsule	1200 ml capsule
V_{PFR}	0.76 ml	240 ml
V_{CSTR}	0.35 ml	300 ml

Table 2
Parameters of the spreading model as determined by fitting the CFD model and the traditional model to a binding BTC of the Pico capsule.

Parameter	CFD model	Traditional model
$k_{a,1}$ [l/(g s)]	6×10^{-2}	5.1×10^{-2}
$k_{d,1}$ [1/s]	1.24×10^{-5}	3.1×10^{-4}
k_{12} [l/(g s)]	5.7×10^{-2}	2.2×10^{-3}
k_{21} [1/s]	8.1×10^{-2}	6.7×10^{-2}
q_m [g/l]	134	190
β	1.08	2.88

parameters of PFR and CSTR, which are connected in series with the CFD model for describing system holdup volumes external to the MC capsule, are estimated from a measured BTC under non-binding conditions (high salt), as shown in Fig. 5a. The PFR and CSTR are essential, as the total volume of the Pico capsule, 0.08 ml, is extremely small compared to the holdup volume of the Äkta system, 1.11 ml. As proven by the following results, this semi-empirical model describes the contribution of the equipment to system dispersion accurately enough, and a mechanistic CFD model of the Äkta is not required. The estimated PFR and CSTR volumes, shown in Table 1, sum up to the true physical holdup volume of the tubing and the Äkta system.

The PFR, CSTR and CFD models are then fixed and combined with the Langmuir and spreading models for simulating BTC under binding conditions. The parameters of both binding models are estimated from measurement data. Fig. 5b shows that the spreading model reproduces the measured BTC very well. The Langmuir model cannot quantitatively reproduce the measured BTC (data not shown), which is in agreement with previous studies of BSA binding on functionalized polyether-sulfone (PES) membrane. Table 2 shows the binding parameters of the spreading model, estimated using the CFD model and the traditional model of the MC capsule. The traditional model can also reproduce the measured BTC very well (data not shown), but with significantly different binding parameters as compared to the CFD model. In particular the spreading factor, β, is much more realistic for the CFD model. A rigorous analysis of the binding mechanism underlying the spreading model will be subject of a separate publication.

4.2. Analysis of the 1200 ml capsule

The CFD geometry of the 1200 ml capsule was constructed on the basis of technical drawings from the manufacturer. The studied

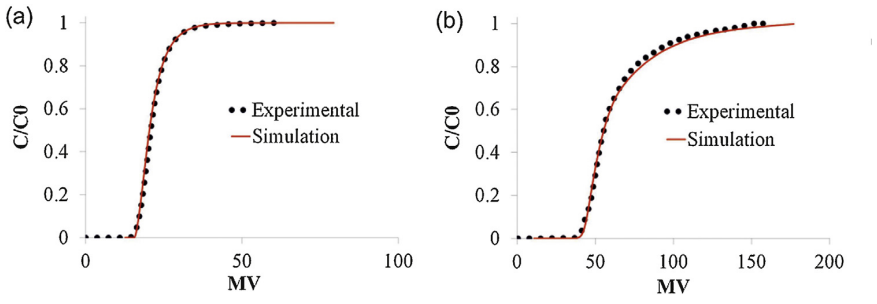

Fig. 5. Comparison of simulated and measured BTC for 0.08 ml capsule under (a) non-binding and (b) binding conditions.

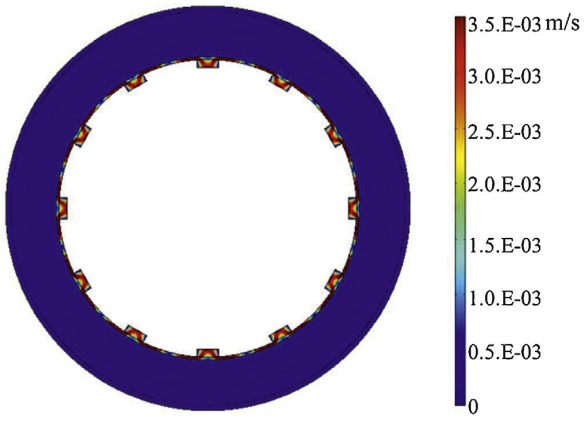

Fig. 6. Velocity field magnitude in the 1200 ml capsule.

MC capsule is a new product with optimized holdup volumes and channel design. It has a spiral wound configuration, which allows to model the membrane layers as a single porous region of given thickness around a solid core. The fluid enters this porous region through a thin void in the outer periphery of the capsule, and exits through another thin void which is connected to several channels that are placed in the solid core of the capsule. For this geometry, it is sufficient to solve the CFD model in a representative 2D axial cross section of the capsule (it will be shown that the holdup volumes at both axial ends of the capsule can be treated by a PFR and CSTR model). Fig. 6 shows the velocity profile, which is computed by solving the Navier-Stokes equations in the void regions on both sides of the membrane stack and the Brinkman equations in the porous domain. In contrast to the Pico capsule, the flow is homogeneously distributed throughout the membrane stack.

The velocity field enters the mass transport equations, which are first solved for non-binding conditions. The CFD model is again combined with a PFR and a CSTR (see Fig. 2), which for the 1200 ml capsule not only account for the holdup volumes that are external to the capsule but also for the holdup volumes in the distributors and collectors at both axial ends of the capsule. The PFR and CSTR parameters are estimated from non-binding BTC data, as shown in Fig. 7a and Table 1. Relative to the membrane volume, the holdup volumes are much smaller in the 1200 ml capsule as compared to the 0.08 ml capsule, but they are still important for quantitatively reproducing the measured BTC data.

4.2.1. Model-based scale-up from 0.08 ml to 1200 ml

The binding parameters of the spreading model that were determined from BTC data of the 0.08 ml Pico capsule, as shown in Table 2, are inserted into the CFD model of the 1200 ml capsule for predicting BTC data under binding conditions. Fig. 7b shows that

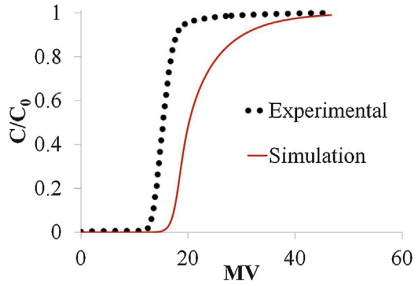

Fig. 8. Attempt to predict binding BTC of the 1200 ml capsule with binding parameters obtained using the traditional mass transfer model.

the result of this model-based scale-up is in excellent agreement with measured BTC data. This result is particularly remarkable, considering the scale-up factor of 15,000 from the Pico capsule used for identifying a suitable binding model and estimating the corresponding binding parameters. The high quality of the prediction is of great relevance for industrial process development, as the presented approach allows to design and optimize separation processes at extremely small scales and directly transfer the obtained results with only one expensive large scale experiment at binding conditions for validating the CFD prediction.

In contrast, an attempt to compute the same prediction with the CFD model of the 1200 ml capsule and binding parameters that were determined from BTC data of the Pico capsule using the traditional model (Fig. 1) completely fails to match the measured BTC, as shown in Fig. 8. This illustrates the importance of quantitatively separating the effects of non-ideal binding and non-ideal flow in MC capsules when the binding parameters are to be transferred across scales. If an inappropriate model is used for describing the mass transfer, flow-related phenomena, that are usually scale-dependent, are lumped into the scale-independent binding mechanism. As shown in Table 2, the effect of this lumping cannot be attributed to individual properties of the binding mechanism but affects all estimated binding parameters. Consequently, not only the binding capacity but also the tailing behavior of the BTC cannot be predicted using binding parameters that were estimated using an oversimplified mass transport model, as shown in Fig. 8.

5. Conclusions and outlook

The presented study extends and substantiates previous results on model-based scale-up of MC capsules. In particular, an extreme scale-up factor of 15,000 has been achieved between the Sartorius Pico capsule with 0.08 ml membrane volume used for process analysis and a production scale capsule from Sartorius with 1.2 l membrane volume and optimized holdup volumes and channel

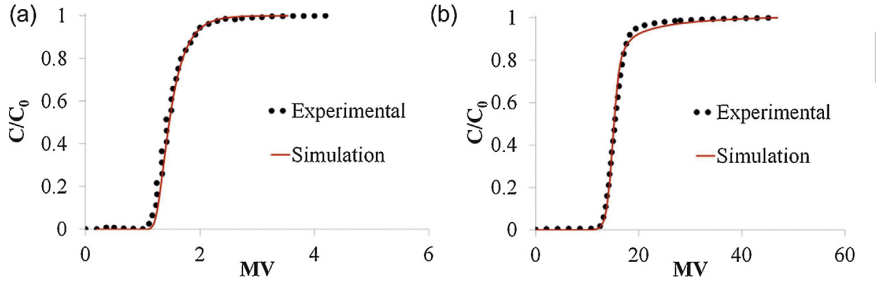

Fig. 7. Comparison of simulated and measured BTC of the 1200 ml capsule under (a) non-binding and (b) binding conditions.

design. The same modeling approach has previously been shown to work equally well for capsules from other vendors (Pall) with different flow-patterns and different membranes. CFD simulations are computationally more expensive than simulations with simplified mass transfer models. However, the additional expense pays off in truly quantitative predictions and can be overcompensated by material savings on the experimental side. The presented results also indicate that the new Sartobind 1.2 l capsule is well designed in that the fluid is homogeneously distributed in the membrane stack and the holdup volumes, resulting in a rather sharp BTC with little tailing. Further studies will focus on further elucidating the binding mechanism hypothesized by the spreading model. However, binding mechanisms are generally very complicated and the presented study proves that a reasonable approximation suffices for quantitative system analysis and design, as long as the impact of flow and binding non-idealities are quantitatively decoupled.

Acknowledgements

This presented work is supported by the Cluster Industrial Biotechnology (CLIB) with a doctoral scholarship for Pranay Ghosh.

References

[1] J.H. Vogel, H. Nguyen, R. Giovannini, J. Ignowski, S. Garger, A. Salgotra, Biotech. Bioeng. 109 (2012) 12.
[2] C. Boi, J. Chrom. B 848 (2007) 1.
[3] C. Charcosset, Biotechnol Adv. 24 (2006) 5.
[4] R. Ghosh, J. Chrom. A 952 (2002) 1.
[5] A. Monster, L. Villain, T. Scheper, S. Beutel, J. Membr. Sci. 444 (2013) 359.
[6] H.F. Zou, Q.Z. Luo, D.M. Zhou, J. Biochem. Biophys. Methods 49 (2001) 1.
[7] D.M. He, M. Ulbricht, J. Membr. Sci. 315 (2008) 1.
[8] M. Phillips, J. Cormier, J. Ferrence, C. Dowd, R. Kiss, H. Lutz, J. Carter, J. Chrom. A 1078 (2005) 1.
[9] J.X. Zhou, T. Tressel, U. Gottschalk, F. Solamo, A. Pastor, S. Dermawan, T. Hong, O. Reif, J. Mora, F. Hutchinson, M. Murphy, J. Chrom. A 1134 (2006) 1.
[10] R. Ghosh, T. Wong, J. Membr. Sci. 281 (2006) 1.
[11] P. Ghosh, K. Vahedipour, M. Lin, J.H. Vogel, C.A. Haynes, E. von Lieres, J. Chrom. A 1305 (2013) 114.
[12] P. Ghosh, K. Vahedipour, M. Lin, J.H. Vogel, C.A. Haynes, E. von Lieres, Biotech. Bioeng. 110 (2013) 4.
[13] S.Y. Suen, M.R. Etzel, Chem. Eng. Sci. 47 (1992) 6.
[14] J. Wang, F. Dismer, J. Hubbuch, M. Ulbricht, J. Membr. Sci. 320 (2008) 1.
[15] D.K. Roper, E.N. Lightfoot, J. Chrom. A 702 (1995) 1.
[16] C. Boi, S. Dimartino, G.C. Sarti, J. Chrom. A 1162 (2007) 1.
[17] P. Francis, E. von Lieres, C.A. Haynes A, Biotech. Bioeng. 109 (2012) 3.
[18] P. Francis, E. von Lieres, C.A. Haynes A, J. Chrom. A 1218 (2011) 31.
[19] A.J. Clark, A. Kotlicki, C.A. Haynes, A.L. Whitehead, Langmuir 23 (2007) 10.
[20] H. Yang, M.R. Etzel, Ind. Eng. Chem. Res. 42 (2003) 4.

Chapter 4

Discussion

4.1 Model building

Membrane chromatography (MC) is increasingly used in the biotechnology industry for downstream processing of large biomolecules such as proteins, antibodies and virus clearance. It can be operated at higher flow rates and offers an economical advantage to the widely applied packed bed chromatography. MC capsules are characterized by the sharpness of their breakthrough curves (BTCs). However, the breakthrough curves (BTCs) of MC capsules frequently suffer from tailing near the saturation. Furthermore, the degree of tailing differs not only between MC capsules from different vendors but also varies between MC capsules at the lab and the large scale from the same vendor. A lab scale MC capsule, built as a physical scale-down model of a large scale MC capsule, therefore, cannot be accurately used for optimization of large scale purification process. Hence, a mathematical model-based approach is required for a holistic process analysis and scale-up in MC.

In this work, two different modeling approaches, the zonal rate model (ZRM) approach and the computational fluid dynamics (CFD) approach, are employed for model based process analysis in MC capsules. Both modeling approaches have been independently utilized for predicting the breakthrough performance of MC capsules at production scale. These predictions are compared with predictions obtained using traditional modeling approaches. MC capsules from Pall Inc. and Sartorius Stedim GmbH are extensively studied using the developed models.

Quantitative reproduction of BTCs in subsequent runs is an essential prerequisite for modeling. Therefore, ***publication I*** first describe the experimental methods that have been developed to obtain consistent BTCs using lab (XT5) and production scale (XT140) MC capsules from Pall Inc. A revised cleaning protocol with NaCl instead of NaOH and minimizing the storage time were identified as most critical for quantitatively reproducing the measured BTCs. These BTCs were used subsequently for model based analysis using ZRM and CFD approaches.

Publication I, thereafter, explains the formulation of ZRM variants for lab scale XT5 and large scale XT140 MC capsules from Pall Inc.. BTC under non-binding and binding conditions, using 1mg/ml BSA at 12MV/min, were analyzed. The non-binding BTC captures flow inhomogeneity in the external hold-up volumes of the studied MC capsule independent of protein binding to the membrane surface. It was found that a two-zone ZRM configuration explains the non-binding BTC of the XT5 capsule in a much better fashion than the traditional model. On the other hand, a one-zone ZRM configuration was found sufficient to explain the non-binding BTC of the XT140 capsule. This implies that the fluid flow in the external hold-up volumes of the XT5 capsule is inhomogeneous while in those of the XT140 capsule is homogeneous.
Employing the two zone ZRM configuration, it was found that BSA binding to the membrane surface in the XT5 capsule can be described accurately by using the spreading model instead of the classical Langmuir model. The binding parameters, thus obtained from XT5 analysis, were used for predicting the BTC under binding conditions of the XT140 capsule. However, an accurate prediction was not successful. MRI investigation of XT140 capsules revealed several structural irregularities in the membrane pleats. It was assumed that such irregularities led to variation of linear velocities within membrane pleats of the XT140 capsule which hindered scale-up. Notably, such velocity variations hardly impact the shape of BTC under non-binding conditions due to low bed height of the membrane stacks. Hence, a BTC under binding condition was required to quantify flow inomogeneity in XT140 capsule. A new ZRM configuration was set-up and a distribution curve for the linear velocity in the XT140 capsule was determined from corresponding BTC at a flow rate of 12MV/min.

Publication II was written in continuation of publication I and further validates the findings of non-idealities in protein adsorption and hydrodynamics in the studied XT5 and XT140 capsules. It was found that a two-zone ZRM configuration also explains non-binding BTCs of the XT5 capsule at 1.2MV/min and 4MV/min using 1mg/ml BSA. The non-binding BTCs are independent of the tracer molecule and it was also found that a two-zone ZRM configuration is required to explain the corresponding BTC obtained

using 1mg/ml ovalbumin at 5.7MV/min. This implies that fluid flow is, indeed, inhomogeneous in the external hold-up volumes of the XT5 capsule. Furthermore, as found earlier in publication I, the spreading model is able to consistently describe theBSA adsorption on the studied membranes at different flow rates as well. The spreading model also accurately explains ovalbumin binding on the studied membrane surface.
It was further shown that the linear velocity distribution in the XT140 capsule, previously determined in publication I, is independent of flow rates and tracer molecules. Thus, the previously determined linear velocity distribution was utilized to independently predict the breakthrough performance of the XT140 capsule using 1mg/ml BSA at flow rates of 1.2MV/min and 4MV/min. Furthermore, the same linear velocity distribution was also used to provide an accurate prediction of the binding BTC of the XT140 capsule using 1mg/ml ovalbumin at a flow rate of 5.7MV/min. Hence, it is concluded that this velocity distribution needs to be determined only once using large scale binding BTC data, and thereafter can be used for quantitative predictions with the ZRM at a variety of operating conditions.

The CFD based model, described in publications III and IV, provides a more mechanistic modeling approach as compared to the ZRM. In ***publication III***, CFD models were constructed based on true internal geometries of XT5 and XT 140 capsules. The geometry of XT5 capsule was reconstructed by measuring internal dimensions while the complicated pleating structure in the XT140 capsule was reconstructed from MRI measurements. The CFD approach is computationally intensive and therefore, the computational requirements were reduced by several assumptions. The 3D complexity of both MC capsules could be reduced to simpler 2D models. Based on geometric information, the CFD simulations were able to predict non-binding BTCs of the XT5 and the XT140 capsules. The CFD simulations also provided a validation of different assumptions in the ZRM approach. It was found that the high length-to-width ratio of the XT5 capsule causes non-ideal flow in the external hold-up volumes. Therefore, the traditional model that assumes homogeneous flow in external hold-up volumes is not able to explain the non-binding BTC of the XT5 capsule. However, since the ZRM of the XT5 capsule discretizes the hold-up volumes in parallel zones, it is successful in accurately explaining the non-binding BTC. On the other hand, the sealing and bend regions in the pleating structure of the XT140 capsule result in locally higher bed heights as compared to the major fraction of the membrane region. Higher bed heights cause higher pressure drops and, consequently, lower velocities in these regions. Therefore, the corresponding ZRM configuration needs to account for linear velocity variations within this capsule.
As observed for the ZRM based modeling approach, the spreading model was also found

to accurately correlate to binding BTC also in the CFD approach. Notably, the binding parameters obtained using both approaches are almost identical. Since, the CFD approach is able to fundamentally decouple the non-idealities in hydrodynamics in XT5 and XT140 capsules, an accurate prediction of BTCs under binding conditions of the XT140 capsule was possible.

The CFD model can accurately capture hydrodynamics within MC capsules irrespective of their scale. The non-idealities in protein adsorption are always conserved for a given protein-membrane interaction. Therefore, once the non-idealities in protein-membrane interaction are rationally captured at a small scale, the CFD framework can be employed to provide a holistic prediction for any arbitrary scale-up factor. In publication III, the CFD approach was employed to perform a scale-up from 5 ml to 140 ml, i.e. a scale-up factor of 28. However, MC devices are further miniaturized in order to save valuable material and time in process development. Sartorius Pico devices are an example of such miniaturization. Here the bed volume is 0.08 ml. In ***publication IV***, the CFD based approach is utilized for modeling MC systems from Sartorius stedim biotech GmbH. Following the same approach as in publication III, an extreme scale-up factor of 15,000 was possible.
Notably, even though membranes in Pall and Sartorius MC capsules exhibit different properties, the spreading model of protein binding is also able to explain BSA adsorption on Sartorius membranes. Thus, the ability of the spreading binding model to rationally explain binding of different proteins on different membranes at different flow-rates indicates that the spreading model is an appropriate model of protein adsorption on membrane. However, this finding cannot be regarded as conclusive and further studies are required.

The ZRM and CFD modeling approaches have different strengths and selecting the right modeling approach depends on the application. Both approaches can also be followed simultaneously which allows the possibility of cross-validation, as has been shown in publication III. The ability to perform faster analysis and low computational requirement make the ZRM particularly attractive process tool for separation scientists for the design and optimization of separation processes utilizing MC capsules. The ZRM is intuitively designed and new configurations can be implemented with minimum effort in order to test new hypotheses. On the other hand, the CFD approach provides a greater mechanistic understanding of fluid flow within MC capsules. Designing MC capsules have been largely an empirical task for manufacturers. As seen in this work, optimum design of a coherently scaled up or a scaled down MC capsule has remained elusive. Thus, a CFD approach leading to a fundamental understanding of hydrodynamics within MC

capsules has proven to be useful for manufacturers to achieve optimum design.

4.2 Applying the models

The developed modeling approaches can be applied for estimating key design parameters that could not be accurately observed using the traditional model. For example, Sartorius MC capsules are routinely used in capture application. The lab scale Pico MC capsule is used for estimating the loading time of the large scale 1.2L MC capsule. The loading is performed until 1% of breakthrough is observed. Figure 4.1 shows the result of such an estimation using the traditional model and the CFD model and compared with the experimentally determined BTC of the Large scale 1.2L MC capsule. Both, the traditional model and the CFD model are equally good in fitting to the BTC data of the Pico MC capsule; however the estimated binding parameters are drastically different. As seen in Figure 4.1, the parameters estimated from the CFD model give a much better prediction of the breakthrough point in comparison to the traditional model. Thus by using the traditional model, one runs the risk of loosing valuable product.

The CFD approach further provides unique insights into the impact of capsule design

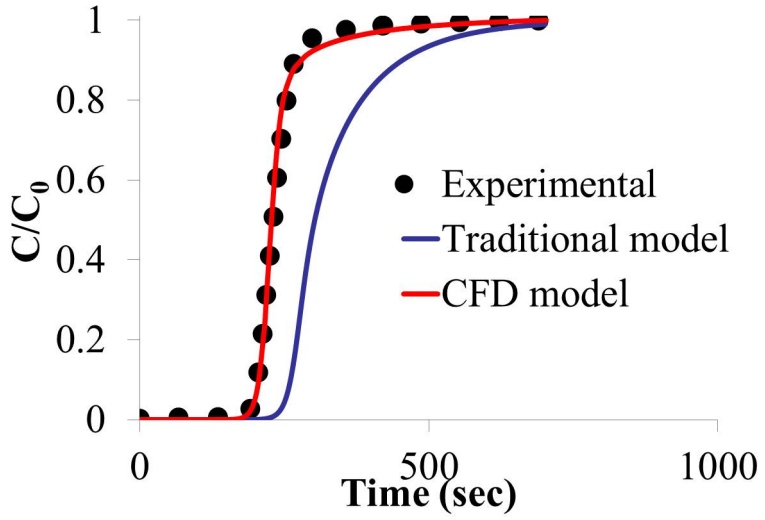

FIGURE 4.1: Prediction of breakthrough performances of Sartorius 1.2L MC capsule using the traditional model (blue line) and the CFD model (red line) for Sartorius 1.2 L capsule.

and suggests ways to improve the performance of MC capsules. Figure 4.2 shows the variation of linear velocity observed within membrane stacks of the studied lab scale Sartorius Pico capsule and the studied large scale Pall XT140 capsule. Both these capsules exhibit greater tailing in their BTCs in comparison to their large scale and lab scale

counterparts, respectively. The CFD approach provides fundamental understanding of such effects and also provides potential solutions to the problem. For example, in the Sartorius Pico capsules, reducing the membrane volume under the clamp region would lead to less tailing in the BTC. Similarly, if the sealing region in Pall large scale XT140 capsules is minimized, there would be much less linear velocity variations within the capsule and that would lead to much less tailing in the corresponding BTC.

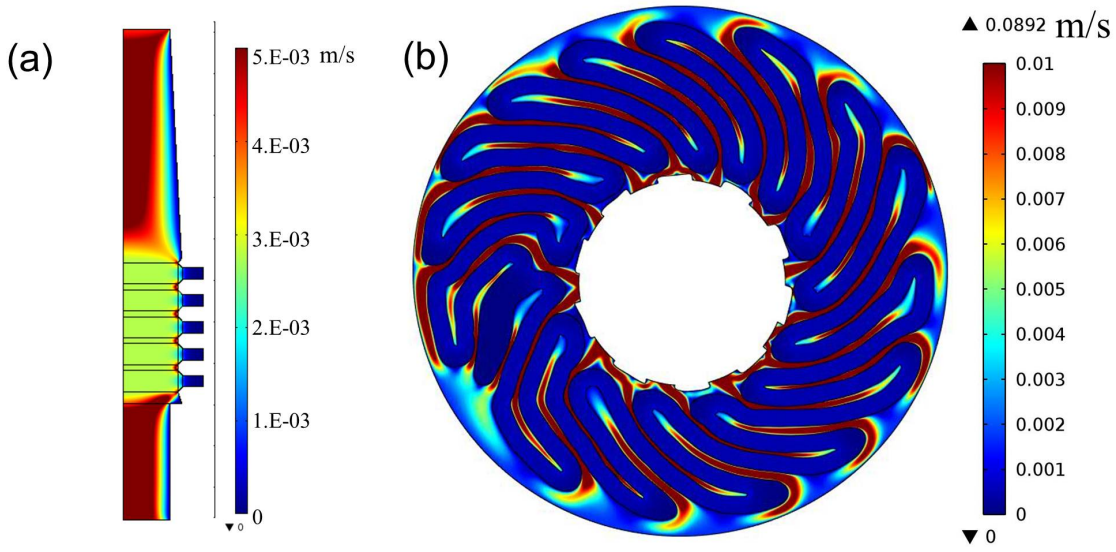

FIGURE 4.2: Variation of linear velocity observed within membrane stacks of MC capsules from different vendors using the CFD approach (a) Linear velocity profile within the studied lab scale Sartorius Pico capsule, (b) Linear velocity proflie within the studied large scale Pall XT140 MC capsule.

4.3 Summary

The breakthrough curve that we observe on a macroscopic level, in fact, depends upon phenomena occurring at much smaller scales of length and time. Protein adsorption on the membrane surface is a result of interactions between small ions and charges at the atomistic level, whereas the mass transport is an outcome of fluid flow occurring in hold-up volumes of the engineered MC capsules and micro scale fluid flow occurring in fine interconnected pores of the membrane. A *super model* of an MC capsule that would span across such different scales of complexity in three dimensions, integrating and passing information from one scale to another, would lead to a true prediction of the system. However, considering our current computational capabilities, creating such a super model remains a distant dream. Furthermore, the amount of experimental effort and validation required in supporting such a modeling task has a certainty of becoming

unmanageable. Therefore, finding the right level of abstraction from reality is crucial in developing simpler modeling strategies that aid in prediction and process analysis but with much smaller computation and experimental requirements. The traditionally employed model for MC capsules assumes protein adsorption as the dominant mechanism that shape the BTC under binding condition and neglects the role of fluid flow. Thus the traditional models lumps the parameters influenced by fluid flow into parameters influenced by protein adsorption.

Such parameter lumping works in performing stand-alone process analysis on one scale of operation; however, as shown in this work, completely fails in providing a holistic model based scale-up. On the other hand, the two modeling approaches developed in this work, go a level deeper, by incorporating the role of fluid flow along with protein adsorption. The parameters influenced by fluid flow are independently analyzed and captured in semi-empirical and mechanistic models, thus avoiding parameter lumping. Notably, the models still do not describe finer details such as fluid flow within the microporous structure of the membrane. The three dimensional design of the MC capsules was also reduced to two dimensional models, that considerably reduced the computation cost. Nonetheless, the developed models were able to provide an accurate model-based scale-up. Thus, by quatitative decoupling of flow related and binding related non-idealities, the developed models provides a superior strategy for process analysis facilitating a rational model based process design.